THE MINISTRY OF NATIONAL INFRASTRUCTURES
GEOLOGICAL SURVEY OF ISRAEL

UNIVERSITY OF HAWAII

Phosphorus accumulation rates in the Upper Cretaceous - Eocene of the southern Tethyan margin - a case study of temporal fluctuations in phosphogenesis and rates of phosphate fluxes

Final Scientific Report (Grant No 1999232)

Submitted to the US-Israel Binational Science Foundation (BSF)

DAVID SOUDRY, YAACOV NATHAN
The Geological Survey of Israel

CRAIG R. GLENN
University of Hawaii

GSI/01/2005

Jerusalem, January 2005

THE MINISTRY OF NATIONAL INFRASTRUCTURES
GEOLOGICAL SURVEY OF ISRAEL

UNIVERSITY OF HAWAII

Phosphorus accumulation rates in the Upper Cretaceous - Eocene of the southern Tethyan margin - a case study of temporal fluctuations in phosphogenesis and rates of phosphate fluxes

Final Scientific Report (Grant No 1999232)

Submitted to the US-Israel Binational Science Foundation (BSF)

DAVID SOUDRY, YAACOV NATHAN

The Geological Survey of Israel

CRAIG R. GLENN

University of Hawaii

GSI/01/2005

Jerusalem, January 2005

Abstract

To try to clarify the question of temporal changes in phosphogenesis, and whether they reflect variations in ocean circulation or continental weathering, we examined the evolution of Tethyan phosphogenesis during the Cretaceous-Eocene. 26 time-stratigraphic phosphorite horizons in the Negev and others sites in Tethys margins, covering a time scale of about 90 Ma from the Hauterivian to the middle Eocene, were analyzed for their Sr, Ca, and Nd isotopic compositions in the carbonate fluorapatite (CFA) phase. P and Ca accumulation rates and rates of bulk sedimentation were also quantified along the middle Cretaceous-Eocene sequence of the Negev to examine changes between isotopic compositions and intensity of Tethyan phosphogenesis. To constrain nutrient recycling by marine circulation, TOC (wt%), C:N:$P_{(org)}$ ratios, $\delta^{13}C_{(org)}$, and $\delta^{15}N_{(org)}$ were also measured along the Coniacian-Eocene interval of the Negev and in the Campanian phosphate section of Egypt.

Several points emerge from the results: 1) A similar tend exists in the distribution of $\delta^{44}Ca$ and $\varepsilon_{Nd(T)}$ in the analyzed time-interval; 2) $\delta^{44}Ca$ and $\varepsilon_{Nd(T)}$ steeply rise after the Cenomanian-Turonian, reaching some of the highest values in the upper Campanian; 3) distinct $\varepsilon_{Nd(T)}$ values are shown by the phosphorites of the Negev and Egypt during the Campanian, and by the phosphorites of the Negev and North Africa during the Maastrichtian-Eocene; 4) the $\delta^{44}Ca$ and $\varepsilon_{Nd(T)}$ peaks during the upper Campanian in the Negev coincide with a peak in rates of P accumulation and a low in rates of Ca accumulation and bulk sedimentation; 5) The evolutions of Sr isotopes and of Ca-Nd isotopes are in general decoupled; 6) TOC, C:$N_{(org)}$, C:$P_{(org)}$, $\delta^{13}C$ and $\delta^{15}N$ generally co-vary in the upper-Coniacian-middle Eocene phosphogenic interval of the Negev.

The general co-variance between $\varepsilon_{Nd(T)}$, $\delta^{44}Ca$, TOC, $\delta^{13}C$ $\delta^{15}N$, and P accumulation rates in the middle Cretaceous-Eocene of the Negev suggests paleogeographic and oceanographic controls in phosphorite accumulation. The steep $\varepsilon_{Nd(T)}$ rise following the upper Cenomanian points to increased Pacific water masses incursion into Tethys, driven by the Late Cretaceous global sea level rise and increased water circulation. It also reflects a weakening of the continental Nd signal as a result of the increasing flooding. $\delta^{44}Ca$ also rising at these times similarly points to a decrease in weathering Ca^{+2} fluxes and expansion of carbonate sedimentation areas in the flooded shelves. The rise of P accumulation in

Campanian times also reflects the combined effect of sea level highstands and plate-tectonics both inducing favorable atmospheric and ocean circulation through the Tethys seaway. The low $\delta^{13}C$ and $\delta^{15}N$ in the Campanian-Maastrichtian organic fraction of the Negev reflect sustained coastal upwelling of P-rich waters in the mainly eastern Tethys, resulting from the increased vertical marine circulation in this area. The overall decoupling between the geochemical evolution of Sr isotopes and Ca-Nd isotopes during the studied time-interval suggests little direct relationship between continental weathering and rates of phosphogenesis. The distinct $\varepsilon_{Nd(T)}$ values between the Middle East phosphorites and the North Africa phosphorites suggest different oceanic P sources for the two phosphorites.

1. Introduction

Phosphorus (P), carbon (C) nitrogen (N) and potassium (K) are all nutrient elements indispensable for plant growth and animal life. By contrast to C, N and K which are virtually of unlimited availability in nature (atmosphere and seawater, respectively), P is far more restricted in nature and is available only via the exploitation of geological phosphate rocks (phosphorites). Apart from being the prime source of P for phosphate fertilizer industry (main use of P), phosphorites are also of high scientific interest as they provide valuable information on the ecology and chemistry of the world's past ocean. As limiting nutrient of living systems, P governs oceanic productivity on Earth as well as the rate of CO_2 removal from the atmosphere and the rate of marine denitrification. This links the P cycle to the carbon (C) and nitrogen (N) cycles (Mackenzie et al., 1993; Schlesinger, 1997), regulating by this way Earth's climate and atmospheric oxygen (Van Cappellen and Ingall, 1996) and N levels over geological time scales (Falkowski, 1997; Tyrrell, 1999). The source of long term P supply to the ocean reservoir is continental weathering of sedimentary and igneous rocks. Once extracted by planktonic organisms from the photic zone of the oceans, P is transferred to sea bottom as part of sedimentary organic matter (OM), and a fraction of it may be fixed as authigenic carbonate fluorapatite (CFA) in bottom sediments during suboxic degradation of OM (Froelich et al., 1978; Glenn, 1990). Large phosphate deposits (phosphorite "giants") were formed at several time-intervals of the Phanerozoic as a result of intensive P accumulation (Glenn et al., 1994). Today, marine phosphate formation is restricted to a few sites in continental margins (off Peru/Chile, Baja California, Namibia,) all associated with intensive coastal upwelling and high productivity

A fundamental question is the meaning of these secular variations in P accumulation (e.g., Baturin et al., 1995). Do or do they not reflect extraordinary (time-bound) oceanographic conditions with accelerated P delivery from the oceanic reservoir? More specifically are global P burial rates constant over geological times or do they show strong deviations at certain periods of Earth history? Cook and McElhinny (1979) following Sheldon (1964) linked variations in phosphogenesis to global changes in paleogeography and paleoceanography in relation with plate tectonic. For phosphogenesis to start, the continents had to be in low latitudes and seaways had to be wide enough to allow strong intensive oceanic circulation and upwelling (see Parrish and Curtis, 1982). As in modern situations (e.g., Hay, 1995), these strong upwelling-times will supply nutrient-rich waters to

continental margins, thus intensifying productivity and P transfer to sea bottom. Indeed, many major phosphate occurrences in the geological past are associated with positive $\delta^{13}C$ shifts indicating increased carbon burial (e.g., Compton et al., 1993). Many used this model to explain phosphogenesis in past times, e.g., McKelvey et al. (1959) for the Permian Phosphoria Formation, Cheney et al. (1979) for the Miocene Sechura phosphorites, Kolodny (1980) and Bein et al. (1990) for the Late Cretaceous Negev phosphorites, and Garrison et al. (1990) for the Miocene Monterey phosphorites.

Yet, a quite different approach has evolved during the last few years. Central to this approach is the view that no "abnormal" oceanographic conditions are required to produce the huge P accumulation of past times, P burial rates via authigenic CFA formation are rather constant over geological timescales, and continental weathering may directly control rates of phosphogenesis in shelves (Barron and Frakes, 1990; Glenn and Arthur, 1990; Delaney and Filippelli, 1994; Filippelli and Delaney, 1994). Reviving earlier views (Bushinski, 1966), Ruttenberg and Berner (1993) claimed that the episodicity of past P accumulations are more a reflection of appropriate depositional settings than the result of increased P removal from the ocean reservoir. In this scenario, phosphate formation in continental margins is mainly via riverine P supply and does not necessarily requires upwelling or high productivity, and the ocean is essentially in steady state with respect to P fluxes (inputs = outputs).

We use the mid-Cretaceous-Eocene of the Negev (southern Israel) and of other areas in Tethys margins as a selected time window to explore this controversy. Two successive contrasting sediment-systems accumulated during this period in the Negev (Fig. 1) and in neighboring Middle East countries (Lewy, 1990). The Barremian – Coniacian consists mainly of platform carbonates. The upper Coniacian – middle Eocene is a phosphate-bearing chert-chalk system associated with a major phosphogenic episode which produced massive phosphorite deposits along the southern Tethys margins (Egypt, Middle-East and North Africa). We 1) quantify the rates of P accumulation over the Cretaceous-Eocene succession of the Negev, and 2) examine how their variations in time are reflected in temporal changes of chemical parameters proxies for continental weathering, ocean circulation, and nutrient recycling.

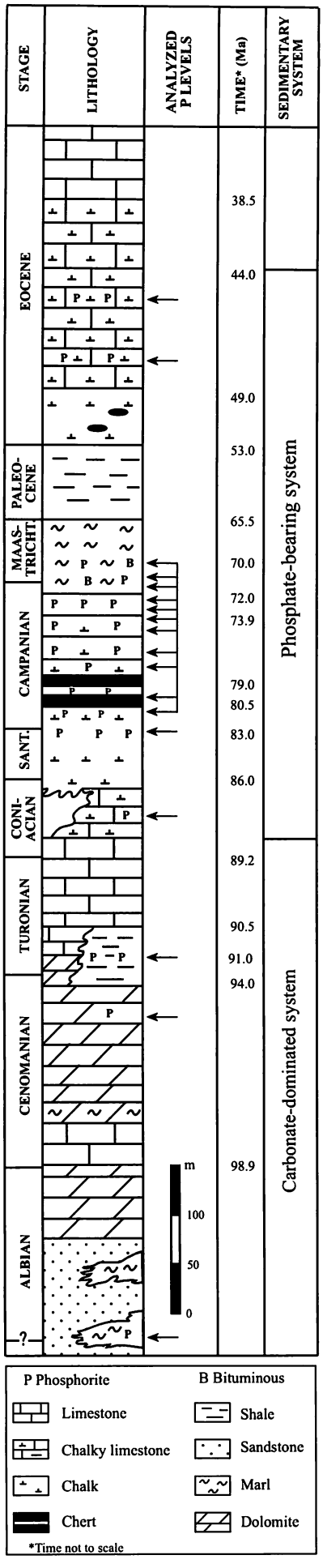

Fig. 1. Chronostratigraphic positions of the phosphate levels (arrowed) analyzed for $\delta^{44}Ca$, $^{143}Nd/^{144}Nd$, and $^{87}Sr/^{86}Sr$ in the Albian-Eocene section of the Negev.

2. Methodology

In addition to conventional analytical techniques, such as XRD, FTIR, wet chemistry, optical petrography, and SEM (with EDAX-coupled) examinations, various isotopic measurements were used to constrain the controls of P accumulation over the studied sequence.

2.1. Sr isotopic analysis

Determination of the variations in P accumulation rates along the upper Cretaceous-Eocene Tethyan sequence (one of the major goals of this research) requires a good stratigraphic control. The use of $^{87}Sr/^{86}Sr$ of past seawater is a potential tool for dating and correlating of marine sequences. Since the reference curve of Burke et al. (1982), this dating technique was refined. Most accuracy in Sr isotope stratigraphy was reached for the Cenozoic (Hoddel et al. 1991, DePaolo and Finger, 1991), although some progress was also made in refining the Late Cretaceous marine Sr isotope curve (e.g., McArthur et al., 1994).

The $^{87}Sr/^{86}Sr$ ratio in francolite was also used to date phosphogenesis (McArthur et al., 1990; Riggs et al., 1997). Sr^{+2} replaces Ca^{+2} in the apatite structure, either in skeletal hydroxyapatite (during biological growth), or in the CFA phase during its precipitation in bottom sediments. The high Sr^{+2} content in CFA (~ 2500 $\mu g.g^{-1}$) makes it particularly suitable to measure the isotopic Sr. Besides, studies of CFA forming today show that their $^{87}Sr/^{86}Sr$ composition is very close or identical to that of present-day seawater, showing that the seawater Sr-isotopic signal is essentially preserved in the formed CFA (see Jarvis et al., 1994). In the present research, the $^{87}Sr/^{86}Sr$ ratio was measured in CFA levels over the Cretaceous-Eocene succession. This, in order to enable detailed quantification of accumulation P rates over the studied sequence, and also to try to try to draw inter-regional correlations between Tethyan phosphate episodes In addition, the determined numerical Sr ages allow us to calculate the initial Nd isotope composition of the CFA samples.

2.2. Nd isotopic analysis

$^{143}Nd/^{144}Nd$ ratios were measured on the same set of CFA samples that were analyzed for Sr isotopes. Nd^{+3} replaces Ca^{+2} in apatite during early diagenesis (while the pore fluids are still in direct communication with seawater), either during CFA precipitation or during post mortem incorporation of Nd^{+3} in skeletal hydroxyapatite. The rational for

measuring the Nd-isotopic ratio is to try to detect variations in ocean circulation and continental weathering over the studied time interval (e.g., Keto and Jacobsen, 1988; Stille, 1992). Due to the short residence time of Nd in seawater (10^2-10^3 years) the oceans are not isotopically homogenous with respect to Nd, allowing to reveal mixing of oceanic water masses of different Nd isotope compositions (e.g., Piepgras and Wasserburg, 1980). In addition, the extremely low concentration of Nd in marine pore fluids together with its low geochemical mobility caused by its high particle reactivity (Martin and Scher, 2004), both make Nd quite resistant to diagenetic alteration, allowing the preservation of seawater Nd isotopic compositions.

2.3. Ca isotopic measurements.

$^{44}Ca/^{42}Ca$ isotopic ratios were measured in many of the CFA samples analyzed for $^{87}Sr/^{86}Sr$ and $^{143}Nd/^{144}Nd$ ratios. Analysis of biological carbonates (Skuklan et al., 1997; Zhu and MacDougall, 1998) together with laboratory experiments (Nägler et al., 2000) indicate that biological fixation of Ca^{+2} discriminates against heavy isotopes, and that this process plays an important role in regulating the isotopic composition of marine Ca. On the other hand, weathering of carbonate rocks will supply to the oceans riverine Ca^{+2} enriched with the lighter isotope. In addition, Ca is a major component of CFA (~ 30% in weight). Such a high Ca concentration in CFA would minimize the effect of isotopic exchange in pore waters and would tend to preserve the Ca isotopic composition during diagenesis. Thus, analyzing the Ca-isotopic compositions may help us to detect deviations in the seawater Ca isotopic composition, and by this way to reveal temporal imbalances between continental weathering and carbonate sedimentation fluxes (De La Rocha and DePaolo, 2000) caused by migrating continents-oceans margins.

2.4. TOC (%), $C:N:P_{(org)}$ atomic ratios, $\delta^{13}C_{(org)}$, $\delta^{15}N_{(org)}$.

To constrain regeneration of nutrients in bottom sediments and their recycling to the euphotic surface water by marine vertical circulation (e.g., Rau et al., 1987; Jenkyns et al., 2001; Murphy et al., 2000), TOC (%), $C:N:P_{(org)}$ ratios, $\delta^{13}C_{(org)}$, and $\delta^{15}N_{(org)}$ were measured throughout the upper Coniacian-middle Eocene succession of the Negev and in the upper Campanian phosphate section of Egypt (Duwy Fm.). In addition, $\delta^{13}C_{(org)}$ might provide useful information on changes in pCO_2 and productivity along the studied time-

interval (e.g., Dean et al., 1986; Hayes et al., 1999), while $C:P_{(org)}$ could help us to better understand the diagenetic fate of P and the conditions of its retention in marine sediments (e.g., Ingall and et al., 1993; Van Cappellen and Ingall, 1996; Filippelli, 2001; Slomp et al., 2004).

2.5. P and Ca accumulation rates and sedimentation rates

To link changes in isotopic compositions with changes in intensity of Tethyan phosphogenesis, P and Ca accumulation rates and sedimentation rates were quantified over the Cretaceous-Eocene of the Negev. The quantified rates allow us to examine how their variations through time are reflected in the isotopic values of the various elements measured along the sequence.

3. Material source

The material analyzed is from two different sources:

1) Drillhole (core/cuttings) material from Negev sections:

- M7 and M13 drillcores (Yarkoni 1982, 1985) of the Mediterranean-Dead Sea hydroelectric project: Taqiye (Paleocene) and Mor - Paran (Eocene) Formations, respectively.

- Har Nishpe S5 drillcore (Soudry and Eyal, 1994) and Pama B124 drillcore (Mishor Rotem): Ghareb Formation (Maastrichtian).

- Har Nishpe S1 and B17 drillcores (Soudry and Eyal, 1994): Phosphate Member, Mishash Formation (upper Campanian).

- ZS28 Zin core (Bein et al., 1990b, Almogi et al., 1993): Menuha Formation (upper Coniacian - Lower Santonian).

We used the drillhole material for the elemental geochemistry of stratigraphic intervals (bulk samples), for the analysis of C_{org}, N_{org}, and P_{org} in the organic fraction (OM), and also to extract CFA fractions for the measurement of $^{87}Sr/^{86}Sr$, $^{143}Nd/^{144}Nd$, and $^{44}Ca/^{42}Ca$ isotope ratios.

2) Outcrop material: mainly phosphate samples in intervals for which no drillhole material was available. The phosphate samples were collected from field outcrops, trenches, cut roads, and open pits and were used for of measurement of Sr, Nd, and Ca isotopes in CFA.

In addition, phosphate samples (drillcore/outcrop material) from other areas in continental Tethys margins (Fig. 2) were obtained from the following sections:

- The Maastrichtian -Ypresian phosphate-bearing suite of the Ganntour deposit, Morocco (Prévôt, 1988).

- The Duwy Formation (upper Campanian), Egypt (Glenn and Arthur, 1990).

- The Amman Formation (upper Campanian), Jordan (Jallad et al., 1989).

- The Sawwaneh Formation (upper Campanian), Syria (Al-Maleh and Mouty, 1994).

- The Mazidagi-Mardin Formation (Coniacian - Santonian), Turkey (Lucas et al., 1979).

- The Vigla Formation (Coniacian - Santonian), Ionian zone, Greece (Pomini-Papaioannou, 2001).

- The "blue marls" (Aptian - Albian) of the Vocontian Basin, SE France (Bréhéret, 1988).

- The Schrattenkalk Formation (Barremian to lowermost Aptian), Helvetic Alps (Föllmi, 1989).

In total, 94 phosphate samples covering a time-span of about 90 Ma over the Cretaceous-Eocene in the continental margins of the Tethys (including a few Cretaceous samples from connected marine provinces) were collected for isotopic measurements in CFA (Table 1). In addition, 104 samples from the upper Coniacian-Eocene of the Negev and some 10 samples from the Campanian of Egypt were analyzed for TOC (wt%), C_{org} and N_{org} (wt%) and $\delta^{13}C_{org}$ and $\delta^{15}N_{org}$ (‰). Of the Negev samples, 36 were also analyzed for P_{org} (wt %).

4. Analytical procedure

4.1. Sample preparation

Separation of the CFA fraction for isotopic analysis was done by two different procedures. In friable samples, phosphate pellets were selectively hand-picked under microscope from the 150-290 μm-sized P-rich fraction of the sample after wet-sieving and oven-drying. In some of these samples, skeletal and pelletal CFA fractions were microscopically separated for selective isotopic analysis of each fraction. In cemented non dolomitic samples, the total CFA fraction was separated by selective dissolution of the calcite fraction with tri-ammonium citrate (TAC), after crushing the sample to 72 μm size. In case of phosphorite with dolomite, the sample was heated at 700° C for one hour, washed with deionized water to remove the free MgO and CaO, then treated with TAC to remove any $CaCO_3$ still remaining in the sample.

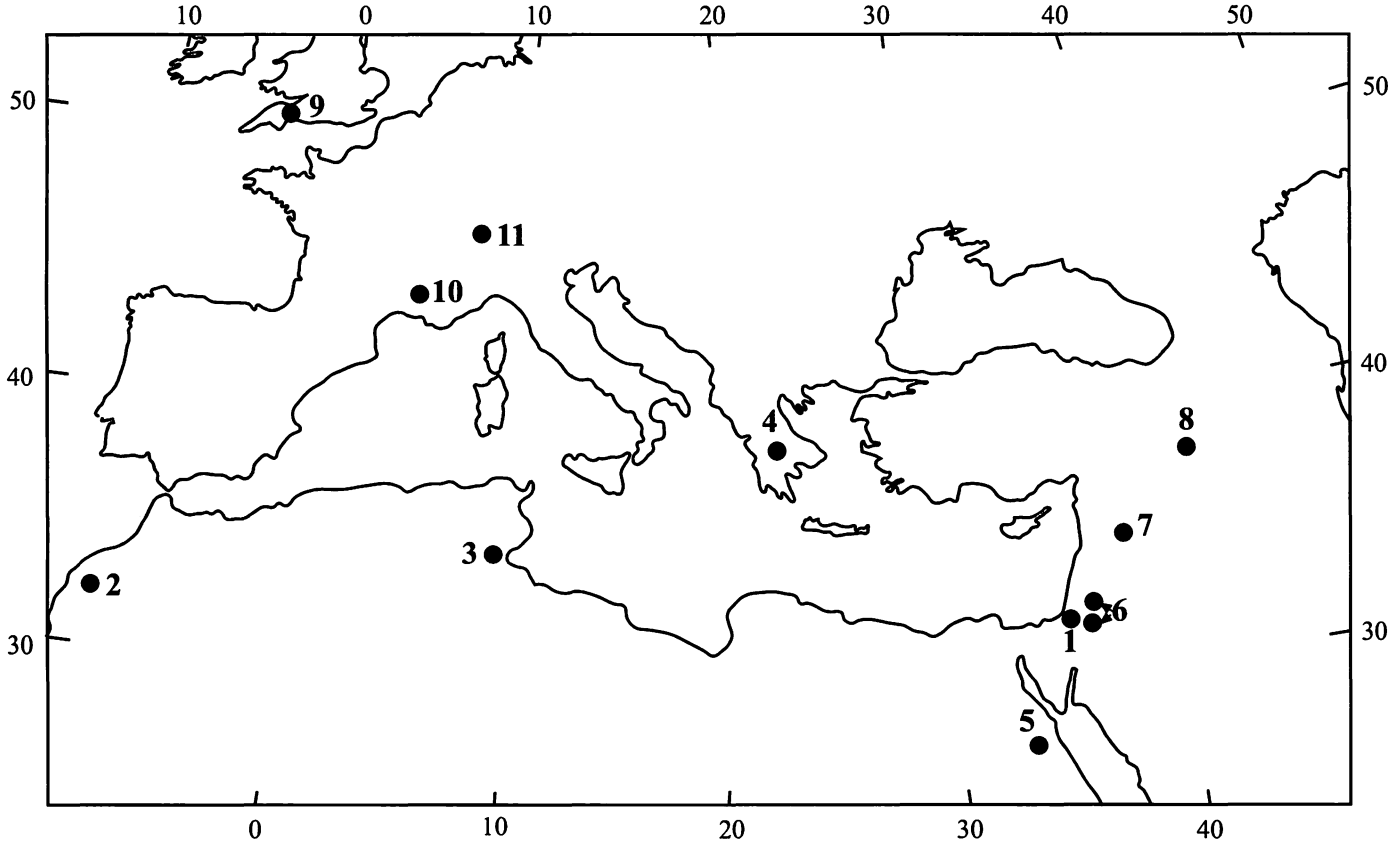

Fig. 2. Location of phosphate samples analyzed for $\delta^{44}Ca$, $^{143}Nd/^{144}Nd$, and $^{87}Sr/^{86}Sr$. 1 - Israel; 2 - Morocco; 3 - Tunisia; 4 - Greece; 5 - Egypt (Red Sea); 6 - Jordan; 7 - Syria; 8 - Turkey; 9 - South England; 10 - SE France (Vocontian Through); 11 - Helvetic Alps.

4.2. Elemental geochemistry

Samples were analyzed by two different procedures:

– bulk samples of stratigraphic intervals were analyzed after sintering the total sample with sodium peroxide (0.5 g sample was mixed with 2 g of Na_2O_2 then heated to 550° C for 30 min.), then the resulting sinter was dissolved in 25 ml 5*M* HCl and made up to 100 ml..

– Separated CFA fractions (samples in which the carbonate fraction was removed) designed for Sr, Nd, and Ca isotope analysis were dissolved in 1/3 HNO_3 and chemically analyzed. The chemical analysis of the separated (carbonate-free) CFA fractions was to ensure that the totality of carbonate was removed, to determine the concentrations of Sr, Mn and Fe, (indicators of weathering), the concentrations of Nd and Sm (the latter for calculation of εNd at initial time T), and the concentrations of U and REEs (the later to calculate various REE ratios also sensible to alteration – see below).

Measurement of major and minors elements is by ICP-AES (JY-48, Jobin Yvon) and trace elements and rare earth elements (REEs) by ICP-MS (Elan 6000, PE-SCIEX). Fluorine (F) contents of the phosphorite samples were determined by a potentiometric method, using a fluoride ion-selective electrode, following the method of Edmond (1969) (see Soudry and Nathan, 2001 for a detailed description of the analytical procedure).

Determination of the oxidation state of U (this was done in various phosphorite samples of the Negev) was performed after the separation of U(IV) following the method of Clarke and Altschuller (1958) (see also Soudry et al., 2002 for a complete description of the procedure).

All the wet chemical analyses were performed at the Israel Geological Survey.

4.3. XRD, FTIR and SEM

Powder X-ray diffraction was run on a Philips diffratometer (PW 3020) with a curved graphite monochromator (Cu radiation). The structural CO_2 in CFA (wt. %) was determined by the Gulbrandsen (1970) X-ray diffraction method, measuring the $\Delta 2\theta$ spacing between the (004) and (410) reflections and using a scan rate of 0.06 θ/min. The absolute accuracy of CO2 content by this technique is ± 15 wt. % while the precision is better than ± 5 %.

Fourier transform infrared (FTIR) spectroscopy was used for analysis of the CFA phase (this was done only on Negev samples). Two pressed pellets were prepared for each bulk phosphorite or separated CFA sample: a 'concentrated' pellet (5 mg sample in 150 mg KBr) and a 'regular' pellet (1mg sample in 150 mg KBr). The pellets were then heated to 150° C and repressed without grinding to expel adsorbed water and obtain better spectroscopic spectra.

Optical and scanning electron microscopy (SEM) together with energy dispersal spectrometry (EDS) were used to examine the ultrastructure and the micro-chemistry of the CFA samples. The microscopic analyses and XRD were performed at the Israel Geological Survey, and FTIR spectroscopy at the Open University (Ramat Aviv).

4.4. Isotopic geochemistry

4.4.1. Checking weathering

Prior to isotopic analysis we checked for possible weathering of the CFA samples from their structural CO_2 content, their Sr/P and Ca/P ratios, and from the $(La/Sm)_N$ and $(Sm/Yb)_N$ ratios of their REEs and the Ce/Ce* anomaly. Normalisation (N) was to the NASC composition (Gromet et al., 1984).

As our CFA are not exclusively skeletal apatites, we used a much higher $(La/Sm)_N$ threshold than that considered (0.3) by Reynard et al. (1999), and decided that $(La/Sm)_N$ lower than 1.0 as indicates possible weathering. Sm/Yb_N ratios above 3 were also considered as indicating alteration (cf. Lécuyer et al., 2004).

Ce (Ce/Ce*) anomaly is defined as $Ce_{anom} = Log\ 3Ce_N/(2La_N+Nd_N)$ (de Baar et al., 1985).

4.4.2. Sr and Nd isotope analytical procedure

The $^{87}Sr/^{86}Sr$ and $^{143}Nd/^{144}Nd$ isotopic ratios in CFA was measured at the University of Hawaii. 100 mg of the powdered decalcified CFA sample was processed with 5 mL of glacial acetic acid for partial dissolution of CFA and the acetic acid leachate was centrifuged, dried, then redissolved in ~ 500 µL of quartz-distilled 6*M* HCl, then taken to dryness and weighted. The Sr, Rb, and bulk REEs were separated using calibrated 2 N and 4N HCl as eluents through a Bio-Rad AG50W-X8 (100-200 mesh) ion-exchange resin in quartz microcolumns. The Sm and Nd were then separated from the REE fraction on quartz

columns following the methods of Mahoney et al. (1991) using α-HIBA (2-Hydroxyisobutyric acid) as eluent, and Bio-Rad AG50W-X8 (200-400 mesh) as ion exchange resin. After dissolution of the various separated dried fractions in 2*M* HCl, Sr was measured using W filament, and Rb, Sm, and Nd using Ta filament. Both Sr and Nd blanks at the time of analysis were less than 20 picograms. gr^{-1}. Sr and Nd isotopes were measured on a VG Sector Multi-collector Mass Spectrometer. The ratio $^{86}Sr/^{88}Sr = 0.1194$ was used for isotopic fractionation correction. The samples were run for at least 300 ratios or 15 blocks for each (Sr or Nd) element. Data were reported relative to $^{87}Sr/^{86}Sr = 0.710248 \pm 0.000018$ for the NBS 987 Sr standard, and relative to $^{143}Nd/^{144}Nd = 0.511847 \pm 0.000009$ for the La Jolla Nd standard.

The measured $^{143}Nd/^{144}Nd$ were then converted to:

$\varepsilon_{Nd(T)} = \{[(^{143}Nd/^{144}Nd)_{sample(T)} / (^{143}Nd/^{144}Nd)_{CHUR(T)}] - 1]\} \times 10^4$,

T = initial time of the samples; CHUR = Chondritic uniform reservoir. (*T*) was obtained either from Sr isotopic measurements (see below), and where these are lacking T was estimated from the stratigraphic positions of the CFA samples in the time scales of Gradstein et al. (1995) and Berggren et al. (1995).

The initial $^{143}Nd/^{144}Nd$ of the sample (at time T) and that of CHUR(*T*) were calculated as follows:

$(^{143}Nd/^{144}Nd)_{sample(T)} = (^{143}Nd/^{144}Nd)_{sample(today)} - {}^{147}Sm/^{144}Nd)_{sample(today)}.(\exp(\lambda_{Sm}T) - 1)]$.

$(^{143}Nd/^{144}Nd)_{CHUR(T)} = (^{143}Nd/^{144}Nd)_{CHUR(today)} - (^{147}Sm/^{144}Nd)_{CHUR(today)}.(\exp(\lambda_{Sm}T) - 1)]$.

(λ_{Sm}) is the rate of radioactive decay of ^{147}Sm to $^{143}Nd = 6.54 \times 10^{-12}.yr^{-1}$.

Common used values for CHUR (*today*) are: $^{143}Nd/^{144}Nd = 0.512638$; $^{147}Sm/^{144}Nd = 0.1967$ (Jacobsen and Wasserburg, 1980).

4.4.3. Ca isotope analysis

The $^{44}Ca/^{42}Ca$ ratio in CFA was measured at the Geological Survey of Israel. 20 mg of powdered decalcified CFA samples was dissolved in 2mL of 1.3*M* HCl, and a aliquot of 0.1-0.2 ml was put into a column (DOWEX 50W × 8 resin, 100-200 mesh) previously preconditioned by the same acid. Elution of Ca was made by 6*M* HCl. The solution was then dried and the precipitate dissolved in 8mL of 0.1*M* HNO_3. Ca isotopes were measured by using a multi-collector ICP-MS (Nu Instruments, Wrexham, UK). In contrast to TIMS (thermal-ionisation mass spectrometer), ^{40}Ca cannot be measured using this new technique

because it is overlapped by ^{40}Ar. Therefore, we used ^{42}Ca and ^{44}Ca isotopes which were measured simultaneously as described in Halicz et al. (1999), using the standard-sample-standard bracketing technique. NIST SRM 915a was used as standard for calculation of $\delta^{44}Ca$. A final $^{44}Ca/^{42}Ca$ ratio comprises the acquisition of 3 data runs, each of 3 blocks of 10 ratio measurements (i.e., 90 ratio measurements). The long term external precision of $\delta^{44}Ca$ (2σ) was 0.1‰.

4.4.4. $C_{(org)}$ and $N_{(org)}$ isotope analysis

Because of problems of reproducibility of $\delta^{15}N$ results when online N_2 and CO_2 extraction technique was used, two different procedures were used for the analysis of $\delta^{13}C$ and $\delta^{15}N$ (these analyses were performed at the University of Hawaii). Both measurements were made on the separated OM-rich IR fraction of the samples (after 1/HNO_3 attack).

a) To determine $\delta^{13}C$, an automated online combustion system was used – a Carlo Erba NC2500 Elemental Analyzer interfaced via a Finnigan ConFloII to a Finnigan DelaS mass spectrometer. Samples and standards were weighted out using a 6-place microbalance and loaded into the EA autosampler, then the sample was flash-combusted (1800° C) amidst a carrier flow of He. The resultant gases were subsequently passed through the oxidation tube maintained at 1150° C, through a reduction column and in a ¼" × 2 m gas chromatographic column where CO_2 is separated. The separated CO_2 was then analyzed in a Finnigan mass spectrometer. External precision for elemental C composition is 2 % or better, and 0.12 ‰ or better for $^{13}C/^{12}C$ values (versus VDP).

b) To determine $\delta^{15}N$ Dumas Combustion offline was used. Samples were weighted out (target 10-20 μmole of N_2) into a 9 mm vycor tube, adding approximately 1 gr of CuO wire and an appropriate amount of Cu wire, and attaching the tube to a vacuum line to remove atmosphere. Once flame-sealed, the tubes were put in a small furnace, heated to 850° C for 6 hrs and slowly cooled to room temperature. Then, the tubes were attached to a vacuum distillation line where N_2 was isolated. Collected N_2 gas was then analyzed via dual inlet in a Finnigan MAT 252 IRMS. External precision for elemental N composition was 1% or better, and 0.11‰ for $^{15}N/^{14}N$ values (versus air).

4.5. $P_{(org)}$ analysis

The bulk phosphorite samples were dissolved in HCl 1:3 to dissolve all inorganic carbonate and phosphate. To 0.4 gr of the insoluble residue was added 10 mL. concentrate HNO_3, left overnight and then heated to 170° C. Some new HNO_3 was added each 8 hrs until the solution was clear (all together ca 40 hrs). Then 10 mL of concentrate $HClO_4$ was added until white solution occur (around 36 hrs). The solution was then transferred to 50 or 100 mL volumetric flasks, and P_{org} spectrometrically measured in the solution using acidic Malachite Green reagent (650 nm, 120 mn). $P_{(org)}$ analysis was done in the Faculty of Agriculture, the Hebrew University, Rehovot (Dr. Moshe Shenkar Laboratory). Sample preparation was done at the Geological Survey of Israel.

4.6. Quantification of P, $C_{(org)}$, and Ca accumulation rates

P , $C_{(org)}$ and Ca accumulation rates and sedimentation rates were quantified using the time scales of Gradstein et al. (1995) for the Mesozoic and Berggren et al. (1995) for the Cenozoic, and on the basis of Negev chronostratigraphic data (Lewy, 2001; Gvirtzman 2004).

Thickness, P and Ca concentrations over the Albian-Eocene of the Negev were collected from various literature sources as well as from sections analyzed in this study (see results of elemental geochemistry). In total, hundreds of sedimentary sections from tens of literature sources were compiled. Data on $C_{(org)}$ contents (upper Coniacian-lower-middle Eocene) are from this study (Table 8).

We used 30.97, 12.01, and 40.01 as atomic weights of P, C and Ca (respectively), and 1.2 g/cm^3 (see also Filippelli et al., 1994) as an estimate of precompaction density (d) of the sedimentary assemblages in the succession.

P and $C_{(org)}$ rates (Φ) are expressed in μmole cm^{-2} kyr^{-1} and calculated as follows:

$$\Phi = \frac{(\text{wt }\%)\ 10^{-2} \times d \times s}{aw} \times 10^6$$

where wt% is the weight content of P or $C_{(org)}$, s the post-compaction sedimentation rate over the quantified stratigraphic interval (cm/kyr), and aw the atomic weight.

Ca accumulation rates are expressed as in μmole cm^{-2} yr^{-1} and calculated in the same way.

5. Results and Discussion

5.1. Elemental geochemistry

The chemical and mineralogical composition of the various stratigraphic intervals along the Cretaceous covering the time of Tethyan phosphogenesis in the Negev are included in previous progress reports and in published articles.

The composition of the Menuha Fm. (upper Coniacian-upper Santonian) is presented in Soudry et al. (2004); the Phosphatic-Carbonate and Porcelanite units (lower and middle part of the Phosphate Mbr., upper Campanian) in Soudry et al. (2001); the Phosphorite unit (upper part of the Phosphate Mbr., uppermost Campanian) in Soudry et al. (2004); the Ghareb Fm (Oil Shale Mbr. and Marly Mbr., Maastrichtian), the Taqiye Fm. (Paleocene) and the Paran Fm. (Eocene) in Soudry et al. (2002).

Table 2 shows the chemical composition of the separated (carbonate-free) CFA samples analyzed for Sr, Nd and Ca isotope compositions.

5.2. Sr isotopic results

The results of Sr isotopic analyses in CFA samples are presented in Tables 3 and 4. Are also included the nature of the CFA phase in the analyzed samples, the structural CO_2 values (wt%), the Sr/P and Ca/P ratios, and the $(La/Sm)_N$, $(Sm/Yb)_N$ ratios and the Ce/Ce* anomaly in their REEs. The numerical Sr ages of the samples were calculated from the statistical LOWESS fit to the marine $^{87}Sr/^{86}Sr$ (Version 3, updated 2000) of McArthur et al. (2001).

Of the 94 samples analyzed, only 34 yielded Sr isotopic compositions matching their stratigraphic position and the secular marine Sr isotope curve (McArthur et al., 2001). The others produced $^{87}Sr/^{86}Sr$ ratios much higher than those expected from their stratigraphy (10-20 Ma younger). The bulk of the samples that yielded consistent Sr isotopic compositions and numerical ages are from the Campanian interval. Part of the Maastrichtian samples and a few Eocene samples also gave consistent results. The causes for the discrepancy between the measured Sr and biostratigraphic ages of part of the samples are not well understood at this stage. Different possibilities could be envisaged:

1) Part of the CFA samples might be weathered. Weathering and extensive diagenesis are known to alter the $^{87}Sr/^{86}Sr$ ratio (e.g., McArthur, 1994). However, no clear relation is seen when examining the composition of the samples and their $^{87}Sr/^{86}Sr$ values

(Table 3). In fact, judging from the structural CO_2 contents (mostly between 4 and 6 wt%), the Ca/P, Sr/P and the $(La/Sm)_N$ ratios (the later consistently > 1.0), it seems that the state of preservation of the major part of the samples is quite fair. Moreover, samples with high Fe and Mn concentrations (supposed to indicate alteration — McArthur, 1994) often yielded $^{87}Sr/^{86}Sr$ values perfectly matching their stratigraphic position, while others with low Fe and Mn contents in contrary produced inconsistent values (higher $^{87}Sr/^{86}Sr$ ratios than expected from their stratigraphy).

2) Retention of the initial $^{87}Sr/^{86}Sr$ is affected by the nature of the CFA phase. In North Carolina phosphorites (Miocene) Riggs et al. (1997) found that skeletal apatite grains generally show higher Sr isotopic ratios than co-occurring phosphate pellets. Recently, Martin and Scher (2004) also found in DSDP sediments (Eocene to Pleistocene) that Sr in fossil fish is consistently altered in the direction of the Sr isotope values of the porefluids, suggesting continual Sr exchange between the fish remain and porewaters during diagenesis and burial. No separate analysis of skeletal and pelletal apatite has been carried in this study and therefore we cannot check the validity of this effect. Nevertheless, a few $^{87}Sr/^{86}Sr$ measurements recently carried out in separated fractions of co-occurring phosphate pellets and fish remains from the Campanian-Negev phosphorites (Gofin, in prep.) showed no difference in the values yielded by the two fractions. Moreover, such an effect, if it was determinant, cannot nevertheless explain the very large age gap (10-20 Ma) in part of our samples, between the Sr ages (as calculated from the Sr isotopic compositions of the samples) and the chronostratigraphic ages. In North Carolina phosphorites this effect contributed to a lowering of the Sr age of fish debris, by comparison to co-occurring phosphate pellets, by only ~ 1 Ma.

3. Contaminants: Contamination with Sr from associated clay minerals during acid attack of the CFA fraction could alter the original $^{87}Sr/^{86}Sr$ of the sample and increase the values (Bailey et al., 2000). We believe however that this effect was negligible in our samples as we used glacial acetic acid (weak acid) for CFA dissolution.

An alternative explanation for the age discrepancies in part of the phosphate samples could be diagenetic Sr exchange (Clauer et al., 1975) between porewaters and some clay fraction (high $^{87}Sr/^{86}Sr$) at the time of CFA precipitation. An important control then would be the rate of sedimentation, this determining how long the growing CFA would be kept near the sediment-water interface, at contact with porewaters exchanging Sr

with the deposited clays. This could perhaps explain why consistent Sr isotopic compositions are produced by most of the Campanian phosphorites of the Negev, while inconsistent values are yielded by most of the other phosphate occurrences above and below in the analyzed section. The Negev phosphorites are mainly granular, generated in conditions of more or less continuous sedimentation; by contrast, most of the other CFAs are nodules formed at sediment discontinuities where the diagenetic impact of exogenic Sr (because of a very slow burial of the CFA phase) was probably more intensive. Detailed Sr isotopic measurements recently made across various phosphate basins of the Negev (Gofin, in prep.) seem to provide some support to the importance of such a diagenetic impact.

5.3. Nd isotopic results.

The results of the measured and initial $^{143}Nd/^{144}Nd$ values and the $\varepsilon_{Nd(T)}$ values over the Hauterivian-Eocene are presented in Table 4. Table 5 shows the $\varepsilon_{Nd(T)}$ results in CFA for various Campanian-Eocene stratigraphic intervals in the Negev, Egypt (Red Sea Coast) and Moroccan (Ganntour) phosphorites. Figure 3 shows the scatter plots of $\varepsilon_{Nd(T)}$ compared to $^{87}Sr/^{86}Sr$ over the Hauterivian-Eocene. In figure 4 are compared the evolutions of $\varepsilon_{Nd(T)}$ in the Negev and the Red Sea (Egypt) phosphorites in the Campanian-Maastrichtian (83-67 Ma), and in figure 5 the $\varepsilon_{Nd(T)}$ evolution in the Negev and the Ganntour (Morocco) phosphorites in the Maastrichtian-Eocene (67-46 Ma).

5.4. Ca isotopic results

The results of the $^{44}Ca/^{42}Ca$ ratios are presented in Table 4. Figure 6 shows the scatter plots of $\delta^{44}Ca$ compared to $^{87}Sr/^{86}Sr$ over the Hauterivian-Eocene; and figure 7 the scatter plots of $\delta^{44}Ca$ compared to $\varepsilon_{Nd(T)}$ in the same interval

5.5. P, Ca and $C_{(org)}$ accumulation rates and sedimentation rates

The rates P and Ca accumulation in the Albian-Eocene of the Negev.are presented in Table 6 ; those of $C_{(org)}$ in the Upper Coniacian-Middle Eocene of the Negev are shown in Table 9.

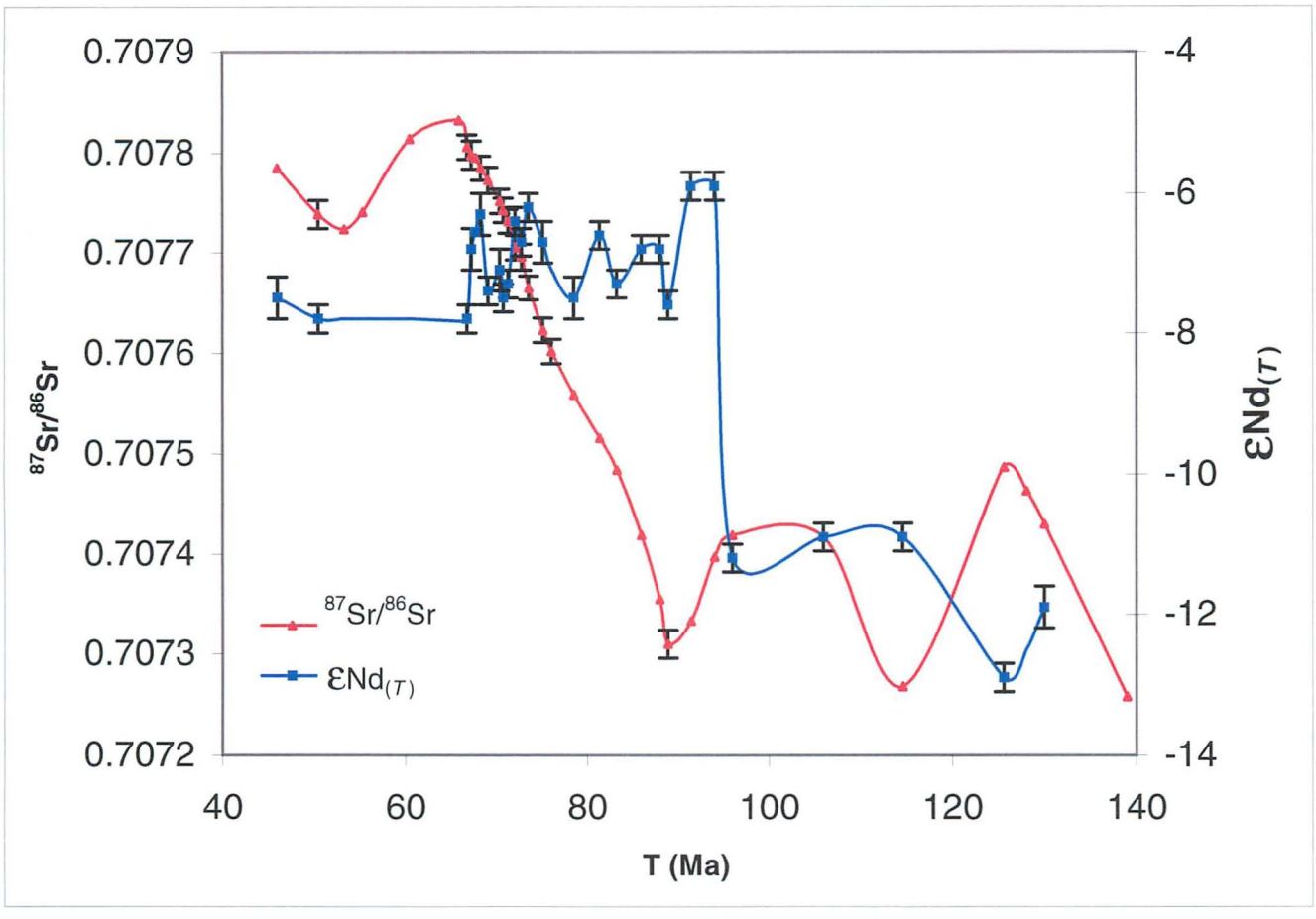

Fig. 3. Scatter plots of $\varepsilon_{Nd(T)}$ and $^{87}Sr/^{86}Sr$ versus time (T) over the Hauterivian-Eocene. Points on the Sr isotope curve (without error bars) are points extracted from the secular isotope curve (McArthur et al., 2001)

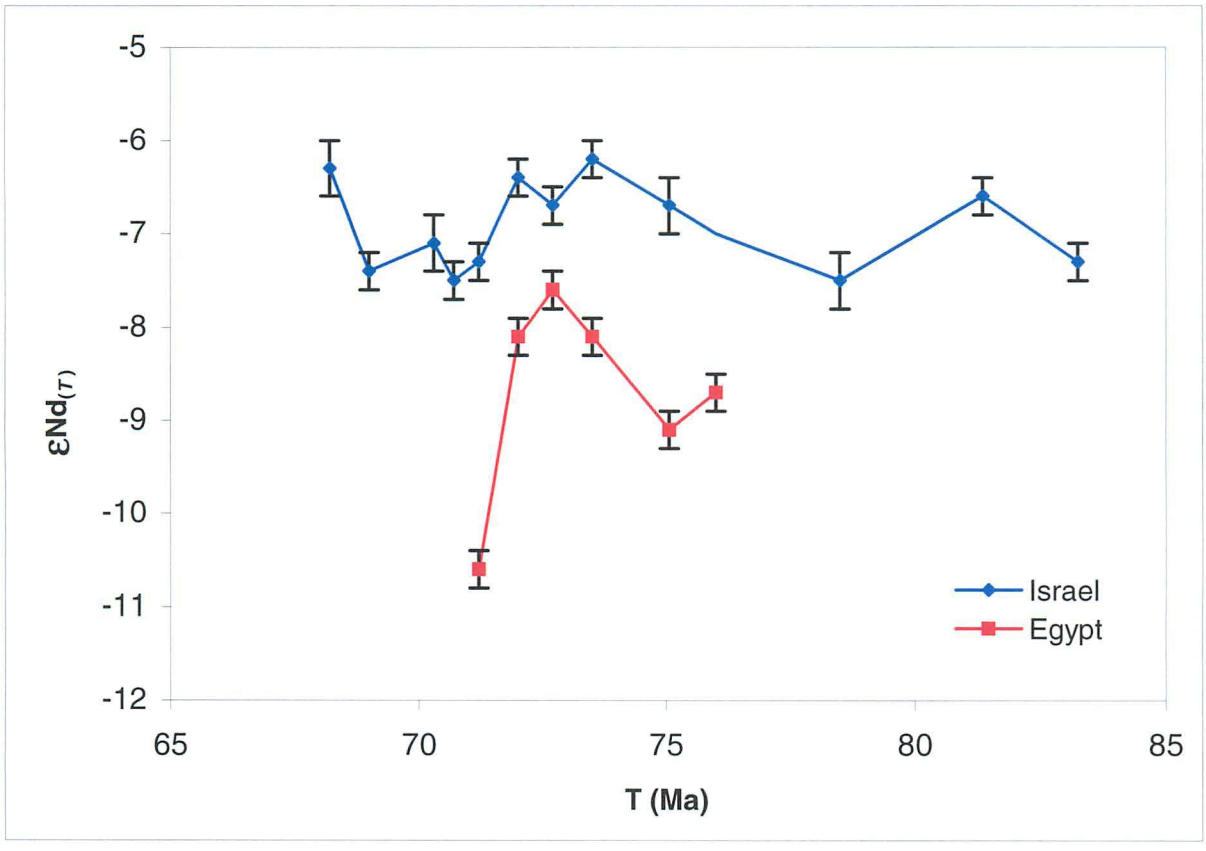

Fig. 4. Comparison of $\varepsilon_{Nd(T)}$ in phosphorites of the Negev and Egypt (Red Sea) in the Campanian-Maastrichtian interval.

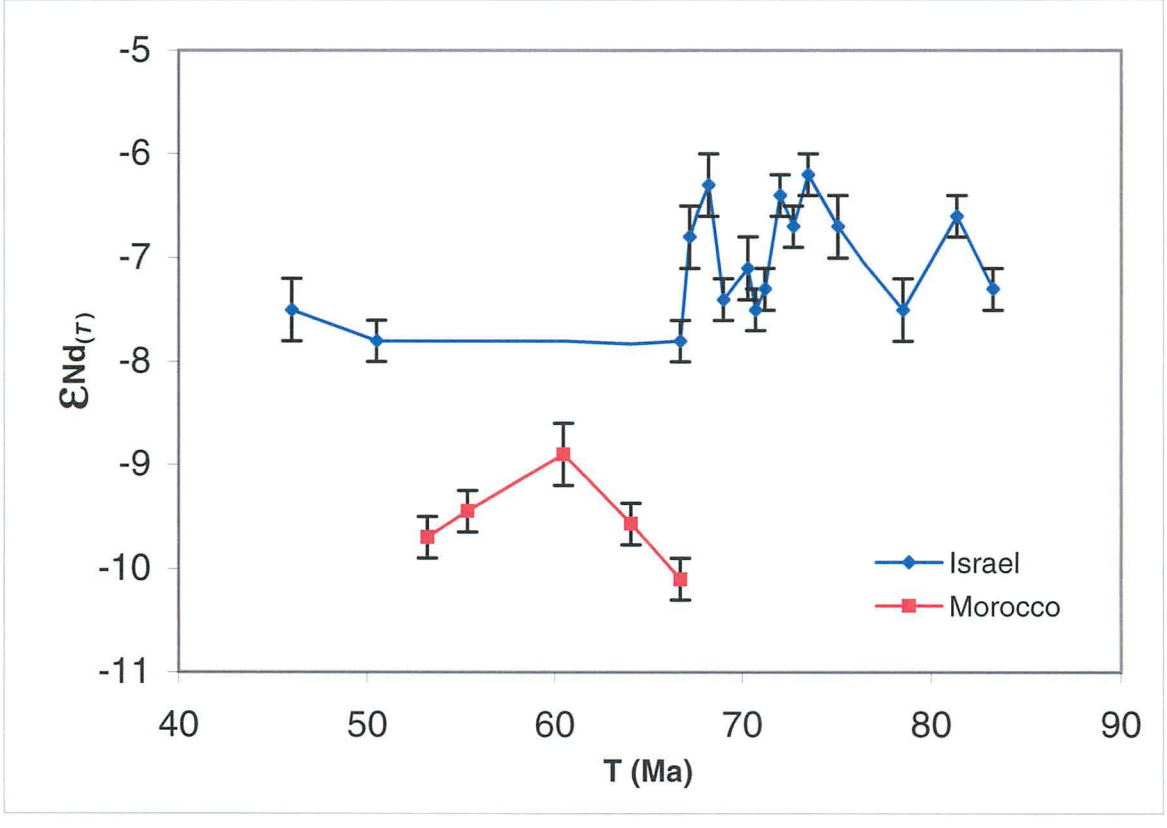

Fig. 5. Comparison of $\varepsilon_{Nd(T)}$ in phosphorites of the Negev and Morocco (Ganntour) in the Maastrichtian-Eocene.

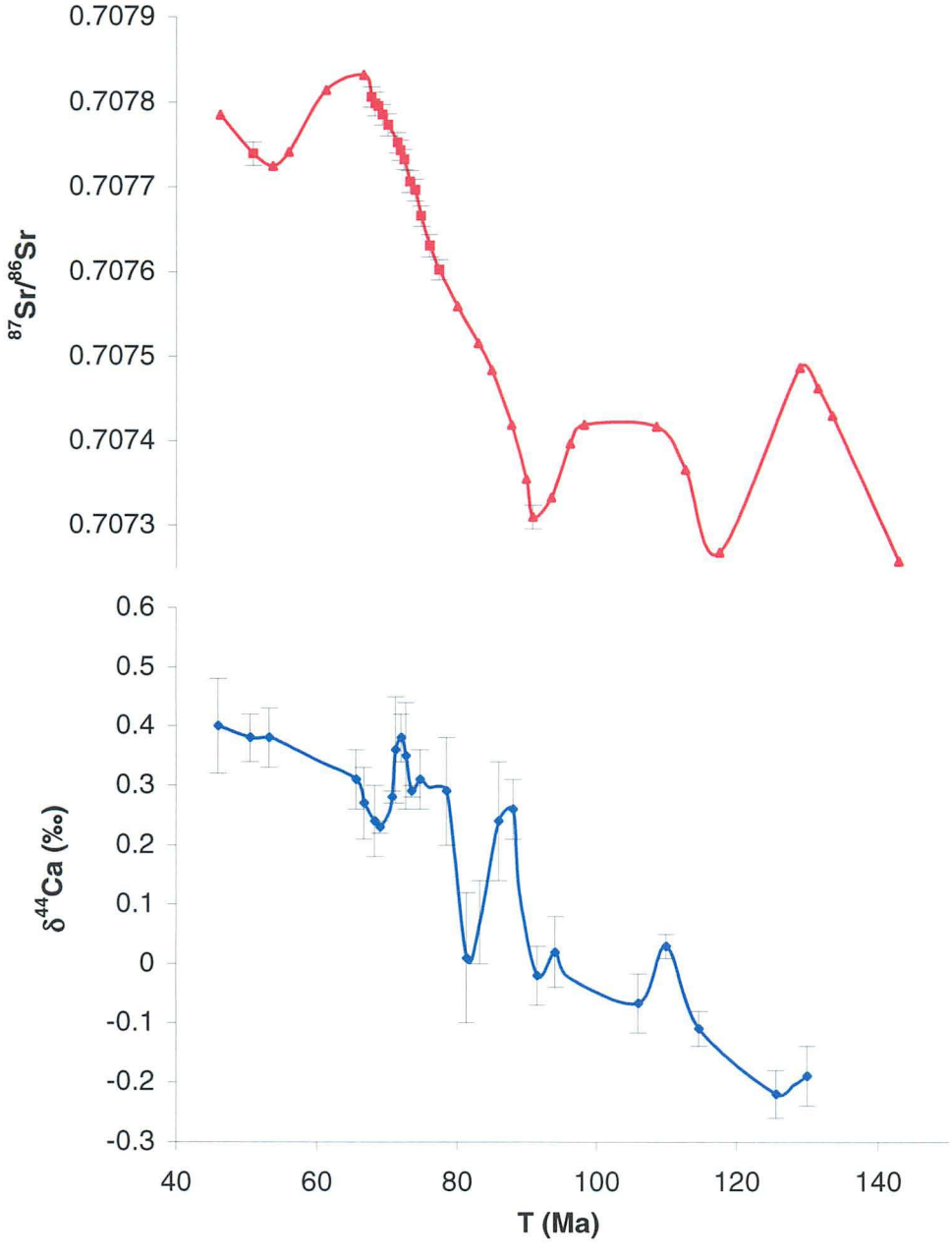

Fig. 6. Scatter plots of $^{87}Sr/^{86}Sr$ and $\delta^{44}Ca$ versus time (T) over the Hauterivian-Eocene. Points on the Sr isotope curve (without error bars) are points extracted from the secular isotope curve (McArthur et al., 2001)

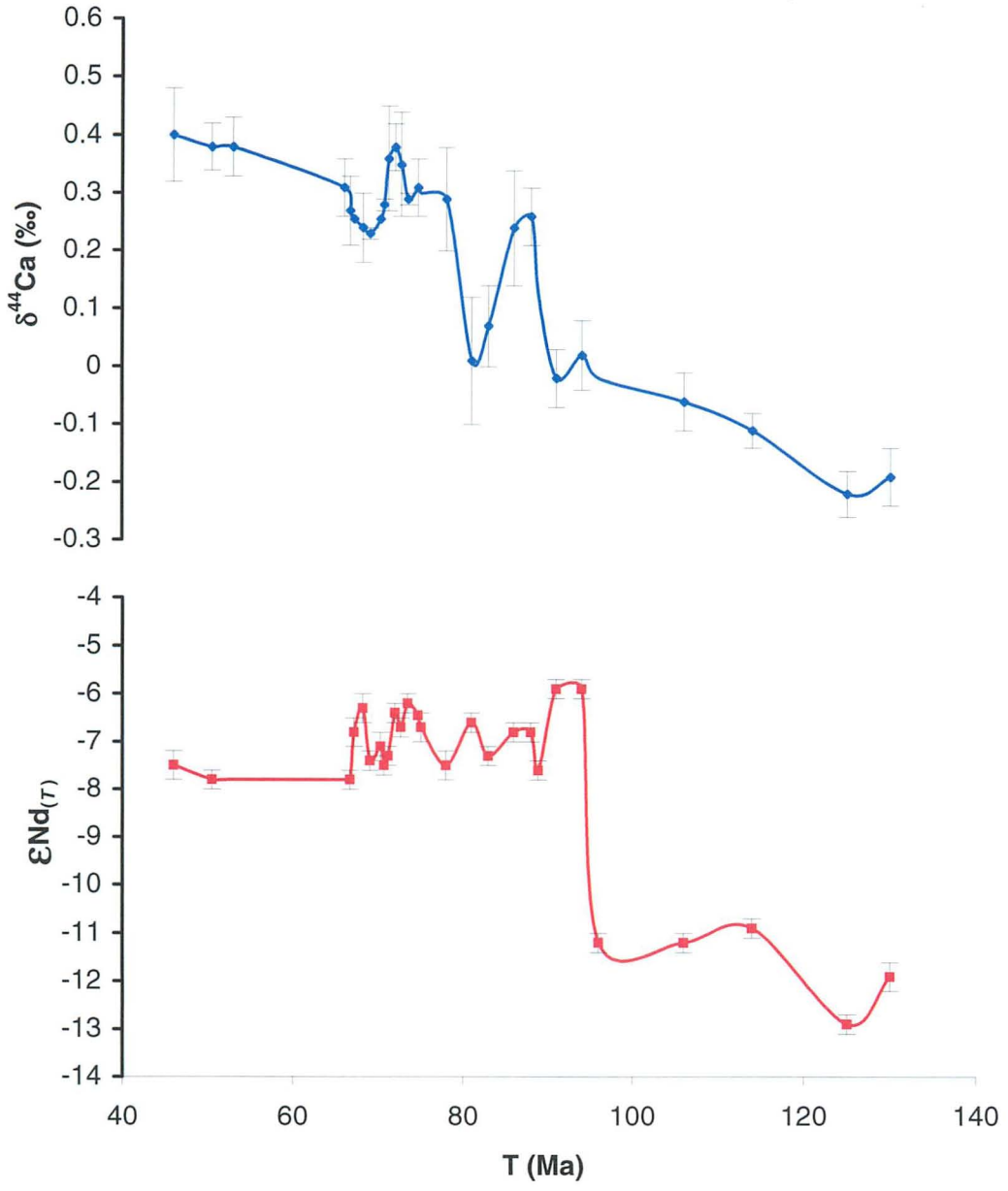

Fig. 7. Temporal evolution of $\varepsilon Nd_{(T)}$ compared to $\delta^{44}Ca$ over the Hauterivian-Eocene.

Figure 8 shows P accumulation rates compared to $\varepsilon_{Nd(T)}$ distribution in the Hauterivian-Eocene; figure 9 – P accumulation rates compared to $\delta^{44}Ca$ distribution; and figure 10 – P accumulation rates compared to $^{87}Sr/^{86}Sr$.

Figure 11 shows the rates of P and Ca accumulation rates in the Albian-Eocene, and and figure 12, the rates of P accumulation compared with the rates of bulk sedimentation. Figure 13 shows the temporal evolution of $\delta^{44}Ca$, $\varepsilon_{Nd(T)}$, rates of P and Ca accumulation, and rates of bulk sedimentation in the Hauterivian-Eocene interval.

5.6. TOC, $C:P_{(org)}$, $\delta^{13}C_{(org)}$ and $\delta^{15}N_{(org)}$ results

Table 7 shows the results of TOC (wt%) in the upper Coniacian-Eocene succession of the Negev and in the Campanian phosphate section of Egypt (Red Sea), as well as the $\delta^{13}C$, $\delta^{15}N$, and C:N atomic values of the separated organic fraction.

Table 8 shows the $C:P_{(org)}$, in part of the samples analyzed for $C:N_{(org)}$, and for $\delta^{13}C$ and $\delta^{15}N$. Figure 14 shows the evolution of TOC, $C:N_{(org)}$, $\delta^{13}C_{(org)}$, $\delta^{15}N_{(org)}$, rates of P accumulation and bulk sedimentation along the upper Coniacian-Eocene of the Negev; and figure 15, the evolution of $C:P_{(org)}$, compared to the rates of P accumulation rates and bulk sedimentation in the same interval.

6. Interpretation of the results and discussion

The results of this study allow, when combined together, to better constrain the development of phosphogenesis in south Tethys margins during the Cretaceous-Eocene. Several points emerge from the various data (figure 11, table 4): 1) A similar trend exists in the distribution of $\delta^{44}Ca$ and $\varepsilon_{Nd(T)}$; 2) $\delta^{44}Ca$ and $\varepsilon_{Nd(T)}$ steeply rise after the Cenomanian-Turonian, reaching some of their highest values in the upper Campanian, 3) distinct $\varepsilon_{Nd(T)}$ are shown by the phosphorites of the Negev and Egypt during the Canpanian, and in the phosphorites of the Negev and N. Africa during the Maastrichtian-Eocene; and 4) the $\delta^{44}Ca$ and $\varepsilon_{Nd(T)}$ peaks during the upper Campanian coincide in the Negev with a peak in rates of P accumulation and a low rates of Ca accumulation and bulk sedimentation. In addition, highly negative $\delta^{13}C_{(org)}$ values (as low as -31‰) and high $C:P_{(org)}$ ratios (Fig. 15) are recorded during the Campanian-lower Maastrichtian.

6.1 Temporal variations of Nd isotopes

The sharp rise of $\varepsilon_{Nd(T)}$ from continental crust-like values in the Hauterivian-lower Cenomanian ($\varepsilon_{Nd(T)}$ = -12.8 to –11.2; n= 11) to Pacific-like seawater values in the upper Cenomanian-Eocene ($\varepsilon_{Nd(T)}$ = -7.8 to –5.9; n = 61), suggest major changes in ocean circulation and sediment deposition between these two periods. Following the global sea regression at the latest Jurassic, much of Europe, the Middle East and the Arabian Peninsula experienced intensive continental weathering as a result of wide exposure of land. In Europe, this regressive event is represented by the Purbecko-Wealdian facies formed by brackish-deltaic sediments and fluvio-lacustrine clastics (Tyson and Funnell, 1987). In the northwest margins of the Arabian craton (Middle east and Arabian Peninsula) this event is represented by widespread terrigenous sediments (Nubian sandstones). The early and mid-Cretaceous was also a warm period (Masse et al., 1993; Barnes, 1999) that enhanced chemical weathering of exposed landmasses (Föllmi et al., 1994). The increased riverine runoff probably caused large input of continental Nd [$\varepsilon_{Nd(0)} \approx$ - 14; e.g., Piepgras and Wasserburg, 1987; Keto and Jacobsen, 1988; Spivack and Wasserburg, 1988) into the Tethys basin, explaining the very low (crust-like) $\varepsilon_{Nd(T)}$ values measured in the Early Cretaceous. In addition, the nearly closure of the Caribbean threshold at those times and shallow blocks in central Tethys (Masse et al., 1993; Hay, 1995) probably impeded marine circulation in the Tethys basin (see also de Boer, 1986) and water exchange with the Pacific.

By contrast, the middle and upper Cretaceous was a time of intense midplate volcanism and crust production. Between 120 and 80 Ma, Earth's oceanic crust formation increased by 50 to 75%, most of it in the Pacific basin (Larson, 1991). A direct consequence would have been be increased injection of radiogenic Nd from hydrothermal activity [$\varepsilon_{Nd(0)}$ from ~ 0 to + 10; Shaw and Wasserburg, 1985; Amakawa et al., 2004) in Pacific water. Many suggested that these mid-ocean ridge volumetric changes induced the Late Cretaceous sea transgression. A thermally induced uplift of the Pacific lithospheric plate linked to mid-plate Cretaceous volcanism was also suggested (Schlanger et al., 1981) as proximal cause of the Cretaceous transgression. The rise in sea level (up to + 250 m; Haq et al., 1977) caused by the Pacific volcanism would have then led to increased incursion of

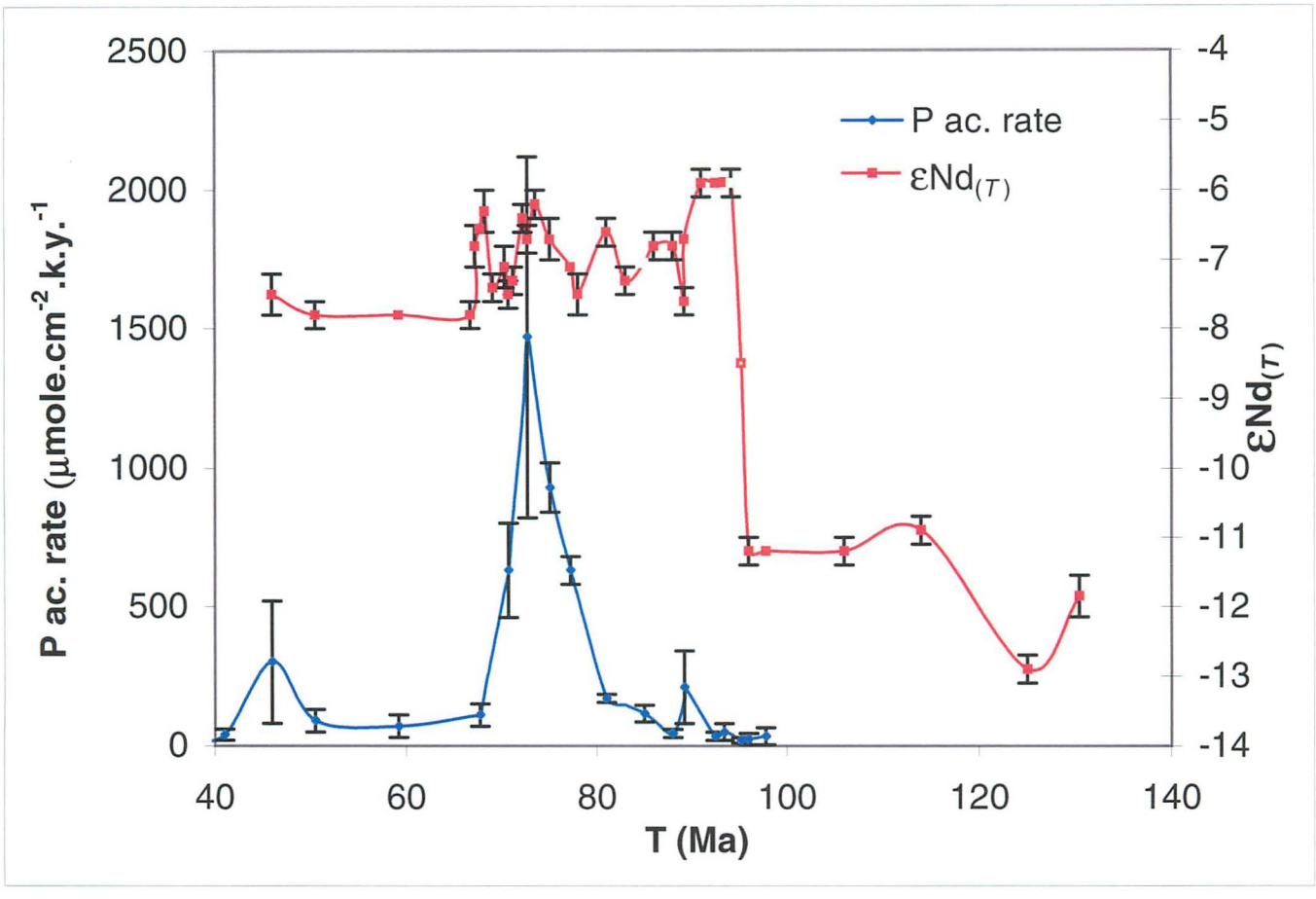

Fig. 8. Temporal evolution of P accumulation rate and $\varepsilon_{Nd(T)}$ over the Hauterivian-Eocene.

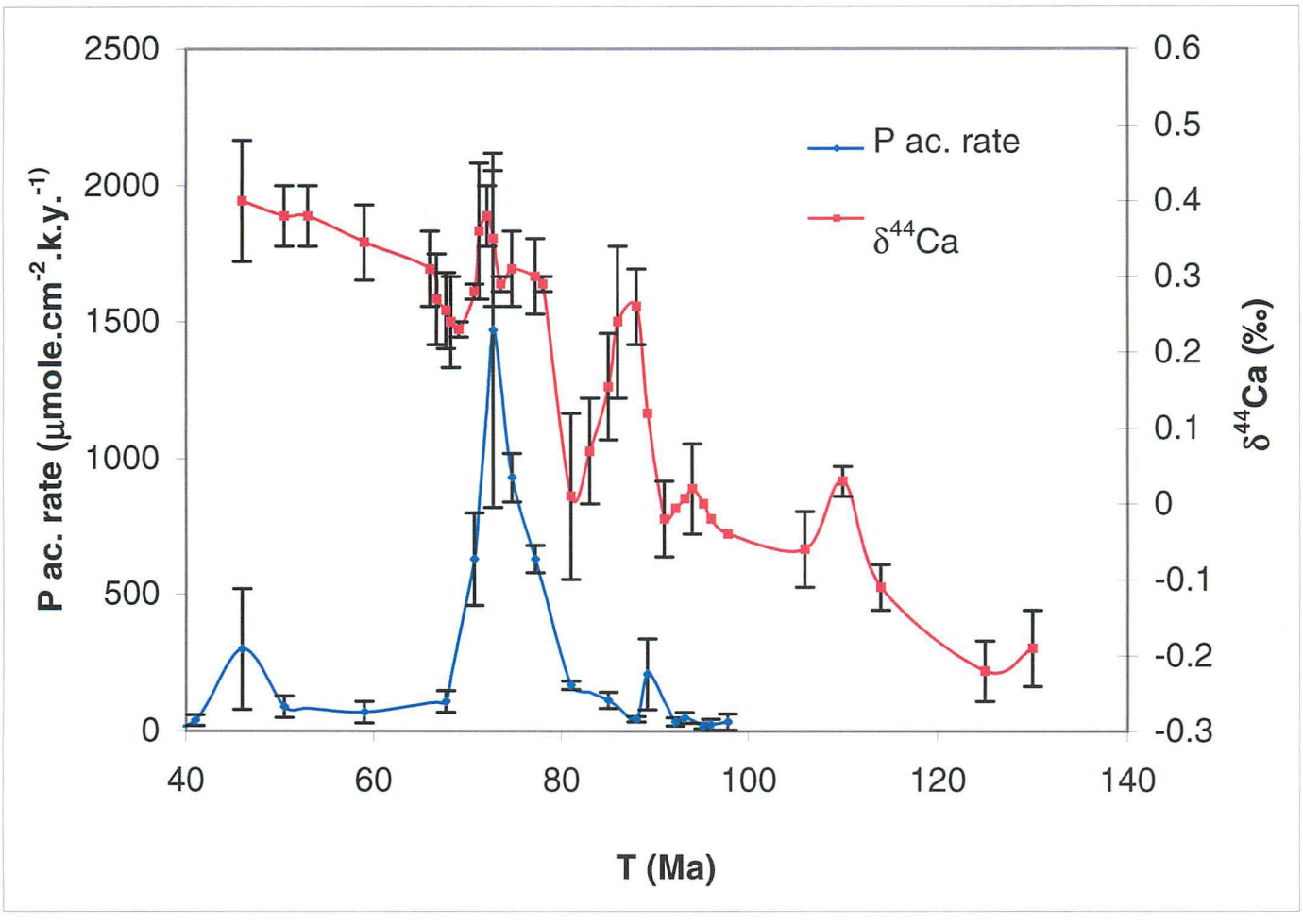

Fig. 9. Temporal evolution of P accumulation rate and $\delta^{44}Ca$ over the Hauterivian-Eocene.

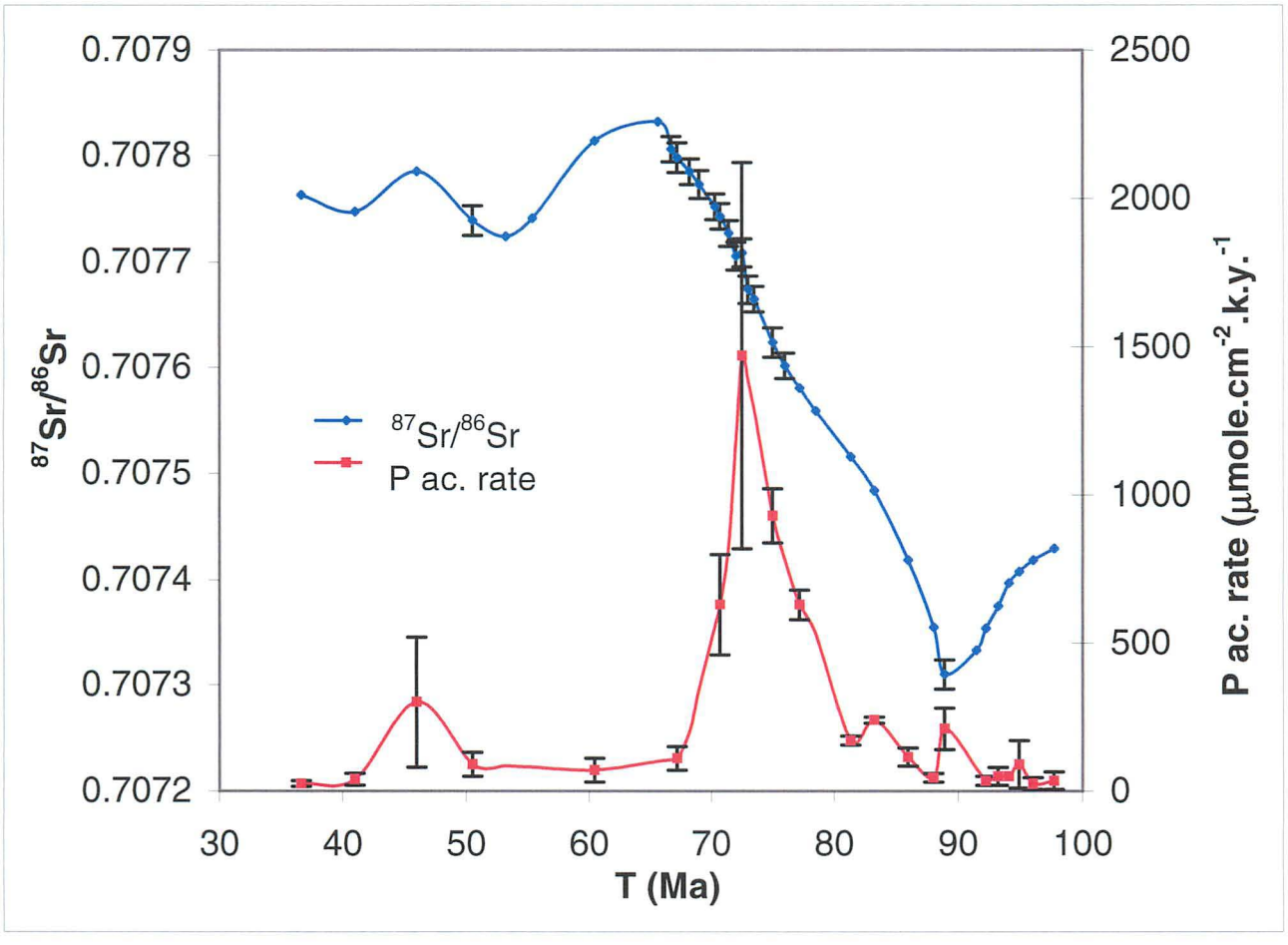

Fig. 10. Temporal evolution of $^{87}Sr/^{86}Sr$ and P accumulation rates over the Albian-Eocene section o the Negev.Points on the Sr isotope curve (without error bars) were extracted from the secular isotop curve (McArthur et al., 2001).

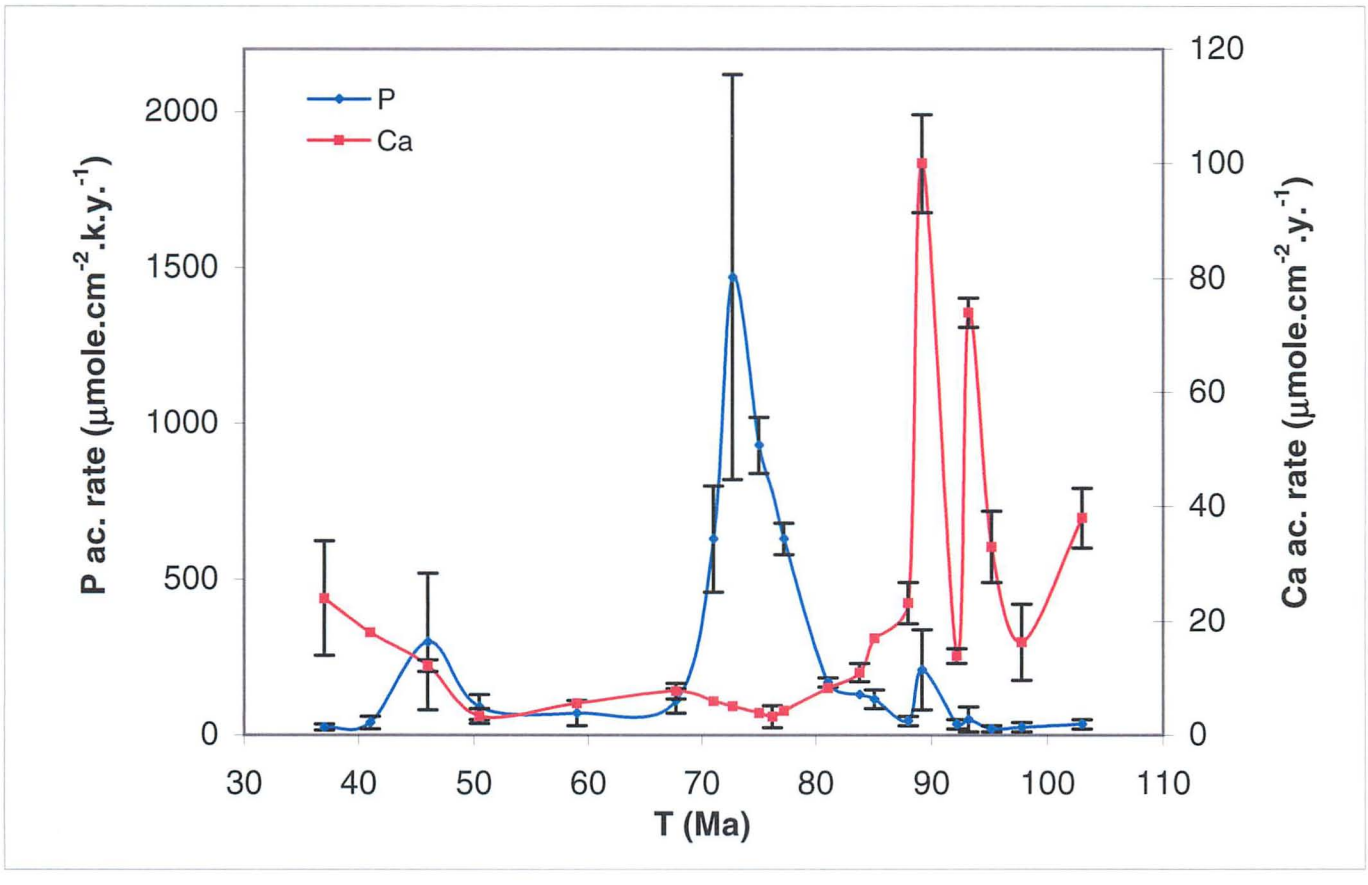

Fig. 11. Temporal evolution of P accumulation rate compared to Ca accumulation rate over the Albian-Eocene of the Negev.

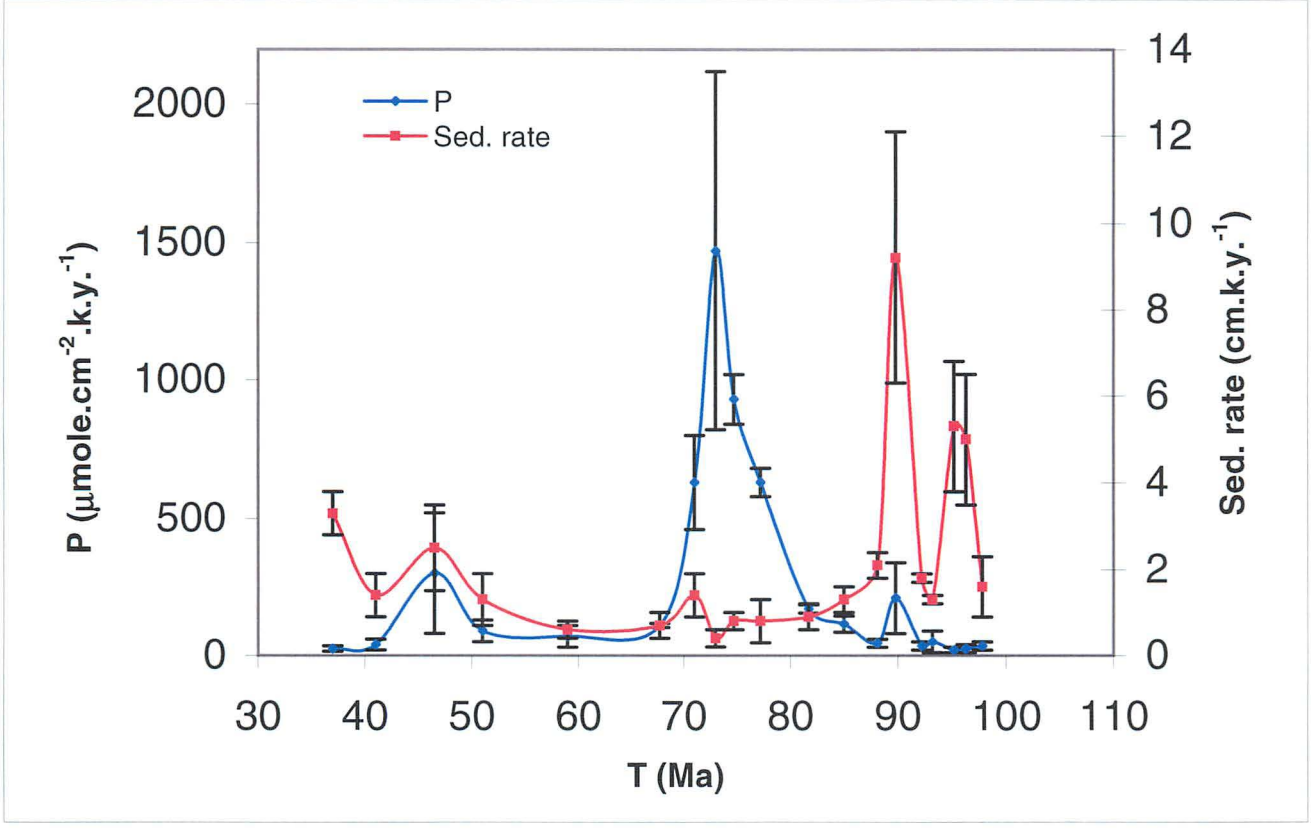

Fig. 12. Temporal evolution of P accumulation rate compared to the rate of bulk sedimentation over the Albian-Eocene.

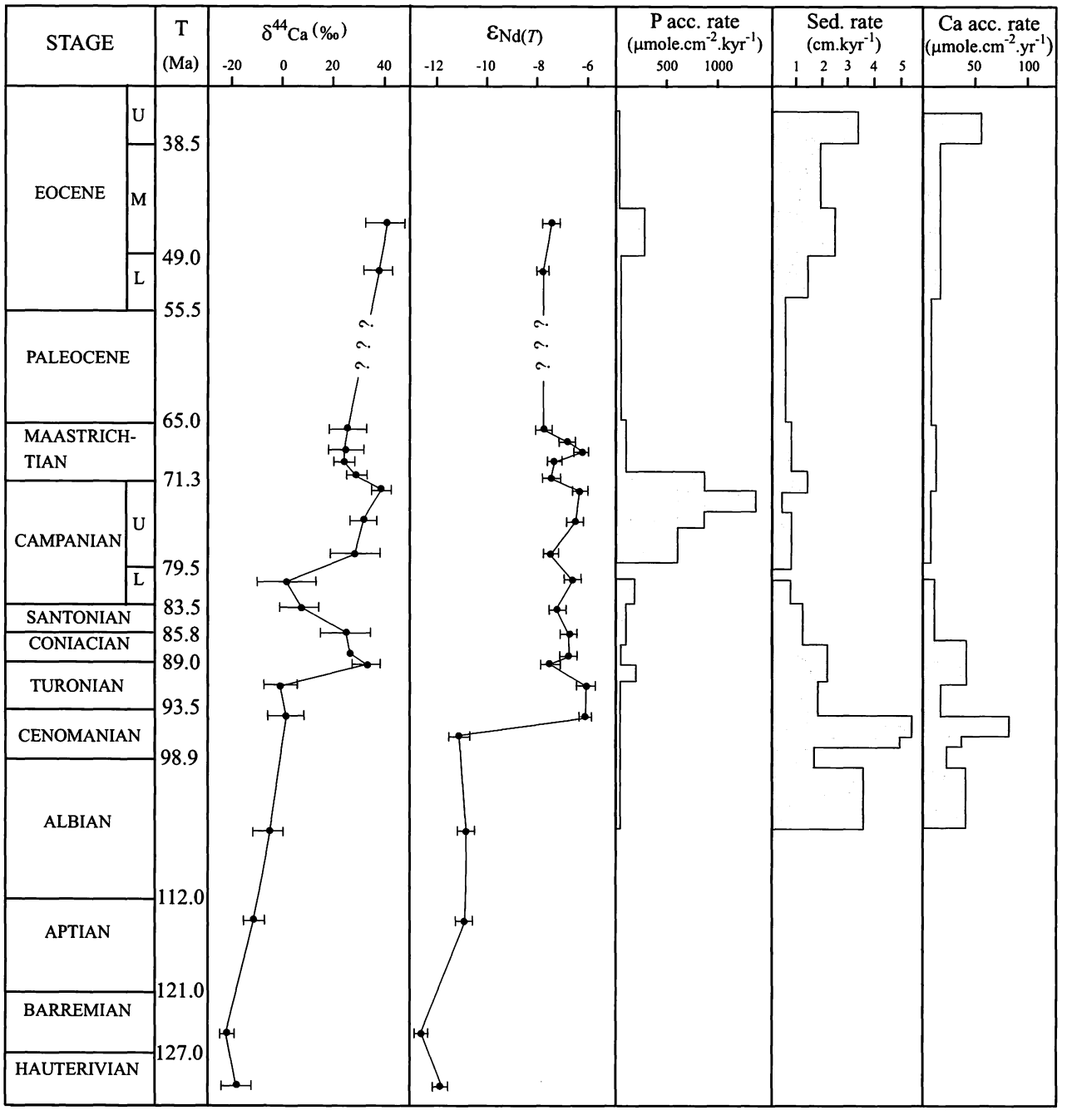

Fig. 13. Temporal evolution of $\delta^{44}Ca$, $\varepsilon Nd_{(T)}$, P accumulation rates, sedimentation rates, and Ca accumulation rates over the Hauterivian-Eocene.

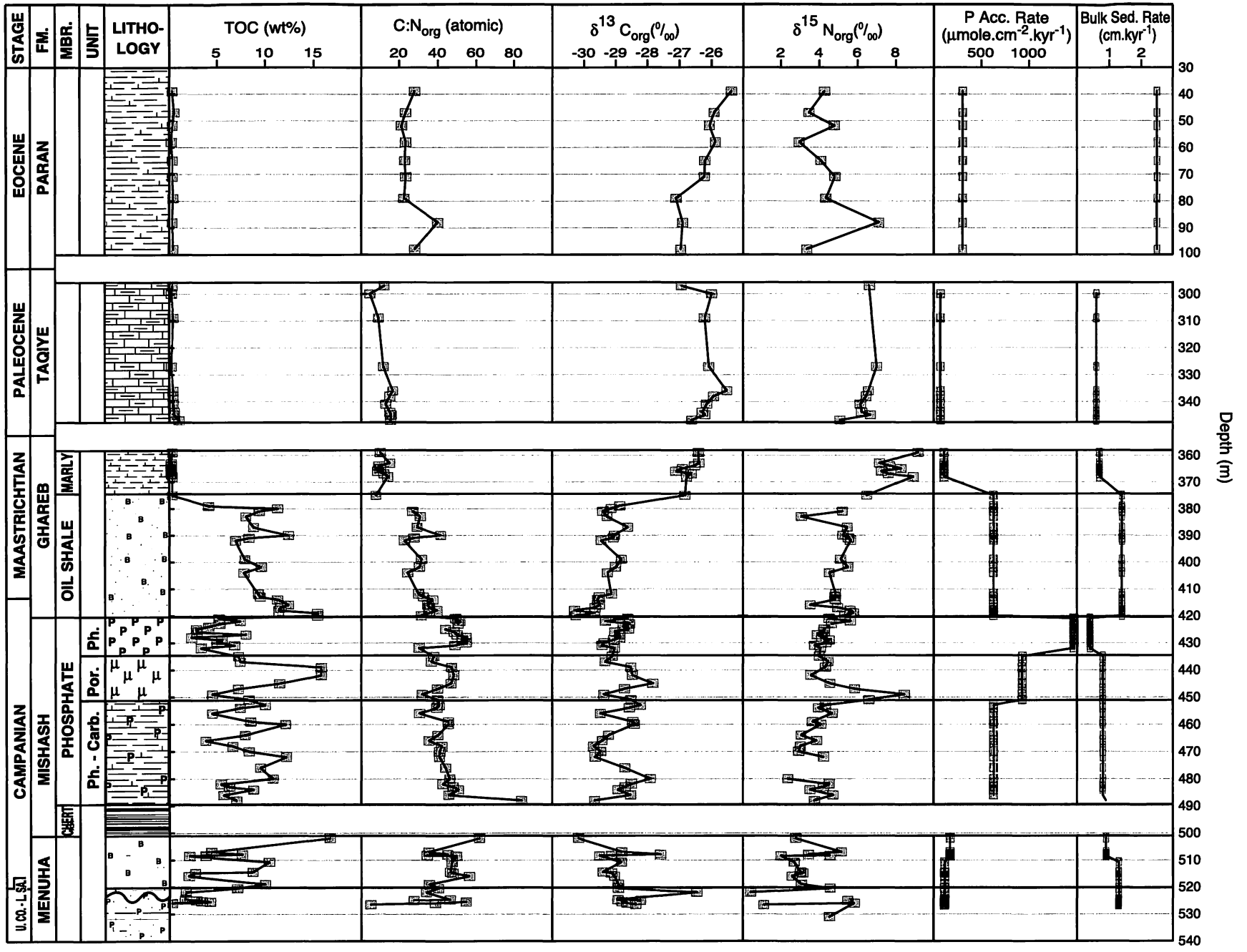

Fig. 14. Temporal evolution of TOC, C:N$_{org}$, δ^{13} C$_{org}$, δ^{15} N$_{org}$, P accumulation and bulk sedimentation rates along the Upper Coniacian-Lower-Middle Eocene of the Negev (composite section).

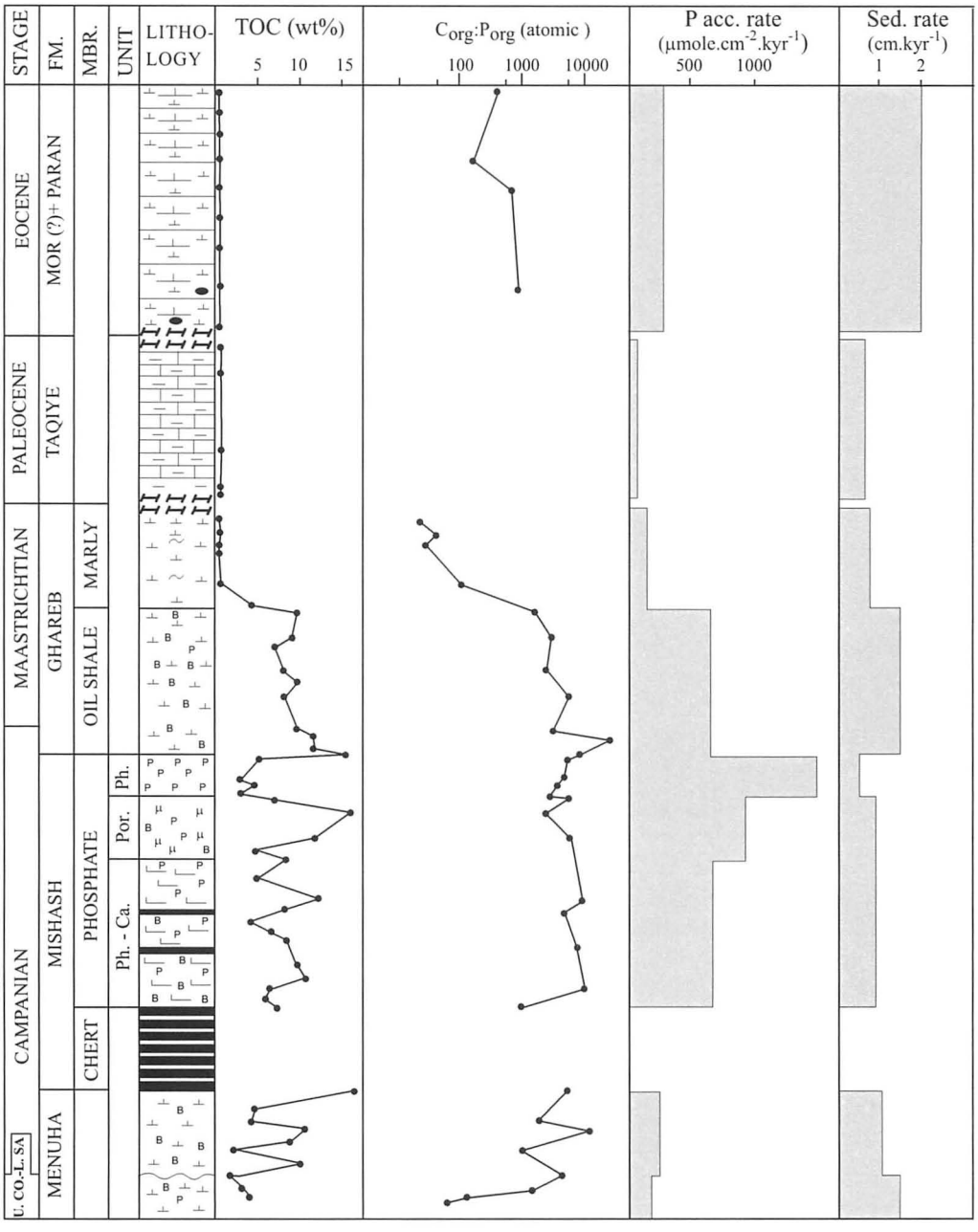

Fig. 15. Temporal evolution of TOC, C(org):P(org), P accumulation rates and rates of sedimentation over the Upper Coniacian-Eocene of the Negev.

Pacific waters into the Tethys seaway and influx of radiogenic (Pacific) Nd. The sharp increase of $\varepsilon_{Nd(T)}$ values in the Negev CFA during the Late Cretaceous reflects this improved water exchange between the Tethys and the open Pacific, causing the Nd isotopic composition of Tethys waters to evolve toward more radiogenic (mantle-like) values. Stille et al., (1996) also observed an increase in $\varepsilon_{Nd(T)}$ (thought more reduced than in our study) in Early Cretaceous-Eocene CFA concretions from the Tethys and linked it to increased water exchange between Tethys and Pacific.

Noteworthy is the distinct $\varepsilon_{Nd(T)}$ in the phosphorites of the Negev and Egypt (Red Sea) during the uppermost Campanian-lowermost Maastrichtian (75-71 Ma) interval (Table 6, fig. 4, 5). While in the Negev $\varepsilon_{Nd(T)}$ is –6.4 to –7.3, in Egypt it is –7.6 to –10.6. We attribute this difference in $\varepsilon_{Nd(T)}$ to the dissimilarity in depositional environments of the two phosphorites. The Egyptian phosphorites are typically associated with abundant glauconitic sands (Glenn and Arthur, 1990) while these are absent in the Negev as well as in other Middle East (e.g., Jordan, Syria) phosphorites. The association of glauconitic sands and phosphorites in Egypt was explained by deep lateritic weathering of the Arabo-Nubian massif followed by abundant fluvial discharge of P and Fe in inner shelf portions of south Tethys. This fluvial supply, rather than upwelled waters (Glenn and Arthur, op. cit.), would have been the main source of P for the formation of the Egyptian phosphorites. The very low (crust-like) $\varepsilon_{Nd(T)}$ values in these Egyptian phosphates confirm this terrigenous impact during their formation, while this impact is lacking in the Negev and other (Jordan, Syria) Middle East phosphorites, as also indicated by their more positive (mantle-like) $\varepsilon_{Nd(T)}$ values (Table 5). Because of the short residence time of Nd in seawater, this distinction in $\varepsilon_{Nd(T)}$ signals is kept in the two groups of phosphorites, indicating the existence of different water masses at the edge of eastern Tethys during the Campanian. The $\varepsilon_{Nd(T)}$ of the Egyptian phosphorites probably integrates two distinct isotopic signals, a crustal-like signal from fluvial discharge, superimposed on the more radiogenic Nd signal that characterized Tethys seawater mass during the Campanian.

It is also interesting to note the general coupling of the Nd and Ca isotopic compositions over the analyzed interval (Fig. 7), indicating that they are both more or less

controlled by the rate of continental runoff. By contrast, no coupling is seen between the isotopic evolution of Sr and Nd (Fig. 3) and that of Sr and Ca (Fig. 6).

6.2. Temporal variations of Ca isotopes

The results of Nd isotopes provide some clues as to the evolution of $\delta^{44}Ca$ in CFA over the analyzed lower Cretaceous-Eocene interval. Geochemical profiles of present-day phosphatization (e.g., off Peru-Chile, Namibia, Mexican continental shelves) indicate that CFA precipitates at the topmost part of bottom sediments together with suboxic bacterial degradation of organic matter (e.g., Jahnke et al., 1993; Glenn and Arthur, 1988). Only there, very close to the sediment-water interface, are the coincident conditions required for CFA precipitation (fluorine supply, carbonate alkalinity, and porewater phosphate concentration) met. Ca^{+2} needed for CFA formation could be supplied from sea-floor dissolution of carbonate and apatite skeletal fragments reaching sea bottoms, and/or directly from seawater infiltrating bottom sediments. Because of the strong biological fractionation of Ca during mineral precipitation (Skukan et al., 1997; Zhu and MacDougall, 1998), these different Ca sources have distinct Ca isotopic compositions. Skeletal carbonate and apatite debris are enriched in isotopically light Ca^{+2} while seawater is enriched in heavy Ca^{+2}.

It is not easy to assess the relative shares of the diverse Ca^{+2} sources (dissolved carbonate and phosphate bioclasts versus seawater) in the formation of the various CFAs and their encoded $\delta^{44}Ca_{(CFA)}$ signatures. Another uncertainty which complicates interpretation of $\delta^{44}Ca$ lies in the composition of the analyzed phosphorites. Many of them (especially the granular ones) are not homogenous in composition and shows phosphate pellets associated with skeletal apatite. Since Ca is more fractioned as it moves through the food chain (Skulan et al., 1997), $\delta^{44}Ca$ of skeletal apatite reaching sea floor is probably more negative than $\delta^{44}Ca$ of phosphate pellets, formed in bottom sediments from P-enriched interstitial seawater. The rather close $\delta^{44}Ca$ values yielded by a few separated CFA pellets and associated bone debris (Table 5) indicate, however, that some isotopic homogeneisation of the different Ca^{+2} sources probably occurred in the CFA-precipitating porewaters. This isotopic exchange between the various Ca^{+2} sources could have occurred during diagenetic stabilization of skeletal hydroxyapatite into CFA. This conversion is

often revealed in fossil phosphorites by local enrichment in fluorine of bone tissues (Soudry and Nathan, 2001).

In spite of these uncertainties, the magnitude of the $\delta^{44}Ca$ change (+ 0.6‰) in the CFA record in the analyzed succession ($\delta^{44}Ca$ = - 0.22 in lower Cretaceous; $\delta^{44}Ca$ = + 0.40 in Eocene) as well as its trend over time (Table 8, Fig. 12) lead us to think that this change reflects temporal variations of the isotopic seawater Ca. This interpretation is supported by results of Schmitt et al. (2003b) in Miocene-Pleistocene phosphates. These found that $\delta^{44}Ca$ varies in phosphates in the same way as in carbonates of the same age (De La Rocha and DePaolo 2000), indicating that $\delta^{44}Ca$ phosphate can detect variations of isotopic Ca in paleoseawater.

Two main stages are distinguished in the evolution of $\delta^{44}Ca$ in CFA along the analyzed lower Cretaceous-Eocene (Fig. 12): 1) a lower Cretaceous-middle Turonian stage with negative $\delta^{44}Ca$ values ($\delta^{44}Ca$ as low as -0.22‰ in the Hauterivian-Albian), and 2) a Coniacian-Eocene stage with positive $\delta^{44}Ca$ values ($\delta^{44}Ca$ mostly between +0.30 and 0.40‰). These two different $\delta^{44}Ca$ stages are explained by changes in paleogeography and paleoceanography caused by eustatic sea level changes and plate tectonics re-arrangement of continents. Biological fixation of Ca+2 into carbonates during calcification is the principal (mainly ^{40}Ca) sink in oceans (Wilkinson and Algeo, 1989). High $CaCO_3$ deposition rates during times of increased flooding of continental shelves will therefore enrich seawater with heavy Ca^{+2}. Conversely, times of increased weathering of carbonate platforms during sea retreats will supply to oceans abundant riverine Ca^{+2} enriched with the lighter Ca^{+2}. The negative$\delta^{44}Ca$ values during the Hauterivian-Albian (130-96 Ma) could reflect high weathering Ca^{+2} fluxes caused by the global latest Jurassic sea regression exposing Jurassic and earlier carbonate platforms. The abundant terrigenous sediments in the lower Cretaceous of N. Europe (The Wealdian-Purbeckian facies) and in the middle East (Nubian sandstone) clearly evidences this intense land-mass erosion after the Jurassic, explaining the negative $\delta^{44}Ca$ values during this period.

It could be argued that the low $\delta^{44}Ca$ values during the Early Cretaceous could be the effect of changing seawater temperature than the result of increased weathering Ca^{+2} fluxes. Data from the natural environment (Zhu and MacDougall, 1998) and laboratory

experiments (Nägler et al., 2000) indicate that fractionation of Ca isotopes during calcification is temperature controlled (fractionation increases with decreasing temperature). Cultured planktonic foraminifera led Nägler et al. (2000) and Hippler et al., (2002) to suggest a $\delta^{44}Ca$ change of 0.24 ± 0.02 per 1°C. A much smaller $\delta^{44}Ca$ temperature dependance (0.05 per 1°C) was later found by Deyhle et al. (2002) in other cultured foraminifera, suggesting that inter-species differences may exist in the magnitude Ca isotopic fractionation. Such a temperature effect on Ca fractionation measured in culture experiments is however not expressed when examining the fossil record. In the Negev sequence, $\delta^{18}O$ in Nodosoria shells (benthonic foraminiferid with negligible "vital effect") increases by +1‰ from the Santonian to the Campanian (Bein et al., 1990b). Such a $\delta^{18}O$ increase would imply a drop of ~ 4°C in seawater temperature from the Santonian to the Campanian. Assuming that most of the CFA-Ca derives from dissolved calcareous shells in bottom sediments, a temperature-dependant Ca fractionation (Nägler et al., 2000) should have shifted $\delta^{44}Ca$ in CFA toward lower values during the Campanian. The results of this study however show that $\delta^{44}Ca$ does not changes and even increases (up to 0.4‰; Table 8) from the Santonian to the Campanian, indicating little dependance between seawater temperatures and Ca fractionation in the studied phosphorites. Schmitt et al. (2003b) also found no correlation between $\delta^{44}Ca$ and $\delta^{18}O$ values in Miocene phosphorites, indicating little temperature effect on Ca isotopic fractionation.

One may also argue that the intense mid-plate Pacific volcanism during the lower Cretaceous (Watts et al., 1980) was also responsible for the low $\delta^{44}Ca$ values during this period. This intense volcanism in mid-ocean ridges would have led to increased Ca-for Mg exchange from hydrothermal alteration of ocean-floor basalt ($\delta^{44}Ca$ = -0.63‰ to –1.16‰; Schmitt et al., 2003a). It is possible that light Ca^{+2} was also contributed from this source to early Cretaceous seawater during these times of high spreading rates. The widespread continental sedimentation during lead us however to think that this hydrothermal source of light Ca^{+2} was subordinate to continental Ca^{+2}. Mass balance calculations also indicate that weathering of carbonate rocks is the main source of Ca^{+2} in seawater. The hydrothermal input of Ca to the oceans was estimated to be around 35 % (Wilkinson and Algeo, 1989) and 22% (Berner and Berner, 1995) of the river input.

The global sea level rise (+200 m) during the Late Cretaceous (Haq et al., 1987), reducing the exposed landmasses and expanding the areas of carbonate sedimentation in shelves, would explain the subsequent increase of $\delta^{44}Ca$ during the Coniacian-Eocene. Nearly 40% of the total continental area was flooded during this period (Howarth, 1981). The more pronounced $\delta^{44}Ca$ increase during the Campanian (80-72 Ma), continuing in the upper Maastrichtian and the Eocene (no $\delta^{44}Ca$ data are available for the Paleocene), is attributed to the increasing abundance and diversification of planktonic foraminifera and calcareous nannoplankton that produced the massive chalks (seaward of the mainly rudist carbonate platforms) during this period (Hay, 1995). This increased carbonate sedimentation would have increased the rate of biological removal of light Ca^{+2}, enriching seawater with heavy Ca^{+2}. A similar trend of increasing $\delta^{44}Ca$ during the Campanian-Eocene (75-45 Ma) is also observed in marine carbonates (De La Rocha and DePaulo (2000), providing additional evidence for a greater imbalance in favor of carbonate sedimentation during this period.

6.3. Variations of P accumulation rates

$\varepsilon_{Nd(T)}$ and $\delta^{44}Ca$ provide some explanation for the changes in P accumulation during the Cretaceous-Eocene. The rise in P accumulation rates starting at the Coniacian and culminating in the Campanian is conjugated with the rise in $\varepsilon_{Nd(T)}$ and $\delta^{44}Ca$, and suggest that they are together related. The low P accumulation rates in the lower Cretaceous of the Negev (less than 50 μmole P cm^{-2} kyr^{-1}) might be due to rather slow marine circulation in the Tethys during these times. The nearly closure of the Carribean threshold during the Early Cretaceous (e.g., Masse et al., 1993) together with shallow blocks and emerging areas (e.g., Apulia, Appenine platform) obstructing parts of the eastern Tethys, would have impeded marine circulation and seawater oxygenation. Blocked from marine circulation, the western Tethys and the Central Atlantic became stagnant and O_2-depleted (Hay, 1995), with black shales forming as a result of nutrient supply from greater riverine runoff (Föllmi et al., 1994). This slow circulation in the large parts of Tethys during the early Cretaceous, causing poor seawater oxygenation, is also indicated by the positive Ce anomalies (up to + 0.7) in biogenic apatites of the Tethyan area during this period (Lécuyer et al., 2004).

The high sea level rise during the Late Cretaceous probably led to intensification of marine circulation in through Tethys seaway. This is evidenced by the sharp $\varepsilon_{Nd(T)}$ rise starting at the upper Cenomanian (Fig. 12), suggesting increased incursion of Pacific waters enriched with radiogenic Nd into Tethys. This intensified circulation is also suggested by the increasingly negative Ce anomalies in Tethyan apatites after the Cenomanian (Lécuyer et al., 2004), pointing to progressive oxygenation of seawater caused by oceanographic changes. Scotese et al. (1988) attributed these changes to the opening of Southern Atlantic and Drake Passage, allowing Pacific waters to travel around south Africa (Stille, 1992) then to flow northwards into the Atlantic. Still, circulation in the Tethys during the Late Cretaceous was mostly E-W (Luyendyk et al., 1972; Berggren and Hollister, 1977; Camoin et al., 1993), driven by widening of the Caribbean threshold (Philip et al., 1993). The development of this westward-flowing circumglobal Tethyan current could have resulted in an increased dissolved P inventory in the water body (Jewell, 1995). Plate tectonic disposition of continents and south Tethys (paleolatitude 8°-15°) at the Campanian-Maastrichtian (Barron et al., 1981) would have induced favorable atmospheric circulation in the Tethys seaway (Parrish and Curtis, 1982). Winds blowing from the NE caused Ekman transport of surface waters to the NW, resulting in coastal upwelling of deoxygenated P-rich, mid-depth waters in mainly the eastern Tethys (the present Middle East area). By contrast, relatively little P reached the western Tethys (the present North Africa belt) during the Campanian-Maastrichtian, perhaps because situated too far from the upwelling center probably situated in -Pacific at these times. Upwelled waters are also quickly depleted of nutrients on relatively short distances (e.g., Barber and Smith, 1981; Parrish and Curtis, 1982; Glenn and Arthur, 1988) and this would cause the eastern Tethys upwelling to dissipate rapidly westward. Although phosphorites also occur in the Maastrichtian of North Africa (Boujo, 1976; Prévot, 1988) they are however much less abundant than in the Middle East. Only in Eocene times, following major changes in paleocirculation (see below) will phosphogenesis reach high intensity in the North Africa area (western Tethys).

The increasing sea level rise, reaching its maximum at the Late Cretaceous (and remaining high until in the Cenozoic), probably caused the shelf front to break (Hay, 1995), allowing subsurface P-rich waters to penetrate up the inner shelves of the eastern Tethys. Such cold upwelled waters are well evidenced by the $\delta^{18}O$ increase in Santonian-

Campanian fish debris (Kolodny and Raab, 1988) and foraminifera (Bein et al., 1990) of the Negev. Continuous nutrient supply from persistent water circulation would have sustained high surface productivity in this area, causing abundant accumulation of organic-rich sediments and increased sea floor phosphogenesis. The extremely reduced sedimentation rates during Campanian times (< 0.4 cm.kyr^{-1}; Table 6) probably also contributed to intense P regeneration (see Table 9) enhancing CFA precipitation. The inverse correlation of P and Ca accumulation rates in the Negev (Fig. 11) fits this depositional scheme. Primary production in areas of upwelling is mostly dominated by diatoms because to their efficiency in P uptake and their high reproduction rates (Reiss, 1988). Such productive zones are less prone (Föllmi, 1996) to calcareous nannoplankton growth (major producers of carbonates), thus explaining the opposite peaks of P and Ca accumulation rates in the Negev during the Campanian.

Configuration of the Tethys basin profoundly changed in the Paleocene-Eocene, the time of maximum phosphate deposition (Thanetian-Ypresian) in North Africa (western Tethys). The increasing plate-tectonic closure of the Tethys basin at these times together with the arrival of the Indian plate at proximity to Eurasia (e.g., Butterlin et al., 1993), probably resulted in a weakening of the westward Tethyan flow, that flow which fuelled phosphogenesis in the eastern Tethys (Middle East) during Late Cretaceous times. Weakening of the Tethyan flow together with widening of the Atlantic, both make that phosphate formation in North Africa during the Paleocene-Eocene is now more fuelled by Atlantic seawater. This shift of oceanic P sources from the Pacific-Tethys during the Late Cretaceous to the Atlantic during the Eocene is well evidenced by the different $\varepsilon_{Nd(T)}$ of the Middle East and North African phosphorites. While $\varepsilon_{Nd(T)}$ is -6 to -7 (Pacific-like) in the Campanian phosphorites of the Middle East, it is -9 to -11 (Atlantic-like) in the Paleocene-Eocene North African phosphates (Table 5, Fig. 5). Therefore, two different oceans and two differently-oriented marine flows, fuelled by turn Tethyan phosphogenesis, following changes in paleogeography and paleocirculation. Pacific-Tethys (westward Tethyan flow) dominant during the Late Cretaceous in the Middle East area (eastern Tethys), followed by the Atlantic (northward Atlantic flow) predominant during the Paleocene-Eocene in North Africa (western Tethys).

6.4. %TOC, atomic C_{org}/N_{org} ratios, $\delta^{13}C_{org}$ and $\delta^{15}N_{org}$ variations

Figure 14 illustrates an up-core composite stratigraphic section displaying the temporal evolution of weight percent total organic carbon (TOC), atomic organic carbon to organic nitrogen ratios (C_{org}:N_{org}), the $\delta^{13}C$ and $\delta^{15}N$ of organic carbon, phosphorus accumulation rates and bulk sedimentation rates along the upper Coniacian through lower middle Eocene of the Negev. There are some clear, yet often subtle relationships between these various important chemostratigraphic parameters.

6.4.1. Total organic carbon and atomic C_{org}/N_{org} ratio variations

Organic geochemical results from the Negev phosphorite sequence (Amit and Bein, 1982) demonstrate a lack of heavy saturated hydrocarbons with odd-over-even predominance, indicating that the organic mater of these units originated from marine microorganisms and thus not from cuticular waxes of terrestrial higher plants. Similary, pyrolysis results from the Negev sequence (Bein et al., 1990) and from organic-rich from temporally equivalent organic–rich shales associated with phosphorite sections of Duwi Group strata across Egypt (Glenn and Arthur, 1990) clearly indicate that the organic matter of these units have undergone little, if any diagenetic alteration during burial. As expected for sequences not deeply buried on stable cratons, all kerogens are thermally immature. In addition, both of these data sets indicate a marine algal (Type I) to possibly slightly mixed marine algal and terrigenous sources (Type II) of the sediments (cf. Tissot and Welte, 1978), a conclusion corroborated by the prevalence of light alkanes in the Negev sections (Bein et al., 1990). TOC contents are markedly enriched in the Campanian and lower Maastrichtian portions of the section (Fig. 14, Table 8) with TOC contents varying between about 5 and 15 weight percent. Although some of the variations in %TOC throughout the section may be attributed to lithologic dilution by other components, as cross plots of TOC versus $\%C_{org}$ extracted from insoluble residues of the same samples for this section display a slightly positive linear correlation of $R^2 = 0.65$ (not shown), the organic carbon accumulation rates are indeed very high, especially through stratigraphic intervals 2 through 6 (Fig. 14, 520m-379m; Table 9) varying between ca. 3,000 to 12,000 $\mu molCorg.cm^{-2}.kyr^{-1}$. These values fall within the lower range of reported C_{org} accumulation rates of many highly productive modern marine coastal upwelling zones, which may range between 10,000 and 450,000 $\mu molC_{org}.cm^{-2}.kyr^{-1}$ (c.f. compilations of

Glenn and Arthur, 1985). In contrast to the above, TOC contents in the post-lower Maastrichtian portions of the Negev are rapidly and dramatically reduced to values typically <1% TOC. Throughout the section C_{org}:N_{org} atomic ratios generally track variations in %TOC, with increasing TOC corresponding to increasing C_{org}:N_{org}. C/N ratios are commonly used to differentiate relative organic inputs of marine algal components versus terrestrially-derived organic matter (algae typically have atomic C/N ratios between 4 and 10 whereas vascular land plants have ratios of 20 or greater; Meyers, 1997). However, pyrolysis data indicate a dominant marine algal source for these sediments. We suspect that the rather high C/N atomic ratios exhibited in the Negev are due to the preferential consumption of N-rich organic matter. Contrary to the expected affect of bacterial degradation on the $\delta^{15}N$ of organic matter, Figure 14 reveals that the up section trend in decreasing C/N ratios correlates with increasing $\delta^{15}N_{org}$. As outlined below, we believe this represents a time-progressive decrease in the availability of dissolved nitrate with time.

6.4.2. $\delta^{13}C_{org}$ and $\delta^{15}N_{org}$ variations

$\delta^{13}C_{org}$ and $\delta^{15}N_{org}$ have become increasingly widespread tracers in deciphering variations in water mass eutrophication, changes in upwelling intensity, and also as clues to the in nature of organisms producing such signals (cf. Meyers, 1997), although systematics of the co-lateral use of these tracers may, at times, prove difficult to interpret. Evidence from recent settings suggest that $\delta^{15}N_{org}$ values of particulate organic matter (POM) in organic-rich sediments are usually very similar to that of the sinking particles from which they were derived and are little affected by post-depositional diagenesis. When there is moderate to good preservation of sedimentary organic matter due to high productivity and/or low bottom water oxygenation, little diagenetic effects in sedimentary $\delta^{15}N_{org}$ are apparent (Altabet et al., 1999b). As noted above, our previous pyrolyses analyses of the sediments associated with Middle East Campanian-lower Maastrichtian phosphorites generally reconfirms this.

The composite chemostratigraphic section (Fig. 14) also illustrates that although with numerous variations, generally low values of $\delta^{13}C_{org}$ and $\delta^{15}N_{org}$ occur in association with elevated TOC values in the Campanian and lower Maastrichtian portions of the studied sequence. $\delta^{13}C_{org}$ values near the base of the section (i.e. from 490m to 420m,

which generally corresponds to a time window from ca. 79 Ma to 72 Ma) have values close to –29‰, while δ^{15}Norg values generally range about +4‰. Above this horizon, both δ^{13}Corg and δ^{15}Norg progressively wax up section to relatively more positive values, with δ^{13}Corg values generally trending from –30‰ at ca. 420m up to ca. –26.5‰ at 360m, and δ^{15}Norg values trending from about 3‰ at 420m to a maximum of 8‰ at 360m. We believe these trends are the result of several possible factors. In comparison with the globally averaged marine $\delta^{13}C_{org}$ for the interval between ca. 79 Ma and 72 Ma (ca. –26‰ to –27‰; Hays et al., 1999), the C_{org} of Campanian interval of the Mishash Fm. is thus anomalously depleted in ^{13}C by about 3‰ to 4‰. We consider the most likely explanation for this anomalous ^{13}C depletion is due to the recycling of upwelled ^{13}C-depleted total dissolved carbon (DIC) that resulted from degradation of settling POC in the water column, although, due to a lack of δ^{13}C of inorganic carbon and of organic biomarker data for these sediments we can not at this time rule out potential contributions due to POM contributions as a result of methane oxidizing bacteria (e.g. Freeman et al., 1990; Hinrichs et al., 1999; Jahnke et al., 1999; Valentine and Reeburgh, 2000; Hollander and Smith, 2001), nor can we dismiss possible biological fractionation effects associated with variations in phytoplankton growth rates and/or cell size (e.g. Laws, et al., 1995; Popp et al., 1998). However, we do strongly favor the water column recycling of degraded DIC on the basis of the combined interplay between up core variations in TOC, $\delta^{13}C_{org}$ and $\delta^{15}N_{org}$, as outlined both previously and more fully examined below.

Traditionally, a general inverse relationship between $\delta^{15}N_{org}$ of suspended and sedimented POM and the dissolved nitrate [NO_3^-] in oxygen-depleted (suboxic) surface waters has been attributed to isotopic fractionation during [NO_3^-] uptake by phytoplankton (e.g. Altabet and Francois, 1994; Altabet et al., 1995, 1999a,b; Altabet and Higginson, 2002; Ganeshram et al., 2000). Nitrate ultilization selectively takes up the lighter nitrogen isotope (^{14}N) during photosynthesis, progressively leaving the residual [NO_3^-] pool relatively enriched in the heavier isotope. Through Raleigh distillation, as assimilation proceeds and nitrate is further depleted, the δ^{15}N of the residual nitrate of the sinking POM that forms by assimilation of that nitrate becomes progressively enriched. However, these systematics must be viewed carefully in order to be correctly interpreted in paleoceanographic reconstructions. Altabet (2001), for example, clearly showed in a study of nitrogen isotope systematics associated with equatorial upwelling in the modern Pacific

that, while entrained upwelled water traveled north and south of the center of equatorial divergence, their [NO_3^-] became progressively reduced simultaneously with enrichments of $\delta^{15}NO_3^-$ (from ca. 0‰ to +14‰), as expected. However, this study also clearly demonstrated that within a broad span of about 8° latitude north to south of locus of the center of equatorial divergence and upwelling, surface waters POM maintained relatively low $\delta^{15}N_{org}$ (plateauing at ca. +2‰) due to sustained [NO_3^-] upwelling in that region. Although this study had the additional caveat that Fe limitation also plays a role in the shaping the extent of the primary export productivity, this model may likely explain the positive correlation in the organic-rich lower portion of the Negev sequence between trends of generally low intervals of δ^{15}Norg (averaging + 4.5‰) corresponding with negative intervals of δ^{13}Corg (averaging –29.0‰). Further up section, at the top of the Ghareb Oil Shale member, as TOC values dramatically diminish, both δ^{15}Norg (averaging 6.1‰) and δ^{13}Corg values (averaging –26.4‰) increase up section. The increase in δ^{15}Norg in the upper portions of the section is likely due to waning productivity and possibly also due to diagenetic effects resulting from a return to oxygenated bottom waters (Altabet et al., 1999a). At the same time, the shift to more positive δ^{13}Corg likely generally reflects a return to average global $\delta^{13}C_{org}$ values for this interval of time (i.e. Hayes et al., 1999), possibly in part to elevated atmospheric pCO_2 in the Late Cretaceous relative to the present (cf. Dean et al., 1986; Berner, 1994). Thus, while there are single up section sample-to sample exceptions where positive excursions in δ^{15}Norg correlate with negative excursions in δ^{13}Corg (e.g. at 450m in the Porcelanite member of the Mishash Fm. where %TOC values fall), the general overall trend for the most organic-rich portions of the Negev section indicate sustained primary productivity as a direct result of continuous [NO_3^-] (and [PO_4^{3-}]) nutrient availability within the core of the maximum locus of upwelling.

6.5. $P_{(org)}$ variations

The results show that $C:P_{org}$.ratios of the sediments in the sequence studied vary by more than two orders of magnitude (Table 8). The first factor which determines these variations is the redox state of the bottom/interstitial waters; oxic conditions lead to C/P_{org} ratios around the Redfield ratio, sometimes higher, sometimes lower; while suboxic and anoxic conditions lead to C/P ratios considerably higher than the Redfield ratio. These results agree with previous studies (Froelich et al., 1982; Coleman and Holland, 2000; Van Cappellen and Slomp, 2002).

Furthermore, they show clearly: 1) there are C/P_{org} ratios that are significantly lower than the Redfield ratio. These are not analytical errors. 2) oxic environments with low C_{org} concentrations do not always result in C/P_{org} ratios that are lower than the Redfield ratio.

The relatively high C/P_{org} ratios found in the suboxic and anoxic parts of the sequence (about 4000, some two orders of magnitude higher than the Redfield ratio) are not surprising for unweathered organic-rich fossil samples (e.g. Ingall and Van Cappellen, 1990; Ruttenberg and Berner, 1993; Ingall and Jahnke, 1997; Van Cappellen and Ingal, 1996; Schenau and De Lange, 2001). We are aware that these results confirm that organic P regeneration is much higher than is indicated by previous estimates. However, this does not mean that all or even most of this regenerated P is returned to the surface waters; most of it is probably used for the formation of authigenic P (francolite) during early diagenesis (Ruttenberg and Berner, 1993; Delaney, 1998; Anderson et al., et al., 2001). This process which is quantitatively much more important in upwelling systems, has been termed sink-switching (Ruttenberg, 1993). It alters significantly our estimates of the P sinks; lowering the organic P sink and increasing the authigenic P sink.

The results also agree with numerous previous findings (e.g. Ingall and Van Cappellen, 1990) which show the importance of the redox potential and sedimentation rate. The $C:P_{org}$ ratio increases with increasing reducing conditions (Table 8, Fig. 15) and decreases with increasing sedimentation rate.

Our results indicate that the present estimates given for the organic P burial in sediments are too high. There is obviously more organic matter buried under suboxic/anoxic conditions than organic matter buried under oxic conditions, at least a 60:40 ratio. Taking as a very conservative estimate an average C/P_{org} ratio of 500 for organic matter buried under suboxic/anoxic conditions and an average C/P_{org} Redfield ratio of 117 (Anderson and Sarmiento 1994) for organic matter buried under oxic conditions we obtain a global estimate of C/P_{org} of 347. Based on C_{org} burial of 1.25×10^{12} mol C yr^{-1} (Jahnke, 1996), we obtain a global estimate of 0.4×10^{10} mole P yr^{-1} buried as organic P. This estimate is significantly lower than all the previous estimates, from 1.1 to 2.0×10^{10} mole P^{-1} buried as organic P (see Table 3 in Delaney, 1998). This, together with our results for the P accumulation rates indicate that most of the estimates for the authigenic P sink are too low and that this have been underestimated, especially the values for phosphogenic environments. This leads to agree with Ruttenberg's estimate (1993) for the average residence time of oceanic phosphate 16-38 kyr. Detailed results of $P_{(org)}$ and their implications are included in a paper now in preparation.

7. Conclusions

The general coupling between total organic carbon, $_{Nd(T)}$, $\delta^{44}Ca$, $\delta^{13}C_{(org)}$, $\delta^{15}N_{(org)}$, and P accumulation rates in the lower Cretaceous-Eocene of the Middle East (eastern Tethys) suggests paleogeographic and oceanographic controls in accumulation of phosphorites in this area. The sharp rise of $\varepsilon_{Nd(0)}$ starting at the upper Cenomanian reflects increased incursion of Pacific water masses into the Tethys seaway, driven by the Late Cretaceous global sea level rise and increased ocean circulation. It also reflects a weakening of the continental Nd isotopic signal intensely recorded during the lower Cretaceous. $\delta^{44}Ca$ also rising at these times reflects a decrease in weathering Ca^{+2} fluxes together with expansion of carbonate sedimentation areas as a result of increased flooding of continental shelves.

The conjugated rise of P accumulation rates, starting at the Coniacian and culminating in the Campanian-Maastrichtian of the Middle east, reflects the combined effect of sea level highstands and plate-tectonics both inducing favorable atmospheric and marine circulation. This resulted in coastal upwelling of P-rich, cold mid-depth waters flowing onto the south edges of eastern Tethys, reaching the inner shelves as the shelf front "broke" with increasing sea level rise. Generally low values of $\delta^{13}C_{(org)}$ and $\delta^{15}N_{(org)}$ occur in association with elevated TOC values. We consider the most likely explanation for this anomalous ^{13}C depletion is due to the recycling of upwelled ^{13}C-depleted total dissolved carbon (DIC) that resulted from degradation of settling POC in the water column. By comparison with modern equatorial Pacific upwelling systematics, we maintain that the relatively low $\delta^{15}Norg$ (plateauing at ca. +2‰) in the Campanian-Maastrichtian of the Negev was due to sustained $[NO_3^-]$ and $[PO_4^{3-}]$ upwelling within the core of the maximum locus of upwelling in this region. In contrast, being situated far from the upwelling center (eastern Tethys-Pacific) at those times, the western Tethys (the present-day N. Africa belt) was less influenced by these nutrient-rich rising waters. In the Negev, these upwelled cold waters are imprinted in the $\delta^{13}C$ of the organic fraction and the $\delta^{18}O$ of fish remains and foraminifera. Increased circulation during the Late Cretaceous is also suggested by the strongly negative Ce anomalies in many biogenic apatites of the Tethyan domain.

The low $\varepsilon_{Nd(T)}$ values in the Egyptian phosphorites reflect local fluvial discharge during the formation of these rocks, suggesting different water masses at the edges of south Tethys during the Campanian. This terrigenous Nd isotopic signal during the formation of these Egyptian phosphorites probably interfered with the more radiogenic Nd signal that characterized Tethys seawater at these times, causing a superimposition of the two signals in these rocks.

Together with the increasing plate-tectonic closure of the Tethys during the Paleocene-Eocene and the arrival of the Indian Plate next Eurasia, paleocirculation changes. The westwards Tethyan flow that fuelled phosphogenesis in the eastern Tethys during the Late Cretaceous is replaced by a northwards Atlantic flow which fuels Paleocene-Eocene phosphogenesis in North Africa area. This shift of oceanic P source from Tethys-Pacific (Late Cretaceous) to the Atlantic (Paleocene-Eocene) is well expressed in the $\varepsilon_{Nd(T)}$ values of the two Middle East and North Africa phosphorites.

The overall decoupling between the geochemical evolution of the Sr isotopes and that of the Ca and Nd isotopes during the analyzed time-interval (while Ca and Nd isotopes are more or less coupled with P rates) suggests little direct relationship between continental weathering and rates of phosphogenesis in south Tethys shelves. It is perhaps significant in this sense that the clastic-rich Wealdian deposits in much of Europe as well as the extensive Nubian sandstone in the Middle East and Arabian Peninsula both deposited during the lower Cretaceous are associated with only limited phosphogenesis.

Additional results (other related studies done as part of the present BSF research)

1) Fluorine (F) geochemistry in Negev phosphorites

Part of the BSF research was devoted to completion of an electron probe, chemical and mineralogical study on the geochemistry of fluorine (F) in the Negev francolites (Soudry and Nathan, 2001). F distribution in phosphorites is strongly connected with the scope of the BSF project as F plays a key role in regulating CFA precipitation. At such, it controls P accumulation in depositing sediments. In addition, preliminary electron probe data have shown that F concentration in the Negev CFA is not uniform and that F could be used as a sensitive control of CFA diagenesis during phosphorite formation.

The results indicate that F concentration (expressed as F/P_2O_5) 1) considerably vary between the various phosphate constituents and even in the same grain, 2) is strongly controlled by the phosphorite facies (increasing with CFA maturation from "pristine" to "recycled" facies), and 3) is inversely related with the Cd and Zn concentration in phosphorite and (to some extent) with the CO_2/F ratio in CFA. All this suggests that CFA (or an amorphous precursor) initially forms with some OH groups in the apatite lattice which are subsequently substituted by F ions during repeated recycling of the pre-formed CFA in the uppermost zone of bottom sediments.

2. Uranium (U) geochemistry in Negev phosphorites

U distribution in phosphorites is an important as CFA is one of the major sinks for U in marine sediments. As such, U is a sensitive control of P accumulation. It was initially suggested that U is originally incorporated in CFA as U(IV) (or in both oxidation states) and that it is converted to U(VI) by subaerial oxidation.

The study the U(IV) fraction in the Negev phosphorites (Soudry et al., 2002) led however to different results, revealing an apparently paradoxical trend: U(IV) fraction is very low in the "pristine", organic-rich laminated phosphorites, whereas it considerably increases in the recycled granular phosphorites deposited under more oxidizing sea-bottom conditions. Moreover, a lower %U(IV) in phosphorites is coupled with lower REE/P_2O_5 and Y/P_2O_5 ratios, higher Cd and Zn concentrations, less negative Ce/Ce* and Eu/Eu* anomalies, a lower HREE (Dy-Er) enrichment, and a lower F/P_2O_5 and higher CO_2/F ratios in CFA. This U(IV) trend is interpreted as reflecting varying time-spans of CFA growth,

changes in burial rates, and mainly different residence times of the CFA fraction near the sediment-water interface.

Publications (Research grant: 1990232)

Soudry, D. and Nathan, Y., 2001. Diagenetic trends of fluorine concentration in Negev phosphorites: Implications for carbonate fluorapatite composition during phosphogenesis. Sedimentology 48: 723-743

Soudry, D., Ehrlich, S., Yoffe, O., and Nathan, Y., 2002. Uranium oxidation state and related variations in geochemistry of phosphorites from the Negev (southern Israel). Chem.Geol., 189: 213-230.

Soudry, D., Segal, I., Nathan, Y., Glenn, C.R., Halicz, L., Lewy, Z., VonderHaar, D.L., 2004. $^{44}Ca/^{42}Ca$ and $^{143}Nd/^{144}Nd$ isotope variations in Cretaceous-Eocene Tethyan francolites and their bearing on phosphogenesis in the southern Tethys. Geology, 32, 389-392.

Scientific presentations.

Soudry, D., Nathan, Y. (2003). Controlling factors in the geochemistry of the Negev phosphorites: clarifying the rules of the game. Ann. Meet. Isr.Geol. Soc., Ein Bokek, p. 120.
and: Ann. Meet. Geol. Soc. America, Seattle, Abstracts with Programs, v. 35, p. 408.

Soudry, D., Segal, I., Nathan, Y., Glenn, C.R., Halicz, L., Lewy, Z., VonderHaar, D., 2004. Tethyan phosphogenesis: a new outlook from $^{42}Ca/^{44}Ca$ and $^{143}Nd/^{144}Nd$ isotopes in Cretaceous-Eocene Tethyan francolites. Ann. Meet. Isr. Geol. Soc., Hagoshrim, p. 107.

Soudry, D., Glenn, C.R., Nathan, Y., Segal, I., VonderHaar, D., 2004. Tracing Tethyan phosphogenesis from temporal variations of $^{44}Ca/^{42}Ca$ and $^{143}Nd/^{144}Nd$ isotope ratios and P accumulation. Eos. Trans. AGU, 85 (47), Fall Meet. Suppl., Abstracts, p. 1007

Acknowledgments

This study was supported by the United States-Israel Binational Science foundation (grant 1999232), the Geological Survey of Israel (GSI Project 40030), and the University of Hawaii School of Ocean and Earth Science and Technology. We thank D. Stieber and O. Yoffe for carrying the elemental geochemistry, N. Teplyakov for assistance in analysis of Ca isotopes, D. Vonderhaar for analysis of Nd isotopes, and T. Rust for analysis of $C_{(org)}$ and $N_{(org)}$ isotopes. We also thank O. Gofin, Y. Mizrahi, S. Ashkenazi, and D. Sidi for technical assistance, and B.-S. Cohen, N. Shragaii, C. Netzer-Cohen for editing the report.

References

Al-Maleh, A.K. and Mouty, M., 1994. Lithostratigraphy of Senonian phosphorite deposits in the Palmyridean region and their general sedimentological and paleogeographical framework. In: Lijima, A., Abed, A.M. and R.E. Garrison, R.E. (Eds.), Siliceous, Phosphatic and Glauconitic Sediments of the Tertiary and Mesozoic. 29th Intern. Geog. Congr. Proceedings, Part C, pp. 225-232.

Almogi-Labin, A., Bein, A. and Sass, E., 1993. Late Cretaceous upwelling system along the southern Tethys margin (Israel): Interrelationship between productivity, bottom water environments, and organic matter preservation. Paleoceanography, 8, 671-690.

Altabet, M.A., 2001. Nitrogen isotopic evidence for micronutrient control of fractional NO_3^- ultilization in the equatorial Pacific. Limnology and Oceanography, 46, 368-380.

Altabet, M. and François, R., 1994. Sedimentary nitrogen isotopic ratios as a recorder for surface ocean nitrogen utilization. Global Biogeochemical Cycles, 8, 103-116.

Altabet, M.A. and Higginson, M.J., 2002. Forcing feedbacks between the nitrogen cycle and global climate, Abstracts Volume, Sixth International Symposium on the Geochemistry of the Earth's Surface, Honolulu, Hawaii, p. 220-223.

Altabet, M.A., Murray, D.W. and Prell, W.L., 1999a. Climatically linked oscillations in Arabian Sea denitrification over the past 1 m.y.: Implications for the marine N Cycle. Paleoceanography, 14, 732-743.

Altabet, M.A., François, R., Murray, D.W. and Prell, W.L., 1995. Climate-related variations in denitrification in the Arabian Sea from sediment $^{15}N/^{14}N$ ratios. Nature, 373, 506-509.

Altabet, M.A., Pilskain, C., Thunnell, R., Priede, C., Sigman, D., Chavez, F., and François, R., 1999b. The nitrogen isotopic biogeochemistry of sinking particles from the margin of the eastern North Pacific. Deep Sea Research, Part I, 46, 655-679.

Amakawa, H., Nozaki, Y., Alibo, D.S., Zhang, J., Fukugawa, K. and Nagai, H., 2004. Neodymium isotopic variations in Northwest Pacific waters. Geochim. Cosmochim. Acta, 68, 715-727.

Amit, O. and Bein, A., 1982. Organic matter in Senonian phosphorites from Israel – origin and diagenesis. Chem. Geol., 37, 277-287.

Anderson, L.D. and Sarmiento, J.L., 1994. Redfield ratios of remineralization determined by nutrient data analysis. Global Biogeochem. Cycles, 8, 65-80.

Anderson, L.D., Delaney, M.L. and Faul, K.L. 2001. Carbon to phosphorus ratios in sediments: Implications for nutrient cycling. Global Biogeochem. Cycles, 15: 65-79.

Barron, E.J. and Frakes, L.A., 1990. Climate model evidence for variable continental precipitation and its significance for phosphorite formation. In: Phosphate Deposits of the World, Vol.3, Neogene to Modern Phosphorites (Burnett W.C. and Riggs S.R., eds.). Cambridge University Press, Cambridge, pp. 260-272.

Barron, E.J., Harrison, C.G.A., Sloan II, J.L. and Hay, W.W., 1981. Paleogeography, 180 million years ago to the present. Eclogae Geologicae Helvetiae, 74, 443-470.

Bailey, T.R., McArthur, J.M., Prince, H. and Thirlwall, M.F., 2000. Dissolution methods for strontium isotope stratigraphy: whole rock analysis. Chem. Geol., 167, 313-319.

Barnes, C.R., 1999. Paleoceanography and paleoclimatology: an Earth system perspective. Chem. Geol., 161, 17-35.

Barber, R.T. and Smith, R.L., 1981. Coastal upwelling ecosystems. In: Longhurst, A.R. (Ed.), Analysis of Marine Ecosystems. Academic Press, New Yprk, N.Y., pp. 31-68.

Baturin, G.N., Lucas, J. and Prévôt-Lucas, L., 1995. Phosphorus behaviour in marine sedimentation. Continuous P-behaviour versus discontinuous phosphogenesis. C.R. Acad. Sci. Paris, 321, 263-278.

Bein, A., Almogi-Labin, A. and Sass, E., 1990a. Sulfur sinks and organic carbon relationships in Cretaceous organic-rich carbonates: implications for evaluation of oxygen-poor depositional environments. Am. J. Sci., 290, 882-911.

Bein, A., Sass, E. and Almogi-Labin, A., 1990b. Paleoceanography and geochemistry of oil shales in the Upper Cretaceous sequence in Israel: Inplications for exploration of a high-energy resource. Isr, Geol. Surv. Rep. GSI/8/90.

Berggren, W.A. and Hollister, C.D., 1977. Plate tectonics and paleocirculation-commotion in the ocean. Tectonophysics, 38, 11-48.

Berggren, W.A., Kent, D.V., Swisher, C.C. and Aubry, M.-P. 1995. A revised Cenozoic geochronology and chronostratigraphy. In: Berggren, W.A., Kent, D.V., Aubry, M.-P. and Hardenbol, J. (Eds), Geochronology, Time Scales and Global Stratigraphic Correlation. SEPM Spec. Publ., 54., pp. 129-212.

Berner, R.A., 1994. GEOCARB II: A revised model of atmospheric CO_2 over Phanerozoic time. Amer. Jour. Sci., 294, 56-91.

Berner, E.K. and Berner, R.A. (1995). Global environment: Water, air and geochemical cycles. Prentice-Hall.

Boujo, A., 1976. Contribution à l'étude géologique du gisement de phosphate Crétacé-Eocène des Ganntour (Maroc occidental). Sci. Geol. Mem., 43, 227p.

Bréhéret, J.-G., 1988. La francolite des concrétions phosphatées, un indicateur de diagenèse; le cas de l'Aptien-Albien du basin vocontien (SE France). C.R. Acad. Sci. Paris, 306, 1017-1022.

Burke, W.H., Denison, R.E., Hetherington, E.A., Koepnick, R.B., Nelson, H.F. and Otto, J.B., 1982. Variation of $^{87}Sr/^{86}Sr$ throughout Phanerozoic time. Geology, 10, 516-519.

Bushinski, G.I., (1966). The origin of marine phosphorites. Lith. Miner. Res., 3, 681-699.

Butterlin, J., Vrienlick, B., Bignot, G., Clermonte, J., Colchen, M., Dercourt, J., Guiraud, R., Poisson, A. and Ricou, L.-E., 1993. Lutetian (46 to 40 Ma). In: Dercourt, J., Ricou, L.E., and Vrielynck, B. (Eds.), Atlas Tethys Palaeoenvironmental Maps, Explanatory Notes. Paris, Gauthier-Villars, p. 197-209.

Camoin, G., Bellion, Y., Dercourt, J., Guiraud, R., Lucas, J., Poisson, A., Ricou, L.E. and Vrielynck, B., 1993. Late Maastrichtian (69.5 to 65 Ma). In: Dercourt, J., Ricou, L.E., and Vrielynck, B. (Eds.), Atlas Tethys Palaeoenvironmental Maps. Maps. BEICIP-FRANLAB, Rueil-Malmaison.

Cheney, T.M., McClellan, G.H. and Montgomery, E.S., 1979. Sechura phosphate deposits, their stratigraphy, origin and composition. Econ. Geol., 74: 232-259.

Clarke, R.S. Jr., Altschuler, Z.S., 1958. Determination of the oxidation state of uranium in apatite and phosphorite deposits. Geochim. Cosmochim. Acta 13, 127-142.

Clauer, N., Hoffert, M., Grimaud, D. and Millot, G., 1975. Composition isotopique du strontium d'eaux interstitielles extraites de sédiments recents: un argument en faveur de l'homogénéisation isotopique des sédiments argileux. Geochim. Cosmochim. Acta, 39, 1579-1582.

Colman, A.S., and Holland, H.D., 2000. The global diagenetic flux of phosphorus from marine sediments to the oceans: redox sensitivity and the control of atmospheric oxygen levels, In: Glenn, C.R., Prevot-Lucas, L., and Lucas, J., eds., Marine Authigenesis: From Global to Microbial: SEPM Special Publication 66, p. 53–75.

Compton, J.S, Hoddel, D.A., Garrido, J.r. and Mallinson, D.J., 1993. Origin and age of phosphorite from the south-central Florida Platform: Relation of phosphogenesis to sea-level fluctuations and $\delta^{13}C$ excursions. Geochim. Cosmochim. Acta, 57, 131-146.

Cook, P.J., and McElhinny, M.W., 1979. A re-evaluation of the spatial and temporal distribution of sedimentary phosphate deposits in the light of plate tectonics. Econ. Geol. 74, 315-330.

Dean, W.E., Arthur, M.A. and Claypool, G.E., 1986. Depletion of ^{13}C in Cretaceous marine organic matter: source, diagenetic, or environmental signal? Mar. Geol., 70, 119-157.

De Baar, H.J.W., Bacon, M.P. and Brewer, P.G., 1985. Rare earth elements in the Pacific and Atlantic oceans. Geochim. Cosmochim. Acta 49, 1943-1959.

De Boer, P.L., 1986. Changes in the organic carbon burial during the Early Cretaceous. In: Sumerhayes, C.P. and Shakelton, N.J. (Eds.), North Atlantic Palaeoceanography. Geol. Soc. London, Spec. Pub. 21, 321-331.

Delaney, M.L., 1998. Phosphorus accumulation in marine sediments and the oceanic phosphorus cycle. Global Biogeochem. Cycles, 12, 563-572.

Delaney, L.M. and Filippelli, G.M., 1994. An apparent contradiction in the role of phosphorus in Cenozoic chemical mass balances for the world ocean. Paleoceanography, 9, 513-527.

De La Rocha, C.L. and DePaolo, D.J., 2000, Isotopic evidence for variations in the marine calcium cycle over the Cenozoic. Science, 289, 1176-1178.

DePaolo, D.J. and Finger, K.L., 1991. High resolution strontium isotope stratigraphy and biostratigraphy of the Miocene Monterey Formation, central California. Geol. Soc. Am. Bull., 103, 112-124.

Deyhle, A., Macdougall, J.D., Macisaac, C. and Paytan, A., 2002, Temperature dependence of Ca isotope fractionation in marine carbonates: 12th Annual Goldschmidt Conference, Davos, Abstracts, p. A181.

Edmond, C.R., 1969. Direct determination of fluoride rock samples using the specific ion electrode. Analytical Chemistry, 41, 1327-1328.

Falkowski, P.G., 1997. Evolution of the nitrogen cycle and its influence on the biological sequestration of CO_2 in the ocean. Science, 387, 272-275.

Filippelli, G.M., 2001. Carbon and phosphorus cycling in anoxic sediments of the Saanich Inlet, British Columbia. Mar. Geol., 174, 307-321.

Filippelli, G.M. and Delaney, M.L., 1994. The oceanic phosphorus cycle and continental weathering during the Neogene. Paleoceanography, 9, 643-652.

Filippelli, G.M., Delaney, M.L., Garrison, R.E., Omarzai, S.K., Behl, R.J., 1994. Phosphorus accumulation rates in a Miocene low oxygen basin: The Monterey Formation (Pismo Basin), California. Mar. Geol., 116, 419-430.

Föllmi, K.B., 1989. Evolution of the Mid-Cretaceous Triad. Lecture Notes of Earth Sciences, 23, Springer-Verlag, Berlin Heidelberg, 153p.

Föllmi, K.B., 1996, The phosphorus cycle, phosphogenesis and marine phosphate-rich deposits. Earth-Sci. Rev., 40, 55-124.

Föllmi, K.B., Weissert, H., Bisping, M. and Funk, H., 1994. Phosphogenesis, carbon-isotope stratigraphy, and carbonate-platform evolution along the Lower Cretaceous northern Tethyan margin. Geol. Soc. Am. Bull., 106, 729-746.

Freeman, K.H., Hays, J.M., Trendel, J.-M. and Albrecht, P. 1990. Evidence for carbon isotope measurements for diverse origins of sedimentary hydrocarbons. Nature, 343, 254-256.

Froelich, P.N., Bender, M.L., Luedtke, N.A., Heath, G.R. and DeVries, T., 1982. The marine phosphorus cycle. Amer. J. Sci., 282, 474-511.

Froelich, P.N., Arthur, M., Burnett, W.C., Deakin, M., Hensley, V., Jahnke, R., Kaul. L., Kim, K., Roe, K., Soutar, A. and Vatakanon, C., 1988. Early diagenesis of organic matter in Peru continental margin sediments: phosphorite precipitation. Mar. Geol., 80, 309-346.

Ganeshram, R.S., Pedersen, T.F., Calvert, S.E., McNeill, G.W. and Fontugne, M.R. 2000. Glacial-interglacial variability in denitrification in the world's oceans: Causes and consequences. Paleoceanography, 15, 361-376.

Garrison, R.E., Kastner, M. and Reimers, C.E., 1990. Miocene phosphogenesis in California. In: Burnett W.C. and Riggs S.R. (Eds.), Phosphate Deposits of the World, Vol.3, Neogene to Modern Phosphorites. Cambridge University Press, Cambridge, pp. 285-299.

Glenn, C.R., 1990. Pore water, petrologic and stable carbon isotopic data bearing on the origin of Modern Peru margin phosphorites and associated authigenic phases. In: Burnett, W.C., Riggs, S.R. (Eds.), Phosphate Deposits of the World, Vol. 3, Neogene to Modern Phosphorites. Cambridge University Press, Cambridge, pp. 47-61.

Glenn, C.R. and Arthur, M.A., 1985. Sedimentary and geochemical indicators of productivity and oxygen contents in modern and ancient basins: The Holocene Black Sea as the "Type" anoxic basin. Chem. Geol., 48, 325-354.

Glenn, C.R. and Arthur, M.A., 1988. Petrology and major element geochemistry of Peru margin phosphorites and associated diagenetic minerals: authigenesis in modern organic-rich sediments. Mar. Geol., 80, 231-26.

Glenn, C.R. and Arthur, M.A., 1990. Anatomy and origin of a Cretaceous phosphorite-greensand giant, Egypt. Sedimentology, 37, 123-154.

Glenn, C.R., Föllmi, K.B., Riggs, S.R., Baturin, G.N., Grimm, K.A., Trappe, J., Abed, A., Galli-Olivier, C., Garrison, R., Ilyin, A.V., Jehl, C., Rohrlich, V., Sadaqah, R.M.Y., Schidlowski, M., Sheldon, R.E. and Siegmund, H., 1994. Phosphorus and phosphorites: Sedimentology and environments of formation. Eclogae geol. Helv. 87, 747-788.

Gradstein, F.M., Agterberg, F.P., Ogg, J.G., Hardenbol, J.,,Van Veen, P., Thierry, J. and Huang, Z., 1995. A Triassic, Jurrassic and Cretaceous time scale. SEPM Spec. Publ., 54, 95-126.

Gromet, L.P., Dymek, R.F., Haskin, L.A., Korotev, R.L., 1984. The North American Shale composite: its compilation, major and trace element characteristics. Geochim. Cosmochim. Acta, 48, 2469-2482.

Guldbrandsen, R.A., 1970. Relation of carbon dioxide content of apatite of the Phosphoria Formation to regional facies. U.S. Geol. Surv. Prof. Paper, 700B, 9-13.

Gvirtzman, Z., 2004. Chronostratigraphic table and subsidence curves of southern Israel. Isr. J. Earth Sci., 53, 47-61.

Halicz, L., Galy, A., Belshaw, N.S. and O'Nions, R.K., 1999. High-precision measurement of calcium isotopes in carbonates and related materials by multiple collector inductively coupled plasma mass spectrometry (MC-ICP-MS). J. Anal. At. Spectom., 14, 1835-1838.

Haq, B.U., Hardenbol, J. and Vail, P.R., 1987. Chronology of fluctuating sea levels since the Triassic. Science, 235, 1156-1167.

Hay, W.W., 1995, Cretaceous paleoceanography. Geologica Carpathica, 46, 257-266.

Hayes, J.M., Strauss, H. and Kaufman, A.J., 1999. The abundance of ^{13}C in marine organic matter and isotopic fractionation in the global biogeochemical cucle of carbon during the past 800 Ma. Chem. Geol., 161, 103-125.

Hinrichs, K.-U., Hayes, J.M., Sylva, S.P., Brewer, P.G. and DeLong, E.F., 1999. Methane-consuming archaebacteria in marine sediments. Nature, 398, 802-805.

Hippler, D., Gussone, N., Darling, K., Eisenhauer, A. and Nagler, T.F., 2002. $\delta^{44}Ca$ in *N. pachy* (left): a new SST-proxy in polar regions. 12th Annual Goldschmidt Conference, Davos, Abstracts, p. A331.

Hodell, D.A., Mueller, R.A. and Garrido, J.R., 1991. Variations in the strontium isotopic composition of seawater during the Neogene. Geology, 19: 24-27.

Hollander, D.J. and Smith, M.A. 2001. Microbially mediated carbon cycling as a control on the d13C of sedimentary carbon in eutrophic Lake Mendota (USA): new models for interpreting isotopic excursions in the sedimentary record. Geochim. Cosmochim. Acta, 65, 4321-4337.

Howarth, M.K., 1981, Palaeogeography of the Mesozoic. In: Cokes, L.R.M. Ed.), The Evolving Earth. Cambridge, Cambridge University Press, p. 197 – 220.

Ingall, E.D. and Van Cappellen, P., 1990. Relation between sedimentation rate and burial of organic phosphorus and organic carbon in marine sediments. Geochim. Cosmochim. Acta, 54, 373-386.

Ingall, E.D. and Jahnke, R.A.,1997. Influence of water- column anoxia on the elemental fractionation of carbon and phosphorus during sediment diagenesis. Mar. Geol., 139, 219-229.

Ingall, E.D., Bustin, R.M. and Van Cappellen, P., 1993. Influence of water column anoxia on the burial and preservation of carbon and phosphorus in marine shales. Geochim. Cosmochim. Acta, 57, 303-316.

Jacobsen, S.B. and Wasserburg, G.J., 1980. Sm-Nd isotopic evolution of chondrites. Earth Planet. Sci. Lett., 50, 139-155.

Jahnke, R.A., 1996, The global ocean flux of particulate organic carbon: Areal distribution and magnitude, Global Biogeochem. Cycles, 10, 71-88.

Jahnke, R.A., Emerson, S.R., Roe, K.K. and Burnett, W.C., 1983. The present day formation of apatite in Mexican continental margins sediments. Geochim. Cosmochim. Acta, 47, 259-266.

Jahnke, L.L., Summons, R.E., Hope, J.M. and Des Marais, D.J., 1999. Carbon isotopic fractionation in lipids from methanotrophic bacteria II: the effects of physiology and environmental parameters on the biosynthesis and isotopic signatures of biomarkers. Geochim. Cosmochim. Acta, 63, 79-93.

Jallad, I.S., Abu Murrey, O.S., Sadaqah, R.M., 1989. Upper Cretaceous phosphorites of Jordan. In: Notholt, A.J.G., Sheldon, R.P. and Davidson, D.F. (Eds.), Phosphate Deposits of the World. Cambridge University Press, Cambridge, pp. 344-351.

Jarvis, I., Burnett, W.C., Nathan, Y., Almbaydin, F.S.M., Attia, A.K.M., Castro, L.N., Flicoteaux, R., Hilmy, M.E., Husain, V., Qutawnah, A.A., Serjani, A. and Zanin, Y.N., 1994. Phosphorite geochemistry: State-of-the-art and environmental concerns. Eclogae geol. Helv. 87, 643-700.

Jenkyns, H.C., Grocke, D.R. and Hesselbo, S.P., 2001. Nitrogen isotope evidence for water mass denitrification during the early Toarcian (Jurassic) oceanic anoxic event. Paleoceanography, 16, 593-603.

Jewell, P.W., 1995, Geological consequences of global encircling equatorial currents: Geology, v. 23, 117–120.

Keto, L.S., and Jacobsen, S.B., 1988, Nd isotopic variations of Phanerozoic paleoceans: Earth and Planet. Sci. Let., 90, 395-410.

Kolodny, Y., 1980. Carbon isotopes and depositional environments of high productivity sedimentary sequence – the case of the Mishash Formation, Israel. Isr. J. Earth Sci., 29, 147-156.

Kolodny, Y. and Raab, M., 1988. Oxygen isotopes in phosphatic fish remains from Israel: paleothermometry of tropical Cretaceous and Tertiary shelf waters. Palaeogeogr. Palaeoclimatol. Palaeoecol., 64, 59-67.

Larson, R.L., 1991, Latest pulse of Earth: Evidence for a mid-Cretaceous superplume. Geology, 19, 547-550.

Laws, E.A., Popp, B.N., Bidigare, R.R., Kennicutt, M.C. and Macko, S.A., 1995. Dependence of phytoplankton carbon isotopic composition on growth rate and $[CO_2]_{aq}$: Theoritical considerations and experimental rsults. Geochim. Cosmochim. Acta 59, 1131-1138.

Lécuyer, C., Reynard, B. and Grandjean, P., 2004. Rare earth element evolution of Phanerozoic seawater recorded in biogenic apatites. Chem. Geol., 204, 63-102.

Lewy, Z., 1990. Transgressions, regressions and relative sea level changes on the Cretaceous shelf of Israel and adjacent countries. A critical evaluation of Cretaceous global sea level correlations. Paleoceanography, 5, 619-637.

Lewy, Z., 2001. Campanian ammonites from the Mishash Formation (southern Israel) and their implication on ammonoid mode of life and functional morphology. Geol. Surv. Isr. Rep., GSI/38/01.

Lucas, J., Prévot, L., Ataman, G. and Gundogdu, N., 1979. Etude minéralogique et géochimique de la série phosphatée du Sul-Est de la Turquie (Mazidagi-Mardin). Sci. Géol. Bull., 39, 59-68.

Luyendyk, B., Forsyth, D., and Phillips, J.D., 1972, Experimental approach to the paleocirculation of the oceanic surface waters: Geological Society of America Bulletin, v. 83, p. 2649–2664.

Mackenzie, F.T., Ver, L.M., Sabine, C., Lane, M., and Lerman, A., 1993. C, N, P, S global biogeochemical cycles and modeling of global change. In: Wollast, R., Mackenzie, F. T., and Chou, L. (Eds.),

Interactions of C, N, P and S Biogeochemical Cycles and Global Change. Berlin, Springer-Verlag, p. 1-61.

Mahoney, J., Nicollett, C., and Dupuy, C., 1991. Madagascar basalts: Tracking oceanic and continental sources. Earth and Planetary Sci. Lett., 104, 350-363.

Martin, E.E., Scher, H.D., 2004. Preservation of seawater Sr and Nd isotopes in fossil fish teeth: bad news and good news. Earth and Planet. Sci. Lett., 220, 25-39.

Masse, J.P., Bellion, Y., Benkhelil, J., Ricou, L.-E., Dercourt, J., and Guiraud, R., 1993, Early Aptian (114 to 111 Ma). In: Dercourt, J., Ricou, L.E., and Vrielynck, B. (Eds.), Atlas Tethys Palaeoenvironmental Maps, Explanatory Notes. Paris, Gauthier-Villars, p. 135-152.

McArthur, J.M., 1994. Recent trends in strontium isotope stratigraphy. Terra Nova, 6, 331-358.

McArthur, J.M., Howarth, R.J. and Bailey, T.R., 2001. Strontium isotope stratigraphy: LOWESS Version 3. Best-fit line to the marine Sr-isotope curve for 0 to 509 Ma and accompanying look-up table for deriving numerical age. J. Geol., 109, 155-169.

McArthur, J.M., Sahami, A.R., Thirlwall, M., Hamilton, P.J. and Osborn, A.O., 1990. Dating phosphogenesis with strontium isotopes. Geochim. Cosmochim. Acta, 54: 1343-1351.

McArthur, J.M., Kennedy, W.J., Chen, M., Thirwall, M.F. and Gale, A.S., 1994. Strontium isotope stratigraphy for Late Cretaceous time: Direct numerical calibration of the Sr isotope curve based on the US Western Interior. Palaeogeogr. Palaeoclimatol. Palaeoecol., 108: 95-119.

McKelvey, V.E., Williams, J.S., Sheldon, R.P., Cressman, E.R., Cheney, T.M. and Swanson, R.W., 1959. The Phosphoria, Park City and Shedhorn Formations in the Western Phosphate Field. U.S. Geol. Surv. Prof. Pap., 313-A, 47 pp.

Meyers, P.A., 1997. Organic geochemical proxies of paleoceanographic, paleolinmologic, and paleoclimatic processes. Org. Geochem, 27, 213-250.

Murphy, A.E., Sageman, B.B. and Hollander, D.J., 2000. Eutrophication by decoupling of the marine biogeochemical cycles of C, N, and P: A mechanism for the Late Devonian mass extinction. Geology, 28, 427-430.

Nägler, Th.F., Eisenhauer, A., Müller, A., Hemleben C. and Kramers, J., 2000, The δ^{44}Ca-temperature calibration on fossil and cultured Globigerinoides sacculifer: New tool for reconstruction of past sea surface temperatures: Geophysics, Geophysics, Geosystems, 1, 1-9.

Parrish, J.T. and Curtis, R.L., 1982. Atmospheric circulation, upwelling, and organic-rich rocks in the Mesozoic and Cenozoic eras. Palaeogeogr. Palaeoclim. Palaeoecol., 40, 31-66.

Philip, J., Babinot, J.-F., Tronchetti, G., Fourcade, E., Ricou, L.-E., Guiraud, R., Bellion, Y., Herbin, J.-P., Combes, P.-J., Cornee, J.-J., and Dercourt, J., 1993, Late Cenomanian (94–92 Ma), *in* Dercourt, J., et al., eds., Atlas Tethys palaeoenvironmental maps, explanatory notes: Paris, Gauthier-Villars, p. 153–178.

Piepgras, D.J., and Wasserburg, G.J., 1980, Neodymium isotopic variations in seawater. Earth and Planet. Sci. Lett., 50, 128-138.

Piepgras, D.J., and Wasserburg, G.J., 1987. Rare earth element transport in the western North Atlantic inferred fron Nd isotopic observations. Geochim. Cosmochim. Acta, 51, 1257-1271.

Pomini-Papaioannou, F., 2001. Lithostratigraphy-sedimentology of the Upper Cretaceous phosphatic formations of the Ionian zone: mechanism of phosphatization – paleotectonic frame. Dept.of Geology, University of Athens, Gaia No 9, 174p.

Popp, B.P., Laws, E.A., Bidigare, R.R., Dore, J.E., Hanson, K.L. and Wakeman, S.G., 1998. Effect of phytoplankton cell geometry on carbon isotopic fractionation. Geochim. Cosmochim. Acta, 62, 69-77.

Prévot, L., 1988. Geochemistry, petrography, genesis of Cretaceous-Eocene phosphorites. The Ganntour deposit (Morocco): a type example. Mem. Soc. Geol. Fr., 158, 230p.

Rau, G.H., Arthur, M.A. and Dean, W.E., 1987. $^{15}N/^{14}N$ variations in Cretaceous Atlantic sedimentary sequences: implication for past changes in nitrogen biogeochemistry. Earth and Planet. Sci. Lett., 82, 269-279.

Reiss, Z., 1988. Assemblages from a Senonian high-productivity sea. Rev. de Paleobiologie, 2, 323-332.

Reynard, B., Lécuyer, C. and Grandjean, P., 1999. Crystal-chemical controls on rare-earth element concentrations in fossil biogenic apatites and implications for paleoenvironmental reconstructions. Chem. Geol., 155, 231-241.

Riggs, S., Stille, P. and Ames, D., 1997. Sr isotopic age analysis of co-occurring Miocene phosphate grain types on the north Carolina continental shelf. J. Sed. Res., 67, 65-73.

Ruttenberg, K.C., 1993. Reassessment of the oceanic residence time of phosphorus. Chem. Geol. 107, 405-409.

Ruttenberg, K.C. and Berner, R.A., 1993. Authigenic apatite formation and burial in sediments from non-upwelling, continental margin environments. Geochim. Cosmochim. Acta, 57, 991-1007.

Schenau, S.J. and De Lange, G.J., 2001. Phosphorus regeneration versus burial in sediments of the Arabian Sea. Mar. Chem., 75:201-217.

Schlanger, S.O., Jenkyns, H.C. and Premoli-Silva, I., 1981. Volcanism and vertical tectonics in the Pacific basin and related to global Cretaceous transgressions. Earth and Planet. Sci. Lett., 52, 435-449.

Schlesinger, W.H., 1997. Biogeochemistry, an analysis of global change. San Diego, Academic Press, 588 p.

Schmitt, A.-D., Chabaux, F., and Stille, P., 2003a. The calcium riverine and hydrothermal isotopic fluxes and the oceanic calcium mass balance: Earth Planet. Sci. Lett., 213, 503–518.

Schmitt, A.-D., Stille, P., and Venneman, T., 2003b, Variations of the $^{44}Ca/^{40}Ca$ ratio in seawater during the past 24 million years: evidence from $\delta^{44}Ca$ and $\delta^{18}O$ values of Miocene phosphates. Geochim., Cosmochim. Acta, 67, 2607-2614.

Scotese, C.R., Gahagan, L.M. and Larson, R.L., 1988. Plate tectonic reconstructions of the cretaceous and and Cenozoic ocean basins. Tectonophysics, 155, 27-48.

Shaw, H.F., and Wasserburg, G.J., 1985, Sm-Nd in marine carbonates and phosphates: Implications for Nd isotopes in seawater and crustal age: Geochimica et Cosmochimica Acta, v. 49, p. 503–518.

Sheldon , R.P., 1964. Paleolatitudinal and paleogeographic distribution of phosphorite. US Geol. Surv. Prof. Paper, 501C, 106-113.

Shields, G., Stille, P. and Brasier, M.D., 2000. Isotope records across two phosphorite giant episodes compared: The Precambrian-Cambrian and the Late Cretaceous – Recent. In: : Glenn, C.R., Prevot-Lucas, L., and Lucas, J. (Eds.), Marine Authigenesis, From Global to Microbial. SEPM Spec. Pub. 66, 103-115.

Skulan, J., DePaolo, D.J., and Owens, T.L., 1997, Biological control of calcium isotopic abundances in the global calcium cycle. Geochim., Cosmochim. Acta, 61, 2505-2510.

Slomp, C.P., Thompson, J. and de Lange, G.J., 2004. Controls of phosphorus regeneration and burial during formation of eastern Mediterranean sapropels. Mar. Geol., 203, 141-159.

Spivack, A.J., and Wasserburg, G.J., 1988. Neodymium isotopic composition of the Mediterranean outflow and the eastern North Atlantic. Geochim. Cosmochim. Acta, 52, 2767-2773.

Soudry, D. and Eyal, A., 1994. Har Nishpe phosphate deposit. Summary of geological survey 1993. Isr. Geol. Surv., Rep. GSI/16/94 and Rotem Deshanim, Rep. G/05/07/94.

Soudry, D. and Nathan, Y., 2001. Diagenetic trends of fluorine concentration in Negev phosphorites: Implications for carbonate fluorapatite composition during phosphogenesis. Sedimentology 48: 723-743

Soudry, D., Nathan, Y., Glenn, C., 2001. Phosphorus accumulation rates in the upper Cretaceous-Eocene of the southern Tethys margin. First year progress report. Submitted to the US-Israel Binational Science Foundation (BSF). Isr. Geol. Surv. and Univ. of Hawaii, Rep. TR-GSI/14/2001.

Soudry, D., Nathan, Y., Glenn, C., 2002. Phosphorus accumulation rates in the upper Cretaceous-Eocene of the southern Tethys margin. Second year progress report (2001-2002). Submitted to the US-Israel Binational Science Foundation (BSF). Isr. Geol. Surv. and Univ. of Hawaii, Rep. TR-GSI/14/2002.

Soudry, D., Nathan, Y., Glenn, C., 2004. Phosphorus accumulation rates in the upper Cretaceous-Eocene of the southern Tethys margin. Third year progress report (2002-2003). Submitted to the US-Israel Binational Science Foundation (BSF). Isr. Geol. Surv. and Univ. of Hawaii, Rep. TR-GSI/01/2004.

Soudry, D., Ehrlich, S., Yoffe, O., and Nathan, Y., (2002). Uranium oxidation state and related variations in geochemistry of phosphorites from the Negev (southern Israel). Chem.Geol., 189: 213-230.

Stille, P., 1992. Nd-Sr isotope evidence for dramatic changes of paleocurrents in the Atlantic Ocean during the past 80 m.y. Geology, 20, 387-390.

Stille, P., Steinmann, M. and Riggs, S.R., 1994a. Nd isotopic evidence for the evolution of the paleocurrents in the Atlantic and Tethys oceans during the past 180 Ma. Earth Planet. Sci. Lett., 144, 9-19.

Tissot, B.P. and Welte, D.H., 1978. Petroleum Formation and Occurrence. Springer, New York.

Tyrrell, T., 1999. The relative influences of nitrogen and phosphorus on oceanic primary production. Nature, 400, 525-531.

Tyson, R.V., and Funell, B.M., 1987, European Cretaceous shorelines, stage buy stage: Palaeogeogr., Palaeoclim., Palaeoecol., 59, 69-91.

Valentine, D.L. and Reeburgh, W.S., 2000. New perspectives on anaerobic methane oxidation: Environmental Microbiology, 2, 477-484.

Van Cappellen, P., and Ingall, D., 1996. Redox stabilization of the atmosphere and oceans by phosphorus-limited marine productivity. Science, 271, 493-496.

Van Cappellen, P.C., Slomp, C.P. (2002) Phosphorous burial in marine sediments. In: Abstracts Volume, Sixth. International Symposium on the geochemistry of the Earth's surface. Honolulu, Hawaii, pp. 239-244.

Watts, A.B., Bodine, J.H., and Ribe, N.M., 1980, Observations of flexure and the geological evolution of the Pacific Ocean Basin. Nature, 283, 532–537.

Wilkinson, B.H., and Algeo, T.J., 1989, Sedimentary carbonate record of calcium-magnesium cycling. Am. J. Sci., 289, 1158-1194.

Yarkoni, M., 1982. Mediterranean – Dead Sea plant, drillcore M-7. Tahal Engeneering and Consulting Ltd., Rep. 04/83/42.

Yarkoni, M., 1985. Hydroelectric plant Mediterranean – Dead Sea (the main tunnel), drillcore M-13. Tahal Engeneering and Consulting Ltd., Rep. 04/85/4.

Zhu, P., and MacDougall, J.D., 1998. Calcium isotopes in the marine envirionment and the oceanic calcium cycle. Geochim. Cosmochim. Acta, 62, 1691-1698.

List of works used for calculation of P and Ca accumulation rates and bulk sedimentation rates (see Table 6)

(1) Avni, Y., 1996. Raw materials for the building industry. Har Hamran (21-I) and Har Lotz (21-III) sheets. Isr.Geol.Surv., Rep. GSI/11/96.

(2) Avni, Y. and Heimann, A., 1996. Raw materials for the building industry. Har Segui (23-I), Har Karkom (23-II) and Har Zenifim (23-IV) sheets. Isr.Geol.Surv., Rep. GSI/14/96.

(3) Avni, Y., Ilani, S. and Itamar, A., 1996. Raw materials for the building industry. Mizpe Ramon (21-II) and Beerot Oded I(21-IV) sheets. Isr. Geol. Surv., Rep. GSI/12/96.

(4) Axelrod, S., 1966. Lithostratigraphy of the Main Phosphorite Member in the vicinity of the Oron syncline. M. Sc. Thesis, Hebrew University, Jerusalem, 68 p.

(5) Bar, Y. and Frishman, M., 1995. Gorer phosphate deposit – geology and phosphorites characteristics. Rotem Ampart Negev, Rep. G/01/08/95.

(6) Bar, G., Minster, T. and Gilat, A., 1996. Raw materials for the building industry. Har ardon (22-I), En Yahav (22-II) and Zofar (22-III, IV) sheets. Isr.Geol.Surv., Rep. GSI/13/96.

(7) Begin, B.Z., 1969. Deposit 5 – Oron. Summary of phosphate reserves. Isr. Geol. Surv., Rep. M.P. 502/69.

(8) Bein, A., Sass, E. and Almogi-Labin, A., 1990. Paleoceanography and geochemistry of oil shales in the Upper Cretaceous sequence in Israel: Inplications for exploration of a high-energy resource. Isr, Geol. Surv., Rep. GSI/8/90.

(9) Ben Ami, S., 1997. Hor Hahar West phosphate deposit: a preliminary report. Negev Rotem Ampart, Rep. G/07/11/97.

(10) Ben Ami, S., 1999. Hazeva B deposit – geological report (summary of the geological model). Rotem Ampart Negev, Rep. G/10/10/99.

(11) Ben Ami, S., 2000. Northern bituminous Yorqe'am and Nahal Gov phosphate deposits. Rotem Ampart Negev, Rep. G/12/09/00.

(12) Ben Ami, S. and Frishman, M., 1996. Hagor phosphate deposit – geology and phosphorites characteristics. Rotem Ampart Negev, Rep. G/11/02/96.

(13) Ben Ami, S., Shitrit, D. and Frishman, M., 1993. Nahash Zame phosphate deposit – geology and phosphorites characteristics. Rotem Ampart Negev, Rep. 1/6/93.

(14) Bloch, N., 1985. 4H phosphate deposit – Oron. Negev Phosphate Co, Rep. G/06/86.

(15) Cook, P.M., Roded, R. and Shiloni, Y., 1974. Phosphorite survey in Orahot and Hazeva deposits. Isr. Geol. Surv., Rep. M.P. 538/73.

(16) Eyal, A. and Frishman, M., 1994. Dimona phosphate deposit – Final geological report. Rotem Deshanim, Rep. 2/6/93.

(17) Eyal, A. and Soudry, D., 1994. The phosphate deposit of Har Nishpe. Rotem Ampart Negev, Rep. G/1/01/94 and Isr. Geol. Surv., Rep. TR-GSI/2/94.

(18) Gill, D. and Shiloni, Y., 1994. Geochemistry of the Arad basin phosphorites. Isr. Geol. Surv., Rep. GSI/8/94.

(19) Ilani, S. and Hirsh, F., 1996. Raw materials for the building industry. Makhtesh Katan (19-II), Sedom (20-I) and Neot Hakikar (19-IV, 20-III) sheets. Isr.Geol.Surv., Rep. GSI/10/96.

(20) Ilani, S., Segev, A., Itamar, A., Shirav (Schwartz) M. and Minster, T., 1977.. Potential of raw materials for the building industry in the Negev. Isr. Geol. Surv., Rep. M.P. 571/77.

(21) Itamar, A., Gilat, A., 1996. Raw materials for the building industry. Nizzana (17-IV), Shivta (18-III) and Sde Boker (18-IV) sheets. Isr.Geol.Surv., Rep. GSI/8/96.

(22) Itamar, A., Segev, A., Shirav, M., 1996. Raw materials for the building industry. Mizpe Sayyarim (25-I), Yotveta (25-II), Har Segov (25-III) and Beer Ora (25-IV) sheets. Isr. Geol. Surv., Rep. GSI/16/96.

(23) Lasman, N. and Folkman. Y., 1966. Raw material for lime industry in the Dimona. Isr. Geol. Surv., Rep. GSI/178/66.

(24) Lewy, Z., 1983. Phosphorite survey in the Har Teref area and the vicinities of Nahal Hawa. Isr. Geol. Surv., Rep. M.A. 8/83.

(25) Levy, Y., 1999a. Zin phosphate field. Strips 4-A, 5A. A geological report. Rotem Ampart Negev, Rep. G/6/6/99.

(26) Levy, Y., 1999b. Hor Hahar phosphate field. Strip 3-A. A geological report. Rotem Ampart Negev, Rep. G/11/12/99.

(27) Minster, T., Yoffe, O., Nathan, Y., Flexer, A., 1997. Geochemistry, mineralogy, and paleoenvironments of deposition of the Oil Shale Member in the Negev. Isr. J. Earth Sci., 46, 41-59.

(28) Nahmias, Y., 1979. Development of phosphate deposit 5 – Oron. A preliminary report. Negev Phosphate Comp., Rep. A/4-12.

(29) Nahmias, Y., Shiloni, Y. and Rotenberg, K., 1974. The phosphate deposit of Hor Hahar. Geological survey, May 1972. Negev Phosphate Comp. Rep. G/10/74 and Isr. Geol. Surv. Rep. M.P 553/74.

(30) Roded, R., 1973. Preliminary investigation of raw material of limestone for cement industry in Oron area. Internal report, Isr. Geol. Surv. (unpublished data)

(31) Roded, R., 1980. Phosphate deposit 5 – Oron. Geology and summary of phosphate reserves. Negev Phosphate Co., Rep. G/55/80.

(32) Roded, R. and Lewy, Z., 1996. Raw materials for the building industry. Dimona (19-I) and Oron (19-III) sheets. Isr. Geol. Surv., Rep. GSI/9/96.

(33) Roded, R., Shiloni, Y., Cook. P. and Ginsburg, D., 1972. The phosphate deposits along Nahal Zin (general report). Part 1, geological survey; part 2, Mechanical beneficiation tests. Isr. Geol. Surv., Rep. M.P. 530/72.

(34) Segev, A., 1975. Porcelanite occurrences in the Hor Hahar area. M. Sc. Thesis, Hebrew University, Jerusalem, 60 p.

(35) Shahar, Y., 1968. Type section of the Campanian - Maastrichtian Ghareb Formation in the Oron syncline (northern Negev). Geological Survey of Israel, Stratigraphic Section, 6, 8 pp.

(36) Shiloni, Y., 1966a. Zefa Ef'e phosphate deposit. Isr. Geol. Surv., Rep. M.P. 154/66.

(37) Shiloni, Y., 1966b. The phosphate deposit at the Makhtesh Katan margins. Isr. Geol. Surv., Rep. M.P. 176/66.

(38) Shiloni, Y., 1967. Zefa – Ef'e phosphate deposit; report No 3. Isr. Geol. Surv., Rep. MP/182/67.

(39) Shiloni,Y., 1969. The phosphate deposit of Nahal Dimona. Isr. Geol. Surv. Rep. M.P. 190/69.

(40) Shiloni, Y. and Shahar, Y., 1969. The phosphate deposit of Ein Ofarim. Isr. Geol. Surv., Rep. M.P. 196/69.

(41) Shiloni, Y. and Roded, R. 1974. The phosphate deposit of Ein Ofarim. Isr. Geol. Surv., Rep. 519/74.

(42) Shiloni, Y. and Rapp, A., 1986. The phosphorite section of Hatrourim area. 8th Meeting of Mineral Engineering, Ashkelon, pp. 231-234.

(43) Shiloni, Y. and Minster, T., 1991. The bituminous section in the Nahal Zin area. Isr. Geol. Surv., Rep. GSI/21/91.

(44) Shirav, M. and Segev, A., 1995. Raw material for the building industry. Har Segov (25 – III), South Beer Ora (25-IV) and Eilat (26-I, II) sheets. Isr. Geol. Surv., Rep. GSI/33/95.

(45) Shitrit, D., 1985. Hazeva phosphate deposits (northern and southern parts). Final geological report, Negev Phosphate Co., Rep. G/138/85.

(46) Shitrit, D., 1989. Hazeva B phosphate deposit. Negev Phosphate Co., Rep. G/2/89.

(47) Shitrit, D., 1995. South Hatrourim phosphate deposit: A geological and technological report. Rotem Ampart Negev, Rep. G/10/11/95.

(48) Shitrit, D., Pinsky, Y. and Shiloni Y., 1985. Saraf – Hagor phosphate deposits. Negev Phosphate Co., Rep. G/134/85.

(49) Soudry, D. (1980) Geological survey for phosphorites in the Nahal Shilhav-Har Omer and Har Nishpe areas. Isr. Geol. Surv. Rep. M.P. 596/80.

(50) Soudry, D., 1982. Data on the Phosphorite Unit in the Nahal Hiyon and Har Nishpe areas. Isr. Geol. Surv., Rep. 432/82.

(51) Soudry, D. and Mor, U. (1985). Phosphorite survey along the northern Arava margins. Isr. Geol. Surv., Rep. 597/80.

(52) Soudry, D. and Eyal, A., 1994. Har Nishpe phosphate deposit. Summary of geological survey 1993. Isr. Geol. Surv., Rep. GSI/16/94 and Rotem Deshanim, Rep. G/05/07/94.

(53) Soudry, D. and Mimran, Y., 1996. Raw materials for the building industry. Paran (24-I, II) and Yahel (24-III, IV) sheets.Isr. Geol. Surv., Rep. GSI/15/96.

(54) Soudry, D., Nathan, Y., Glenn, C.R., 2001. Phosphorus accumulation rates in the Upper Cretaceous – Eocene of the southern Tethys margin. Isr. Geol. Surv. and University of Hawaii, Rep. TR-GSI/14/2001

(55) Tsur, A., 1998. Rotem mine – Eastern marginal strips (Dekel 3, 4, 5). Rotem Ampart Negev, Rep. G/04/07/98.

(56) Wollin, S., 1997. Phosphate deposit 6 – a preliminary geological report. Rotem Ampart Negev, Rep. G/06/09/97.

(57) Wurzburger, U. and Shilo, A., 1963. Ein Yahav phosphate deposits – Shizaf field. Isr. Geol. Surv., Rep. M.P. 133/63.

(58) Wurzburger, U., Shilo, A. and Gross, S., 1964. Hameishar phosphate deposit. Isr. Geol. Surv., Rep. M.P. 141/64.

(59) Wurzburger, U., Lasman, N., Gross, S., and Shiloni, Y., 1963. The Zefa – Ef'e phosphate deposit (Arad Region – southern Israel). Isr. Geol. Surv., Rep. M.P. 126/62.

(60) Yastrov, U., 1990. Northern Negev – summary of results. Negev Phosphate Co.

(61) Zohar, E. and Shiloni, Y., 1987. The Arad basin phosphate deposit. Isr. Geol. Surv., Rep. GSI/19/87.

Table 1. CFA samples analyzed for $^{87}Sr/^{86}Sr$, $^{143}Nd/^{144}Nd$ and $^{44}Ca/^{42}Ca$

Sample No	Stratig. interval	CFA phase	Source	Procedure of CFA separation			Natural sample (without carbonate)	Isotopic measurements		
				TAC	Heating	Hand-picking		$^{87}Sr/^{86}Sr$	$^{143}Nd/^{144}Nd$	$^{44}Ca/^{42}Ca$
OG-5	L. Eo.	N	1	+				+	+	+
D4/01	L. Eo.	Mm	1	+				+	+	+
D10/01	L. Eo.	S	1	+				+	+	n.d.
D17/01	L. Eo.	N	1	+				+	+	+
D32a/01	L. Eo.	Mm	1	+				+	+	+
S1/02a	L. Eo.	N	1	+				+	+	+
S1/02b	L. Eo.	N	1		+			+	+	+
S17/02	Ypr.	P	2	+				+	+	+
S18/02	Ypr.	P	3	+				+	+	+
S19/02	Mont.	P	2	+				+	+	n.d.
S16/02	U. Ma.	P	2	+				+	n.d.	+
S20/02	U. Ma.	P	2	+				+	+	+
S29/03	U. Ma.	P	2	+				+	+	n.d.
S30/03	U. Ma.	P	2	+				+	+	+
S7/02	U. Ma.	P	4	+				+	+	+
OG-4	U. Ma.	N	1	+				+	+	n.d.
S13/02	U. Ma.	P ± S	1	+				+	+	+
S6/02	L. Ma.	N	1	+				+	+	+
OG-12	L. Ma.	N	1	+				+	+	n.d.
D8/01	L. Ma.	N	1	+				+	+	+
D26/01	L. Ma.	N	1	+				+	+	+
S5/64-65a	L. Ma.	P	1	+				+	+	+
AT/85	U. Ca.	P	5	+				+	+	n.d.
S10/02	U. Ca.	N	1	+				+	n.d.	+
D9/01	U. Ca.	Mm	1	+				+	n.d.	+
D29/01	U. Ca.	N	1	+				+	+	+
Dis 13	U. Ca.	N	1	+				+	+	+
S14/02	U. Ca.	P	6	+				+	n.d.	n.d.
S15/02	U. Ca.	P	6	+				+	+	n.d.
D9/98	U. Ca.	P	6	+				+	+	+
S12/02	U. Ca.	P	6	+				+	+	+
SG/45	U. Ca.	P ± S	5	+				+	+	n.d.
OG-9	U. Ca.	P	1	+				+	+	n.d.
B2/L8	U. Ca.	P	1	+				+	+	n.d.
D12/01	U. Ca.	P	1	+				+	+	+
D18/01	U. Ca.	Int	1	+				+	+	+
B2/L7	U. Ca.	P	1	+				+	+	+
OG-11	U. Ca.	P	1	+				+	+	n.d.
SG/40	U. Ca.	P ± S	5	+				+	+	+
AS-1	U. Ca.	P	7	+				+	+	+
D11/01	U. Ca.	S	1	+				+	+	n.d.
OG-1	U. Ca.	P	1	+				+	+	n.d.
B2/L5	U. Ca.	P	1	+				+	+	n.d.
B2/L4	U. Ca.	P	1	+				+	+	n.d.
B2/29	U. Ca.	P	1			+		+	+	n.d.
B2/L2	U. Ca.	P	1	+				+	+	n.d.
15/31	U. Ca.	P	1			+		n.d.	n.d.	+

Table 1. (continued)

Sample No	Stratig. interval	CFA phase	Source	Procedure of CFA separation			Natural sample (without carbonate)	Isotopic measurements		
				TAC	Heating	Hand-picking		$^{87}Sr/^{86}Sr$	$^{143}Nd/^{144}Nd$	$^{44}Ca/^{42}Ca$
B2/L6	U. Ca.	P	1	+				+	+	n.d.
B2/L3	U. Ca.	P	1	+				+	+	+
B2/L1	U. Ca.	P	1	+				+	+	+
SG/32	U. Ca.	P ± S	5	+				+	+	+
SG/34	U. Ca.	P ± S	5	+				+	+	+
S1/71 -72	U. Ca.	P	1			+		n.d.	n.d.	+
D2/01	U. Ca.	N	1	+				+	+	+
D3/01	U. Ca.	S	1	+				+	+	+
SG/38	U. Ca.	P ± S	5	+				+	+	n.d.
SG/15	U. Ca.	P ± S	5	+				+	+	n.d.
SG/27	U. Ca.	P ± S	5	+				+	+	+
SG/12	U. Ca.	P ± S	5	+				+	+	n.d.
D34/01p	U. Ca.	P	1			+		n.d.	n.d.	+
D34/01s	U. Ca.	S	1			+		n.d.	n.d.	+
D14/01	U. Ca.	N	1	+				+	+	+
D15/01	U. Ca.	S	1					+	+	+
D30/01	L. Ca.	S	1	+				+	+	+
D6/01	Sa-Ca*	S	1	+				+	+	+
D27/01	Sa-Ca*	S	1	+				+	+	+
S2/02	Sa-Ca*	N	1	+				+	+	n.d.
32/01p	Sa-Ca*	P	1					+	+	+
32/01s	Sa-Ca*	S	1					+	+	+
ZS/18	U.Co.	P ± S	1	+				+	+	+
ZS/21	U.Co.	P ± S	1	+				+	+	n.d.
ZS/23	U.Co.	P ± S	1	+				+	+	n.d.
Ar-2	L. Co.	P± S	8	+				+	+	+
Ar-10a	L. Co.	P± S	8	+				+	+	+
Ar-10b	L. Co.	P± S	8		+			+	+	+
Ar-20a	L. Co.	P± S	8				+	+	+	n.d.
Ar-21	L. Co.	P± S	8	+				+	+	+
Ar-20c	L. Co.	P± S	8	+				+	+	+
S31/03	L. Co.	P± S	8	+				+	+	+
S32/03	L. Co.	P± S	8	+				(+)	+	+
6007	L. Co.	P± S	4	+				+	n.d.	+
6014	L. Co.	P± S	4	+				+	+	+
S33/03	M. Tu.	P± S	8	+				+	+	+
S34/03	M. Tu.	P± S	8					+	+	+
S3/02	M. Tu	N	8	+				+	+	+
D1/01	U. Ce.	N	6	+				+	+	+
S4/02	U. Ce.	Mm	9	+				+	+	n.d.
S5/02	L. Ce	Mm	9	+				+	+	n.d.
D42/01	L. Alb.	N	10	+				+	+	+
D7/01	L. Alb.	Mm	1	+				+	+	+
D43/01	L. Alb.	N	10	+				+	+	+
D49/01	L. Alb.	N	10	+				+	+	+
S27/03	E. Alb.	N	11	+				+	+	+

Table 1. (continued)

Sample No	Stratig. interval	CFA phase	Source	Procedure of CFA separation			Natural sample (without carbonate)	Isotopic measurements		
				TAC	Heating	Hand-picking		$^{87}Sr/^{86}Sr$	$^{143}Nd/^{144}Nd$	$^{44}Ca/^{42}Ca$
D45/01	U. Apt.	N	10	+				+	+	+
S26/03	U. Apt.	N	11					+	+	n.d.
S25/03	L. Bar.	N	11	+				+	+	+
S24/03	M. Haut.	N	11	+				+	+	+

Eo. – Eocene (undifferentiated); Ypr. – Ypresian; Mont. – Montian; Ma. – Maastrichtian; Ca. – Campanian; Sa-Ca* - Santoanian-Campanian transition; Co. – Coniacian; Tu. – Turonian; Ce. – Cenomanian; Alb. – Albian; Apt. – Aptian; Bar. – Barremian; Haut. – Hauterivian. L. – lower; M. – middle; U. – upper.
N – nodular; S – skeletal; Mm – megafossil mold; P – pelletal.
1 – Israel (Negev); 2 – Morocco (Ganntour); 4 – Tunisia (Gafsa); 5 – Greece (Ionian zone); 6 – Egypt (Red sea coast); 7 – Jordan (Al Abiad, Resaifa); 8 – Syria (Er Rakheime); 9 – Turkey (Mardin-Mazidagi); 10 – S. England (Isle of Wight, Lyme Regis); 11 – SE France (Fossé Vocontien); 12 – Helvetic Alps.
n.d. – not determined.

Table 2a. Elemental composition of separated (carbonate-free) CFA samples analyzed for $^{87}Sr/^{87}Sr$, $^{144}Nd/^{144}Nd$, and $\delta^{44}Ca$ (Major elements in wt%; minor and trace elements in $\mu g\ g^{-1}$)

Sample No	Ca	Mg	Na	K	Sr	SiO_2	Al	Fe	Ti	P	SO_4	Ca/P	Sr/P ($\times 10^{-4}$)
OG-5	30.0	0.18	0.53	400	1300	1.3	2000	2250	73.5	11.5	1.5	2.60	113
D4/01	29.1	0.30	0.96	170	2100	0.02	275	650	n.d	11.2	2.2	2.59	187
D17/01	34.4	0.09	0.34	170	1250	0.68	285	1000	n.d	13.5	2.2	2.52	93
D32a/01	34.9	0.26	0.87	310	2250	0.54	460	900	20	11.3	1.7	3.06	199
S1/02a	32.9	0.19	0.76	445	1620	0.14	940	1160	23	11.4	1.9	2.88	142
S1/02b	34.5	0.15	0.67	750	1800	0.14	2250	9950	80	11.4	1.1	2.99	158
S28/03	20.6	0.25	0.42	3000	1150	1.5	3650	1.0%	24	7.4	1.4	2.78	155
S17/02	9.5	0.12	0.13	200	420	0.43	725	360	8	3.5	0.5	2.71	120
S18/02	29.0	0.16	0.88	320	1800	0.53	700	530	20	10.9	5.7	2.66	165
S19/02	33.5	0.19	0.26	55	1700	0.35	300	220	37	14.0	1.4	2.39	121
S16/02	13.5	0.32	0.12	215	615	0.55	1100	700	13	5.2	0.6	2.59	118
S20/02	26.0	0.14	0.37	485	1100	1.4	2250	1050	27	10.5	1.2	2.47	105
S29/03	16.9	0.75	0.11	825	815	1.6	8300	0.3%	204	6.7	0.6	n.d.	2.52
S30/03	16.2	0.28	0.09	525	835	1.2	2500	0.2%	80	6.3	0.6	n.d.	2.57
S7/02	24.0	0.25	0.45	235	3070	0.83	2800	6100	24	9.6	1.0	2.50	319
OG-4	34.0	0.15	0.54	250	1850	0.77	1500	1400	26.0	13.3	1.6	2.55	139
S13/02	31.0	0.16	0.55	115	1720	0.70	1300	670	14	11.8	1.0	2.62	145
S6/02	33.0	0.26	0.65	545	1250	1.8	1900	2300	39.0	12.2	2.0	2.70	102
OG/12	36.0	0.15	0.63	185	2120	0.25	500	600	10	14.0	1.3	2.57	151
D26/01	33.8	0.19	0.65	135	2700	0.19	375	915	25	12.2	2.3	2.77	221
S5/64-65a	11.8	0.062	0.11	145	670	0.37	900	7000	21	4.4	1.8	2.68	152
AT/85	31.0	0.24	0.64	1700	1760	0.64	1600	2.2%	16	11.5	1.5	2.69	153
S10/02	35.0	0.16	0.53	135	2980	0.23	510	1350	11	13.5	0.8	2.59	220
D9/01	31	0.19	0.60	98	2450	0.13	200	1170	n.d	12.0	2.0	2.58	204
D29/01	36.9	0.12	0.43	170	2280	0.19	355	295	21	12.2	0.8	3.02	186
Dis13	30.6	0.20	0.87	340	2500	0.42	420	3000	25	11.4	1.7	2.68	219
S14/02	31.5	0.11	0.35	65	1770	0.39	730	200	9	13.1	0.9	2.40	135
S15/02	35.0	0.12	0.35	43	1690	0.19	340	102	8	14.0	0.6	2.50	121
D9/98	31.5	0.12	0.41	100	1680	0.32	500	230	9	12.7	0.7	2.48	132
S12/02	30.0	0.10	0.34	415	1460	0.12	160	80	8	11.8	0.9	2.54	124
SG/45	16.1	0.08	0.16	60	620	0.39	550	0.11	7	6.5	0.2	2.48	69
OG-9	35.5	0.08	0.30	65	1500	0.26	380	135	8	14.4	0.6	2.46	104
B2/L8	28.6	0.31	0.23	585	1600	1.2	3100	2700	29.2	11.3	0.65	2.53	142
D12/01	36	0.08	0.40	42	1700	0.13	50	54	n.d	15.0	2.0	2.40	113
D18/01	36.2	0.10	0.37	135	2000	0.13	235	280	19	12.7	0.7	2.85	157
B2/L7	38.2	0.08	0.23	200	2100	0.29	570	450	22.7	15.5	0.65	2.46	135
OG-11	30.5	0.08	0.34	26	1470	0.17	135	125	7	11.8	0.8	2.58	124
SG/40	25.6	0.11	0.26	80	1530	0.39	350	0.06	9	10.0	0.4	2.56	153
AS-1	32.5	0.13	0.37	73	1800	0.15	180	115	8	13.1	0.7	2.48	137
D11/01	36.0	0.10	0.53	85	2250	0.18	100	170	15.3	15.0	0.9	2.40	150
OG-1	31.5	0.16	0.45	270	1800	1.0	1900	930	27.7	12.0	1.3	2.62	150
B2/L5	27.5	0.04	0.16	40	1550	0.33	255	105	15.7	11.5	0.3	2.40	134
B2/L4	31.8	0.08	0.21	150	1800	0.58	855	350	24.0	13.7	0.4	2.32	131
B2/L2	36.0	0.05	0.20	15	1750	n.d.	160	165	21.0	15.0	0.45	2.40	116
B2/L6	38.0	0.06	0.18	75	2450	0.21	370	310	19.0	15.5	0.55	2.45	158
B2/L3	35.0	0.06	0.20	85	1700	0.40	530	250	21.5	14.8	0.4	2.36	114
B2/L1	36.0	0.07	0.25	15	1700	0.26	725	180	21.8	14.8	0.5	2.43	114
SG/32	25.7	0.11	0.13	70	990	0.63	1100	400	9	10.5	0.2	2.48	94
SG/34	22.2	0.10	0.09	185	815	0.75	1450	120	8	8.9	0.2	2.49	92
D3/01	33	0.13	0.45	41	1900	0.19	125	345	n.d	13.5	1.0	2.44	140

Table 2a. (continued)

Sample No	Ca	Mg	Na	K	Sr	SiO_2	Al	Fe	Ti	P	SO_4	Ca/P	Sr/P ($\times 10^{-4}$)
SG/38	26.1	0.05	0.13	65	955	0.36	500	200	8	10.7	0.2	2.43	89
SG/15	17.9	0.12	0.20	165	860	0.68	2300	0.12%	11	7.1	0.3	2.52	121
SG/27	19.5	0.05	0.13	225	760	0.52	600	0.06%	13	7.9	0.2	2.47	96
SG/12	8.8	0.05	0.10	90	440	0.49	1250	0.17%	7	3.4	0.2	2.58	129
D14/01	35.4	0.17	0.52	95	1950	0.12	72	200	17	12.2	1.7	2.90	160
D15/01	34.9	0.12	0.46	95	1580	0.13	150	280	18	12.7	0.9	2.74	124
D30/01	32.6	0.07	0.32	80	1650	0.16	160	250	n.d	13.5	0.9	2.42	122
D27/01	22.7	0.09	0.34	170	1250	0.68	1230	1000	n.d	9.2	1.2	2.47	135
S2/02	33.2	0.20	0.73	460	2150	0.63	900	1800	22.5	12.7	1.7	2.61	169
ZS/18	26.5	0.29	0.43	125	1790	0.76	900	3400	15	10.0	1.4	2.65	179
ZS/21	28.5	0.24	0.48	125	1910	0.74	515	3250	18	10.9	1.6	2.61	175
ZS/23	29.0	0.24	0.49	165	1920	0.53	700	4450	20	10.9	1.8	2.66	176
Ar-2	36.7	0.11	0.59	61	1570	0.05	53.5	50	24	14.4	1.1	2.54	109
Ar-10a	35.6	0.12	0.63	66	1560	0.06	68.5	67	23	13.9	1.1	2.56	112
Ar-10b	35.2	0.13	0.29	42.5	1580	0.85	235	910	45	14.4	1.1	2.44	110
Ar-20a	36.3	0.11	0.58	87	1530	0.11	160	64	27	13.5	1.1	2.68	113
Ar-21	36.4	0.11	0.61	73	1630	0.08	88	68	25	13.5	1.1	2.68	120
Ar-20c	36.6	0.11	0.61	74.5	1620	0.08	110	55	27	14.0	1.1	2.61	115
S31/03	20.3	0.07	0.34	60	750	0.11	40	190	11	7.3	0.8	2.78	102
S32/03	19.1	0.06	0.24	42	575	0.18	115	250	12	7.1	0.9	2.69	81
6007	35.6	0.37	1.1%	230	2280	0.08	220	110	23	12.2	2.2	2.91	187
6014	35.5	0.38	1.08%	240	2370	0.11	315	160	25	12.7	2.2	2.79	187
S33/03	27.1	2.1%	0.14	755	950	1.5	9700	2900	600	9.6	1.7	2.82	98
S34/03	29.7	0.09	0.67	620	1170	0.41	665	120	24	10.6	1.7	2.80	110
S3/02	31.8	0.11	0.87	340	1950	0.32	570	735	15.0	12.8	2.4	2.48	152
D1/01	15.9	0.19	0.19	165	650	0.44	900	2200	n.d	6.3	0.6	2.52	103
S4/02	27.0	0.12	0.41	710	1100	0.87	1200	2750	31.3	10.4	1.0	2.59	106
S5/02	28.0	0.16	0.54	620	1500	0.62	900	1950	30.0	10.8	1.3	2.59	139
D42/01	18.3	0.17	0.10	215	2080	0.77	4600	9850	19	6.5	0.1	2.77	320
D43/01	34.2	0.09	0.37	70	6360	0.22	775	2700	26	11.8	0.4	2.89	538
D49/01	28.1	0.16	0.10	190	2320	0.04	4350	8000	22	10.0	<0.1	2.81	232
S27/03	21.2	0.45	0.06	285	760	1.1	8350	2.2%	15	8.7	0.4	2.43	87
D45/01	24.5	0.065	0.13	345	1870	0.48	930	3150	16	8.7	0.5	2.81	214
S26/03	20.4	0.16	0.03	220	1400	0.40	1250	7100	19	7.9	0.9	2.58	177
S25/03	7.2	0.10	0.04	235	350	0.32	1700	3800	350	2.9	0.2	2.48	120
S24/03	13.1	1.2%	0.05	115	660	1.5	17000	4.6%	18	5.2	0.4	2.52	127

Table 2b. Elemental composition of separated (carbonate-free) CFA samples analyzed for $^{87}Sr/^{87}Sr$, $^{144}Nd/^{144}Nd$, and $\delta^{44}Ca$ (Trace elements in $\mu g\ g^{-1}$)

Sample No	Ag	As	Ba	Be	Cd	Co	Cr	Cu	Mn	Mo	Ni	Pb	Th	Sb	U	V
OG-5	0.7	22	20	0.3	20	1	180	15	290	0.8	23	19	0.8	0.6	150	230
D4/01	0.2	n.d	690	n.d	0.4	<1	28	5	20	0.6	7	4.5	n.d	n.d	n.d	33
D17/01	<0.2	n.d	21	n.d	5	<1	26	25	4	3.3	27	7.5	n.d	n.d	n.d	85
D32a /01	<0.5	5	775	775	0.3	<2	35	<2	18	0.8	8	2.5	0.1	0.3	81	38
S1/02a	2	4	1380	1380	17	<2	20	8	102	2.2	27	20	0.4	1.3	185	85
S1/02b	2.7	6	1440	1440	22	<2	33	8	135	6.5	40	22	0.5	1.8	164	100
S28/03	<0.1	3.5	46	n.d.	<0.1	4	80	5	200	3	14	n.d.	2.2	0.1	29	25
S17/02	<0.1	1.3	200	n.d.	8	<1	40	2.3	5.5	0.2	3.5	n.d.	2	0.1	16	23
S18/02	<0.1	1.8	320	n.d.	19	<1	75	<1	8	2.5	4	n.d.	15	0.1	27	28
S19/02	0.1	1.5	55	n.d.	12	<1	150	3.2	3	4	12	n.d.	0.9	0.5	55	100
S16/02	0.1	2.5	215	n.d.	14	<1	38	4	12	1.2	8	n.d.	4	0.3	33	21
S20/02	0.2	2.5	485	n.d.	13	<1	85	9.5	6	7.5	14	n.d.	5	0.4	88	43
S29/03	0.5	4	30	n.d.	12	1	74	7	20	1.5	12	n.d.	6.3	0.4	24	36
S30/03	0.3	3	22	n.d.	6	<1	53	4	8	1	9	n.d.	5	0.3	17	20
S7/02	<0.1	4	235	n.d.	0.6	3	23	11	94	0.3	17	n.d.	16	0.5	28	40
OG-4	0.4	20	40	0.3	32	1	90	7	7650	0.9	10	12	1.0	0.4	110	68
S13/02	<0.1	3.5	115	n.d.	0.3	3	43	21	100	0.5	14	n.d.	2.3	0.3	97	28
S6/02	0.2	10	250	<0.2	0.2	2	95	21	470	0.6	33	27	1.0	2.2	50	53
OG-12	0.4	1.1	185	n.d.	20	<1	40	9	33.5	3.8	8.5	n.d.	0.6	0.2	93	48
D26/01	<0.1	2	255	n.d.	12	<1	41	9	44	0.7	11	6	1	0.3	72	60
S5/64-65a	<0.5	30	140	140	11	<2	45	55	13	11	55	15	2.8	3.7	81	25
AT/85	0.1	16	73	n.d.	1.3	5	38	12	1000	3	43	n.d.	13	0.4	27	40
S10/02	<0.1	5	135	n.d.	10	<1	45	1	63	2.5	20	n.d.	0.2	0.4	55	18
D9/01	<0.2	n.d	150	n.d	0.4	<1	32.5	<1	80	0.4	13	1.2	n.d	n.d	n.d	11
D29/01	3.3	4	110	110	68	<2	42	17	6	8	20	15	0.7	3.4	132	38
Dis13	<0.5	7	230	230	0.6	<2	40	7	17	1	10	3.5	0.3	1.5	102	25
S14/02	<0.1	1.3	65	n.d.	1.0	<1	55	5	5	0.3	13	n.d.	3.5	0.1	73	57
S15/02	<0.1	3.5	140	n.d.	6	<1	40	9	6.5	0.3	4.5	n.d.	0.8	0.2	65	58
D9/98	<0.1	1.3	79	n.d.	1.0	<1	50	7.9	7	0.5	1	n.d.	4.5	0.1	56	36
S12/02	<0.1	1.0	415	n.d.	1.0	<1	28	2	6	0.4	3	n.d.	3.5	<0.1	53	31
SG/45	0.1	0.3	46	n.d.	13	<1	70	3	30	1	5	n.d.	0.2	<0.1	58	51
OG-9	0.3	1.5	65	n.d.	23	<1	40	20	7	1.3	8	n.d.	0.7	0.3	145	165
B2/L8	0.9	7	150	0.6	11	2	130	45	15	12	36	6	4	0.6	140	38
D12/01	<0.2	n.d	70	n.d	8	<1	13	6	6.5	9.5	1.5	0.9	n.d	n.d	n.d	97
D18/01	2	5	93	93	65	<2	33	15	5.5	10	10	15	0.6	3.6	155	50
B2/L7	1.0	4.5	200	0.6	22	<1	44	24	3.8	12	26	10	0.3	1.1	170	26
OG-11	0.1	5.5	26	n.d.	7	<1	65	15	7	1.4	8.5	n.d.	0.5	0.1	135	170
SG/40	0.5	0.9	115	n.d.	25	<1	60	11	13	3	4	n.d.	1.5	0.1	70	51
AS-1	0.1	1.0	77	n.d.	3.5	<1	40	4.3	3.8	0.4	1	n.d.	1.2	0.1	45	38
D11/01	0.4	5.5	185	1.0	55	1	17	11	5.5	5	7	9	0.3	0.8	85	110
OG-1	0.7	8	300	0.3	25	<1	75	6	37	0.6	8	12	5	0.6	130	60
B2/L5	0.4	1.4	110	0.6	24	<1	34	17	2.2	5	16	3	1.3	0.3	120	85
B2/L4	<0.2	4.0	125	1.2	80	<1	75	53	3	11	75	3	1.0	0.8	170	350
B2/L2	<0.2	2.5	160	0.7	94	<1	37	43	2.2	9	24	8	0.9	0.7	210	185
B2/L6	0.2	3.2	290	0.7	27	<1	50	15	3.3	8	25	3	0.2	0.5	155	180
B2/L3	0.2	2.3	145	1.0	50	<1	68	32	2.2	9	41	3	0.5	0.6	200	290
B2/L1	0.2	2.5	290	1.1	97	<1	50	27	3.8	9	28	9	1.0	0.7	160	155
SG/32	0.4	0.2	78	n.d.	4.8	<1	55	7	3	0.8	44	n.d.	1	0.3	26	8
SG/34	0.1	1	65	n.d.	4.3	<1	85	4	9	0.6	22	n.d.	2	<0.1	24	15

Table 2b. (continued)

Sample No	Ag	As	Ba	Be	Cd	Co	Cr	Cu	Mn	Mo	Ni	Pb	Th	Sb	U	V
D3/01	<0.2	n.d	160	n.d	4	,1	13	2.5	7.5	5.5	7	3.7	n.d	n.d	n.d	5
SG/38	<0.1	0.1	55	n.d.	4.5	<1	47	1	3	0.6	200	n.d.	0.4	<o.1	41	18
SG/15	0.2	0.5	85	n.d.	7	<1	94	9	170	0.5	9	n.d.	3.2	0.2	22	37
SG/27	0.4	0.3	165	n.d.	3	<1	50	7	6	0.5	225	n.d.	0.3	0.2	18	11
SG/12	0.5	0.7	1300	n.d.	3.5	<1	80	9	95	1.5	5	n.d.	3.5	0.2	8.5	16
D14/01	<0.5	3	100	100	6.5	<2	22	7	5	7	5	3	<0.1	0.7	117	22
D15/01	4	5	125	125	130	<2	23	15	2.8	13	22	64	0.3	2.8	104	23
D30/01	<0.2	n.d	49	n.d	56	<1	20	8	1	0.6	1	19	n.d	n.d	n.d	8
D27/01	0.3	n.d	41	n.d	30	<1	26	25	4	3.3	27	7.5	n.d	n.d	n.d	130
S2/02	0.4	4.2	320	0.7	20	<1	53	34	9	1.3	12	9	0.4	0.6	60	38
ZS/18	<0.1	8	55	n.d.	1.1	<1	62	17	6.5	1.7	21	n.d.	2.8	0.5	38	11
ZS/21	<0.1	13	125	n.d.	1.4	<1	65	20	4.5	1.7	24	n.d.	4	0.6	55	17
ZS/23	0.1	4	165	n.d.	1.2	<1	75	25	5	2.8	37	n.d.	3.5	0.7	58	22
ZS/18	<0.1	8	55	n.d.	1.1	<1	62	17	6.5	1.7	21	n.d.	2.8	0.5	38	11
ZS/21	<0.1	13	125	n.d.	1.4	<1	65	20	4.5	1.7	24	n.d.	4	0.6	55	17
ZS/23	0.1	4	165	n.d.	1.2	<1	75	25	5	2.8	37	n.d.	3.5	0.7	58	22
Ar-2	<0.5	6	98	0.5	6	<2	75	15	2.5	0.8	<5	4	0.2	0.5	60	75
Ar-10a	<0.5	6	105	0.6	23	<2	75	13	7.6	1.4	<5	5	0.2	0.5	52	63
Ar-10b	0.6	8	97	0.6	41	<2	120	32	20	0.8	22	1.8	0.1	0.5	61	87
Ar-20a	<0.5	7	96	0.8	18	<2	115	100	6.2	1.2	<5	1.5	0.1	0.6	67	94
Ar-21	0.5	6	108	0.9	25	<2	85	45	4.8	1.1	<5	7.5	0.3	1.4	66	79
Ar-20c	<0.5	6	100	0.9	15	<2	95	40	8	1.3	5	2.2	0.2	0.6	62	80
S31/03	0.2	2	60	n.d.	1.5	<1	48	12	3	0.5	68	0.5	0.1	0.2	32	64
S32/03	0.2	1.5	67	n.d.	14	1	53	17	14	0.4	110	0.8	<0.1	0.2	25	72
6007	<0.5	<1	22	<0.2	0.3	<2	15	<2	80	0.8	7	1.5	0.1	0.2	38	130
6014	<0.5	1	29	<0.2	0.3	<2	15	4	94	0.6	<5	2.6	0.3	0.2	44	165
S33/03	0.2	8	60.5	n.d.	1	1	85	12	13.5	1	20	3	3	0.3	40	120
S34/03	<0.1	2	63	n.d.	0.4	<1	20	10	3.5	0.4	15	1	8	0.2	43	15
S3/02	1.5	5.5	45	0.9	46	<1	5	7	1250	0.4	<2	12	8	0.6	5	5
D1/01	1.5	n.d	26	n.d	16	7.5	11	10	320	0.9	26	8.5	n.d	n.d	n.d	11
S4/02	0.6	2.4	25	0.8	9.5	1	13	3	95	0.1	2	22	1.2	0.7	34	50
S5/02	3.0	3.0	20	0.8	18	1	6	4	155	0.3	4	23	2.5	0.6	50	20
D42/01	8.5	6	450	450	33	<2	10	5	10	0.5	12	24	3.5	1.2	23	23
D43/01	8.5	3	2400	2400	54	<2	10	2	95	1.5	<5	20	1.2	2.7	102	22
D49/01	<0.5	5	425	425	0.15	<2	10	<2	10	0.1	11	13	2.5	0.1	216	6
S27/03	0.1	2	27	n.d.	0.2	2	68	5	30	0.6	16	n.d.	2.5	0.1	24	60
D45/01	1.5	16	550	550	3.5	<2	10	2	15	1	18	46	2.0	1.8	78	5
S26/03	0.3	6	14.5	n.d.	0.1	3	64	8	63	2.5	15	17	4	0.4	46	17
S25/03	0.4	1	5.7	n.d.	<0.1	<1	11	10	17	0.3	6	6.5	1.5	<0.1	13	4
S24/03	0.4	2	26	n.d.	0.1	1	83	3	6	0.3	15	n.d.	4	<0.1	20	55

Table 2c. Elemental composition of separated (carbonate-free) CFA samples analyzed for $\delta^{87}Sr/^{87}Sr$, $^{144}Nd/^{144}Nd$ and $\delta^{44}Ca$ (REEs in $\mu g\ g^{-1}$)

Sample No	Y	La	Ce	Pr	Nd	Sm	Eu	Tb	Gd	Dy	Ho	Er	Tm	Yb	Lu
OG-5	59	37	16	4.7	18.3	3.4	0.8	4.4	0.75	5.1	1.5	4.4	0.82	4.6	0.77
D4/01	n.d	18	4	1.4	6.6	1.1	0.2	0.31	2.2	2.5	0.7	2.6	0.37	2.4	0.38
D17/01	n.d	30	6.5	2.6	12.2	2.1	0.5	0.6	4.1	4.5	1.3	4.5	0.63	3.9	0.62
D32a/01	35	20	5	2.5	9.9	1.8	0.3	3.0	0.42	2.8	0.72	2.4	0.35	2.0	0.33
S1/02a	141	70	21	7.6	29	5.1	1.2	8.7	1.27	9.0	2.46	8.5	1.31	8.3	1.36
S1/02b	121	66	21	7.3	7.3	4.7	1.1	8.1	1.16	8.2	2.18	7.5	1.14	7.2	1.17
S28/03	23	23	54	5.5	22	4.3	1.2	0.65	4.4	3.5	0.68	1.9	0.29	1.48	0.22
S17/02	53	27	16	4.7	19.7	4.0	0.9	0.75	4.5	4.6	1.0	3.1	0.41	2.6	0.49
S18/02	113	100	118	21.3	85.4	16.4	2.6	2.56	16.3	14.2	3.0	8.9	1.17	7.5	1.4
S19/02	34	17	9	2.1	8.6	1.6	0.4	0.38	2.0	2.5	0.7	2.3	0.35	2.4	0.50
S16/02	34	19	23	4.2	17.1	3.5	0.7	0.59	3.6	3.5	0.8	2.3	0.30	1.9	0.37
S20/02	57	33	30	6.5	26.4	5.3	0.9	0.98	5.8	5.9	1.3	4.1	0.56	3.6	0.69
S29/03	32	23	37	6.1	24	4.7	1.3	0.68	4.3	3.8	0.78	2.2	0.35	1.82	0.28
S30/03	24	18	30	4.9	19	3.8	1.1	0.55	3.4	2.0	0.62	1.7	0.26	1.38	0.21
S7/02	538	375	153	70	280	57	11	11	62	62	14	39	5.0	29.6	5.3
OG-4	24	14	7	2.1	8.4	1.7	0.4	2.0	0.34	2.2	0.62	1.8	0.33	1.8	0.30
S13/02	134	68	24	9.0	37.4	7.5	1.5	1.67	9.4	11.1	2.8	9.0	1.3	8.5	1.7
S6/02	186	121	34	15	59	10.5	2.5	13.6	2.3	16	4.60	14	2.5	13.8	2.3
OG-12	34	17	8	2.5	10	2.1	0.3	0.46	2.6	3.0	0.7	2.4	0.35	2.3	0.46
D26/01	n.d	17	14	2.8	11	2.4	0.7	0.51	3.5	3.4	0.81	2.6	0.38	2.5	0.42
S5/64 -65a	84	30	19	5.2	21	4.2	1.0	6.3	0.90	5.9	1.45	4.8	0.72	4.5	0.75
AT/85	290	204	385	55	205	42	13.5	7.4	45	43	9.3	27	4.4	23	3.5
S10/02	22	14	10	2.0	7.4	1.3	0.2	0.30	1.7	2.1	0.5	1.9	0.30	2.2	0.47
D9/01	n.d	4.3	3.7	0.62	2.5	0.45	0.15	0.11	0.72	0.79	0.22	0.83	0.14	1.07	0.20
D29/01	37	17	6	2.2	8.4	1.6	0.3	2.7	0.39	2.7	0.71	2.4	0.38	2.5	0.44
Dis13	30	17	7	2.0	7.3	1.4	0.3	2.2	0.31	2.1	0.54	1.8	0.27	1.8	0.30
S14/02	51	36	29	7.9	27.3	5.3	0.9	0.87	5.4	5.0	1.1	3.4	0.45	2.0	0.54
S15/02	106	47	18	7.5	29	6.0	1.2	1.32	7.4	8.5	2.1	6.7	0.93	6.0	1.2
D9/98	71	48	40	9.0	36.3	7.2	1.3	1.2	7.4	6.8	1.5	4.6	0.60	3.8	0.71
S12/02	38	27	24	5.6	22.7	4.6	0.8	0.73	4.6	4.1	0.9	2.6	0.34	2.1	0.39
SG/45	18	10	11	4.3	5.8	1.0	0.3	0.20	1.2	1.3	0.34	0.9	0.15	0.90	0.14
OG-9	27	11	6	1.6	6.5	1.3	0.2	0.30	1.7	2.0	0.5	1.7	0.24	1.6	0.35
B2/L8	130	57	33	9.8	39	8.3	2.0	10.1	1.7	11.6	3.2	9.5	1.7	8.9	1.5
D12/01	n.d	9.8	3.3	1.13	4.9	0.92	0.25	0.25	1.66	1.83	0.51	1.78	0.25	1.76	0.30
D18/01	46	20	4	2.6	10	2.0	0.4	3.3	0.49	3.3	0.87	3.0	0.46	2.9	0.52
B2/L7	117	62	21	10	41	8.5	1.7	10.6	1.8	12.2	3.4	10	1.8	9.2	1.6
OG-11	30	11	5	1.5	6.3	1.3	0.3	0.30	1.7	2.0	0.5	1.8	0.26	1.7	0.37
SG/40	81	29	21	6.9	20	4.1	1.3	0.92	5.1	6.1	1.56	4.9	0.82	4.50	0.75
AS-1	40	19	10	3.4	11.9	2.3	0.5	0.48	2.7	3.0	0.7	2.4	0.32	2.1	0.41
D11/01	30	12	5	1.4	5.6	1.1	0.3	1.4	0.26	1.9	0.57	1.8	0.34	1.8	0.33
OG-1	86	50	30	9.4	38	8.0	1.7	9.0	1.5	9.4	2.4	6.9	1.2	6.0	0.99
B2/L5	30	12	6	1.7	6.8	1.3	0.3	1.8	0.31	2.2	0.64	2.0	0.36	2.0	0.36
B2/L4	32	11	7	1.6	6.7	1.4	0.4	1.7	0.30	2.1	0.59	1.8	0.33	1.7	0.31
B2/L2	38	14	7	2.0	8.1	1.6	0.4	2.1	0.36	2.5	0.72	2.2	0.40	2.1	0.38
B2/L6	30	14	6	2.0	8.1	1.6	0.3	2.1	0.36	2.5	0.74	2.3	0.42	2.2	0.39
B2/L3	32	11	5	1.4	5.8	1.2	0.3	1.5	0.27	1.9	0.55	1.7	0.31	1.7	0.30
B2/L1	44	15	9	2.3	9.4	1.9	0.5	2.4	0.41	2.8	0.82	2.5	0.45	2.5	0.43
SG/32	21	8.4	10	1.6	6.2	1.2	0.4	0.25	1.4	1.6	0.40	1.3	0.22	1.25	0.21
SG/34	26	12	19	4.8	11	2.2	0.7	0.39	2.2	2.3	0.57	1.6	0.27	1.51	0.24
D3/01	n.d	7.6	2.0	0.64	2.7	0.51	0.2	0.16	1.03	1.34	0.40	1.6	0.26	2.1	0.39

Table 2c. (continued)

Sample No	Y	La	Ce	Pr	Nd	Sm	Eu	Tb	Gd	Dy	Ho	Er	Tm	Yb	Lu
SG/38	17	6.6	7.5	4.0	4.5	0.9	0.3	0.19	1.0	1.1	0.32	0.9	0.16	0.90	0.15
SG/15	62	39	75	9.7	40	8.0	2.7	1.35	8.1	7.9	1.71	5.0	0.83	4.41	0.68
SG/27	5	1.7	1.2	0.30	1.2	0.25	<0.1	0.05	0.3	0.3	0.09	0.3	0.05	0.29	0.05
SG/12	35	23	48	6.5	27	5.8	1.6	0.94	5.5	5.5	1.14	3.4	0.55	2.93	0.44
D14/01	18	7.1	2.0	0.7	2.5	0.47	0.1	0.9	0.14	1.0	0.30	1.2	0.20	1.4	0.27
D15/01	15	6.5	2.6	0.7	2.4	0.48	0.1	0.8	0.13	0.9	0.26	1.0	0.18	1.3	0.25
D30/01	n.d	54	19	6.2	29	5.3	1.1	1.2	8.9	8.2	2.0	6.7	0.91	5.8	0.96
D27/01	n.d	140	97	23	103	19	4.0	3.4	27	20	4.4	13.5	1.7	9.7	1.5
S2/02	17	9	4	1.1	4.5	0.9	0.2	1.1	0.19	1.3	0.36	1.1	0.19	1.0	0.19
ZS/18	144	75	39	11	46	9.4	2.0	2.0	11.4	12.8	3.1	9.6	1.32	8.5	1.7
ZS/21	223	123	53	18	73	15.0	3.1	3.2	18.3	20.0	4.8	14.6	1.95	12.2	2.4
ZS/23	225	124	53	18	73	14.8	3.0	3.2	18.2	19.9	4.7	14.4	1.91	11.9	2.3
Ar-2	35	14	3.5	1.7	6.3	1.15	0.3	2.0	0.29	2.0	0.52	1.8	0.26	1.6	0.26
Ar-10a	39	15	3.8	1.7	7	1.28	0.3	2.2	0.32	2.2	0.59	2.0	0.29	1.8	0.32
Ar-10b	39	15	3.9	1.8	7.2	1.30	0.3	2.3	0.33	2.3	0.61	2.1	0.30	1.9	0.33
Ar-20a	38	14	3.6	1.7	6.4	1.17	0.3	2.0	0.29	2.0	0.54	1.8	0.27	1.7	0.29
Ar-21	36	13	3.9	1.7	6.1	1.11	0.1	2.0	0.28	1.9	0.51	1.7	0.25	1.6	0.27
Ar-20c	39	15	3.8	1.9	6.5	1.18	0.3	2.1	0.30	2.0	0.66	1.8	0.27	1.7	0.29
S31/03	n.d.	4.8	1.7	0.5	2.1	0.4	0.1	0.10	0.7	0.75	0.20	0.67	0.09	0.61	0.11
S32/03	n.d.	3.8	1.4	0.4	1.7	0.3	0.1	0.08	0.6	0.59	0.15	0.53	0.07	0.48	0.08
6007	6.5	5.7	3.1	0.8	2.8	0.50	0.3	0.8	0.10	0.6	0.13	0.4	0.05	0.3	0.049
6014	12	10	6	1.7	6.3	1.20	0.3	1.7	0.22	1.2	0.28	0.8	0.11	0.6	0.094
S33/03	n.d.	87	49	13	56	11	2.4	1.7	14	9.8	2.0	5.9	0.67	4.2	0.60
S34/03	n.d.	141	127	28	117	26	6.4	4.4	34	26	5.5	16.2	2.0	12	1.85
S3/02	410	505	1420	220	880	200	45	165	24	105	19	37	4.0	15	1.9
D1/01	n.d	98	145	22	103	19	4.2	3.1	27	16	3.1	8.2	0.87	4.8	0.66
S4/02	24	19	17	3.4	13.3	2.5	0.7	2.8	0.42	2.4	0.58	1.5	0.24	1.1	0.16
S5/02	48	55	85	14	56	10.8	2.5	10.8	1.6	8.2	1.7	3.9	0.53	2.1	0.28
D42/01	505	480	665	120	470	88	18	85	16	86	16	41	4.0	18	2.1
D43/01	590	440	605	100	390	75	15	83	15	84	18	49	5.4	29	4.0
D49/01	635	755	830	190	800	142	27	143	23	117	21	52	4.9	24	3.1
S27/03	35	35	68	8.1	25	4.3	1.3	0.71	4.7	3.9	0.83	2.3	0.34	1.60	0.22
D45/01	405	585	460	145	615	11	13	100	16	74	13	31	2.8	14	1.8
S26/03	n.d.	73	153	15	60	11	2.4	1.5	14	7.8	1.5	4.2	0.44	2.4	0.33
S25/03	n.d.	24	50	7.2	32	7.0	1.7	1.2	9.5	6.6	1.2	3.1	0.29	1.4	0.18
S24/03	55	38	55	8.4	35	7.4	2.1	1.21	7.7	6.6	1.34	3.6	0.50	2.28	0/32

Table 3. Sr isotopic composition and numerical Sr ages of separared (carbonate-free) CFA samples

Sample no	CFA phase	Biostr. Age[1] (Ma)	$^{87}Sr/^{86}Sr$	Sr age (Ma)	Fe (ppm)	Mn (ppm)	CO_2 (wt%)	Sr/P ($\times 10^{-4}$)	Ca/P	$(La/Sm)_N$	$(Sm/Yb)_N$	Ce/Ce*
OG-5	N	46	0.707842 *0.000013*	33.18	2250	290	5.4	113	2.60	1.98	0.40	- 0.62
D4/01	Mm	46	0.707774 *0.000002*	44.50	650	20	3.9	187	2.59	2.94	0.25	- 0.89
D10/01	S	46	0.707863 *0.000015*	32.79	n.d.	n.d.	3.2	179	2.59	n.d	n.d	n.d
D17/01	N	46	0.707758 *0.000014*	69.89	1000	4	5.7	133	2.52	2.57	0.29	- 0.91
32a/01	**Mm**	**46**	**0.707780 *0.000014***	**46.02**	**900**	**18**	**6.1**	**199**	**3.06**	**1.99**	**0.49**	**- 0.87**
S1/02a	**N**	**50**	**0.707739 *0.000014***	**50.54**	**1160**	**102**	**5.3**	**142**	**2.64**	**2.47**	**0.36**	**- 0.77**
S28/03	*P*	*53*	0.707979 *0.000014*	*30.11*	1.0%	200	n.d.	155	2.78	0.96	1.60	+ 0.02
S17/02	*P*	*53*	0.708028 *0.000012*	*28.89*	360	5.5	n.d.	120	2.71	1.21	0.84	- 0.53
S18/02	*P*	*53*	0.707823 *0.000011*	*33.57*	530	8	4.4	165	2.66	1.09	1.20	- 0.25
S19/02	*P*	*60*	0.708254 *0.000012*	*24.05*	220	3.2	2.9	121	2.39	1.92	0.35	- 0.53
S16/02	*P*	*66*	0.708427 *0.000014*	*20.48*	700	12	4.0	118	2.59	0.98	1.00	- 0.25
S20/02	*P*	*66*	0.708507 *0.000014*	*19.19*	1050	6	2.4	105	2.47	1.12	0.80	- 0.36
S29/03	*P*	*66*	0.708423 *0.000014*	*20.54*	0.3%	20	2.3	121	2.52	0.88	1.42	- 0.15
S30/03	*P*	*66*	0.708419 *0.000014*	*20.61*	0.2%	8	2.6	132	2.57	0.83	1.51	- 0.13
S7/02	**P**	**67**	**0.707806 *0.000012***	**66.68**	**6100**	**94**	**5.3**	**319**	**2.50**	**1.18**	**1.04**	**- 0.69**
OG-4	**N**	**67**	**0.707798 *0.000014***	**67.20**	**1400**	**7650**	**5.3**	**139**	**2.55**	**1.48**	**0.57**	**- 0.45**
S13/02	**P±S**	**68**	**0.707785 *0.000012***	***68.21***	**670**	**100**	**5.1**	**145**	**2.62**	**1.62**	**0.48**	**- 0.72**
OG-12	**N**	**70.5**	**0.707752 *0.000012***	**70.31**	**600**	**33.5**	**6.0**	**151**	**2.57**	**1.45**	**0.49**	**- 0.50**
D8/01	**N**	**70.5**	**0.707745 *0.000012***	**70.64**	**n.d.**	**n.d.**	**6.0**	**145**	**2.58**	n.d	n.d	n.d
S6/02	**N**	**70**	**0.707773 *0.000013***	**69.05**	**2300**	**470**	**5.8**	**102**	**2.70**	**2.08**	**0.41**	**- 0.81**
D26/01	***N***	***71***	**0.707741 *0.000014***	***70.82***	**915**	**44**	**5.6**	**221**	**2.77**	**1.25**	**0.53**	**- 0.37**
D29/01	**N**	**71**	**0.707701 *0.000015***	**71.97**	**295**	**6**	**5.9**	**186**	**2.62**	**1.90**	**0.35**	**- 0.71**
S5 64-65a	P	71	0.707686 *0.000013*	72.76	7000	13	6.1	152	2.68	1.28	0.51	- 0.48
AT-85	***p***	***71.5***	**0.707735 *0.000012***	***71.08***	**2.2%**	**1000**	**3.8**	**153**	**2.69**	**0.97**	**1.00**	**- 0.07**

Table 3. (continued)

Sample no	CFA phase	Chrono str. age[1] (Ma)	$^{87}Sr/^{86}Sr$ (Ma)	Sr age	Fe (ppm)	Mn (ppm)	CO_2 (wt%)	Sr/P ($\times 10^{-4}$)	Ca/P	$(La/Sm)_N$	$(Sm/Yb)_N$	Ce/Ce*
S10/02	**N**	**71.5**	**0.707727** ***0.000012***	**71.38**	**1350**	**63**	**5.2**	**220**	**2.59**	**1.95**	**0.32**	**- 0.41**
D9/01	**Mm**	**72**	**0.707713** ***0.000013***	**71.87**	**1170**	**80**	**6.1**	**204**	**2.58**	**1.72**	**0.22**	**- 0.34**
S14/02		*72*	0.707834 *0.000014*	*65.06*	200	5	n.d.	135	2.40	1.22	1.44	- 0.40
S15/02	*P*	*72*	0.707807 *0.000012*	*66.64*	102	6.5	4.4	121	2.50	1.41	0.64	- 0.70
D9/98	P	72	0.707826 *0.000012*	65.84	230	7	4.2	132	2.48	1.20	1.03	- 0.38
S12/02	P	72	0.707748 *0.000012*	70.50	80	6	4.5	124	2.54	1.04	1.20	- 0.37
Dis 13	**N**	**72**	**0.707710** ***0.000014***	**71.97**	**3000**	**17**	**5.9**	**219**	**2.68**	**2.18**	**0.43**	**- 0.63**
SG/45	P±S	72	0.707763 *0.000014*	*69.68*	1100	30	2.8	95	2.47	1.76	0.77	- 0.23
OG-9	**P**	**72**	**0.707708** ***0.000012***	**72.03**	**135**	**7**	**3.8**	**104**	**2.46**	**1.52**	**0.44**	**- 0.54**
D12/01	**P**	**72**	**0.707705** ***0.000014***	**72.13**	**54**	**6.5**	**5.4**	**113**	**2.40**	**1.92**	**0.28**	**- 0.74**
D18/01	**In**	**72**	**0.707694 0.000015**	**72.49**	**280**	**5.5**	**4.5**	**157**	**2.65**	**1.80**	**0.38**	**- 0.96**
OG-11	P	73	0.707743 *0.000012*	74.50	125	7	5.6	124	2.58	1.52	0.41	- 0.61
SG/40	**P±S**	**73**	**0.707690** ***0.000012***	***72.62***	**600**	**13**	**3.8**	**153**	**2.56**	**1.27**	**0.49**	**- 0.42**
AS-1	P	73	0.707835 *0.000014*	65.25	115	4.3	4.0	137	2.48	1.48	0.60	- 0.49
D11/01	S	73	0.707832 *0.000014*	65.50	170	5.5	2.2	150	2.40	1.96	0.33	- 0.64
OG-1	P	73	0.707811 *0.000015*	66.47	930	37	5.0	150	2.62	1.11	0.73	- 0.53
B2/L3	**P**	**73**	**0.707663** ***0.000013***	**73.54**	**250**	**2.2**	**3.1**	**114**	**2.36**	**1.63**	**0.39**	**- 0.60**
B2/L4	**P**	**73**	**0.707679** ***0.000014***	**73.00**	**350**	**3**	**3.1**	**131**	**2.32**	**1.40**	**0.45**	**- 0.47**
B2/L7	**P**	**72**	**0.707694** ***0.000013***	**72.49**	**450**	**3.8**	**3.8**	**135**	**2.46**	**1.30**	**0.50**	**- 0.75**
B2/L8	**P**	**72**	**0.707708** ***0.000014***	**72.03**	**2700**	**15**	**4.1**	**142**	**2.53**	**1.23**	**0.51**	**- 0.53**
B2/L2	**P**	**73.5**	**0.707670** ***0.000014***	**73.30**	**165**	**2.2**	**n.d.**	**116**	**2.40**	**1.57**	**0.42**	**- 0.58**
B2/L1	**P**	**74**	**0.707664** ***0.000014***	**73.50**	**180**	**3.8**	**3.2**	**114**	**2.43**	**1.41**	**0.41**	**- 0.51**
B2/L5	P	73	0.707633 *0.000013*	74.66	105	2.2	2.9	134	2.40	1.67	0.35	- 0.58
SG/32	**P±S**	**75**	**0.707638** ***0.000012***	***74.46***	**400**	**3**	**3.3**	**94**	**2.44**	**1.28**	**0.52**	**- 0.23**
SG/34	**P±S**	**75**	**0.707633** ***0.000012***	***74.66***	**120**	**9**	**3.2**	**91**	**2.49**	**0.97**	**0.79**	**- 0.13**

Table 3. (continued)

Sample no	CFA phase	Chrono str. age[1] (Ma)	$^{87}Sr/^{86}Sr$	*Sr* age (Ma)	Fe (ppm)	Mn (ppm)	CO_2 (wt%)	Sr/P ($\times 10^{-4}$)	Ca/P	$(La/Sm)_N$	$(Sm/Yb)_N$	Ce/Ce*
D2/01	N	75	0.707706 *0.000014*	72.10	n.d.	n.d	5.3	n.d	n.d	n.d	n.d	n.d
D3/01	S	75	0.706676 *0.000002*	73.10	345	7.5	3.8	140	2.44	2.68	0.13	- 0.81
SG/38	**P±S**	**75**	**0.707624 *0.000015***	***75.04***	**200**	**3**	**3.4**	**89**	**2.43**	**1.31**	**0.55**	**- 0.24**
SG/15	**P±S**	**75**	**0.707623 *0.000014***	***75.09***	**1200**	**170**	**4.1**	**121**	**2.52**	**0.87**	**0.99**	**- 0.07**
SG/27	**P±S**	**75**	**0.707617 *0.000012***	***75.35***	**600**	**6**	**3.9**	**96**	**2.46**	**1.22**	**0.46**	**- 0.47**
SG/12	**P±S**	**76**	**0.707602 *0.000012***	***76.04***	**1700**	**95**	**4.5**	**129**	**2.58**	**0.72**	**1.08**	**- 0.05**
D14/01	N	78	0.707652 *0.000013*	73.93	200	5	6.0	160	2.70	2.85	0.17	- 0.79
D15/01	S	78	0.707663 *0.000013*	73.54	280	2.8	6.2	124	2.70	2.61	0.19	- 0.64
D30/01	S	81	0.707665 *0.000015*	73.45	250	1	3.6	122	2.42	1.83	0.50	- 0.72
D6/01	S	83	0.707611 *0.000013*	75.62	n.d.	n.d	3.0	n.d	n.d	n.d	n.d	n.d
D27/01	S	83	0.707551 *0.000014*	78.78	1000	4	5.7	135	2.47	1.32	1.07	- 0.42
S2/02	N	83	0.707618 *0.000011*	75.31	1800	9	6.0	169	2.61	1.80	0.50	- 0.61
ZS/18	P±S	86	0.707652 *0.000012*	73.93	3400	6.5	6.1	179	2.65	1.43	0.60	- 0.36
ZS/21	P±S	86	0.707637 *0.000014*	74.50	3250	4.5	5.4	175	2.61	1.47	0.67	- 0.64
ZS/23	P±S	86	0.707637 *0.000014*	74.50	4450	5	5.2	176	2.66	1.49	0.68	- 0.64
Ar-2	P±S	88	0.707610 *0.000015*	75.83	50	2.5	n.d.	109	2.54	2.19	0.39	- 0.86
Ar-10a	P±S	88	0.707600 *0.000015*	76.31	67	7.6	4.8	112	2.56	2.11	0.38	- 0.86
Ar-20a	P±S	88	0.707590 *0.000013*	76.64	64	6.2	4.7	113	2.68	2.28	0.38	- 0.84
Ar21	P±S	88	0.707578 *0.000014*	77.25	68	4.8	4.7	120	2.68	2.11	0.38	- 0.78
S31/03	P±S	88	0.707619 *0.000013*	*75.26*	190	3	4.7	102	2.77	2.20	0.35	- 0.70
S32/03	P±S	88	*n.d.*	*n.d*	250	14	3.9	94	2.44	2.44	0.32	- 0.70
6007	**P±S**	**88**	**0.707311 *0.000013***	***88.79***	**110**	**80**	**6.0**	**187**	**2.91**	**2.05**	**0.90**	**- 0.53**
6014	**P±S**	**88**	**0.707310 *0.000015***	***88.82***	**160**	**94**	**5.8**	**187**	**2.79**	**1.50**	**1.09**	**- 0.51**
S33/03	P±S	*91*	0.707598 *0.000013*	*76.41*	2900	13.5	4.4	99	2.82	1.42	1.43	- 0.53
S34/03	P±S	*91*	0.707462 *0.000013*	*84.14*	120	3.5	5.6	91	2.49	0.97	4.04	- 0.36

Table 3. (continued)

Sample no	CFA phase	Chrono str. age[1] (Ma)	$^{87}Sr/^{86}Sr$ (‰)	Sr age (Ma)	Fe (ppm)	Mn (ppm)	CO_2 (wt%)	Sr/P (× 10^{-4})	Ca/P	$(La/Sm)_N$	$(Sm/Yb)_N$	Ce/Ce*
S3/02	N	91	0.707408 *0.000013*	86.24	735	1250	6.1	152	2.48	0.45	7.2	0.00
D1/01	N	94	0.707475 *0.000012*	83.55	2200	320	5.7	104	2.52	0.93	2.16	-0.19
S3/02	N	91	0.707408 *0.000013*	86.24	735	1250	6.1	152	2.48	0.45	7.2	0.00
D1/01	N	94	0.707475 *0.000012*	83.55	2200	320	5.7	104	2.52	0.93	2.16	-0.19
S4/02	Mm	96	0.707438 *0.000013*	85.15	2750	95	5.7	106	2.59	1.38	1.22	-0.34
S5/02	Mm	96	0.707443 *0.000013*	84.95	1950	155	6.0	139	2.59	0.91	2.83	-0.16
D42/01	N	106	0.707506 *0.000014*	81.80	9850	10	3.0	210	2.65	0.98	2.67	-0.20
D7/01	Mm	106	0.707855 *0.000012*	32.98	n.d.	n.d.	6.1	n.d	n.d	n.d	n.d	n.d
D43/01	N	106	0.707602 *0.000015*	76.04	2700	95	4.2	200	2.63	1.05	4.55	-0.19
D49/01	N	106	0.707544 *0.000014*	79.25	8000	10	3.3	214	2.59	0.95	3.25	-0.31
S27/03	*N*	*110*	0.707764 *0.000012*	*69.61*	2.2%	30	2.0	87	2.43	1.45	148	-0.01
D45/01	N	114	0.707508 *0.000013*	81.68	3150	15	3.4	*212*	*2.59*	n.d	n.d	-0.46
S26/03	*N*	*114*	0.707688 *0.000014*	*72.69*	7100	63	5.6	177	2.58	1.21	2.51	0.00
S25/03	*N*	*125*	0.707631 *0.000014*	*74.75*	3800	17	2.3	123	2.52	0.51	2.77	-0.08
S24/03	*N*	*130*	0.707660 *0.000014*	*73.64*	4.6%	6	2.3	127	2.52	0.92	1.75	-0.17

[1] estimated chronostratigraphic ages according to the stratigraphic position of the samples in time scales of Gradstein et al. (1995) and Berggren et al. (1995).
In bold – samples for which chronostratigraphic and Sr ages are matching

Table 4. (continued)

Table 4. $^{87}Sr/^{86}Sr$, $^{143}Nd/^{144}Nd$ and $\delta^{44}Ca$ results in separated CFA fractions.

Sample no	A.	Str.	T (Ma)	CFA phase	CO_2 (wt%)	Sr/P ($\times 10^{-4}$)	Ca/P	$(La/Sm)_N$	$(Sm/Yb)_N$	Ce/Ce*	Nd ($\mu g\ g^{-1}$)	Sm ($\mu g\ g^{-1}$)	$^{143}Nd/^{144}Nd$ ($\pm 2\sigma \times 10^{-6}$) (measured)	$^{147}Sm/^{144}Nd_{(T)}$	$^{143}Nd/^{144}Nd_{(T)}$ ($\pm 2\sigma \times 10^{-6}$)	$\varepsilon Nd_{(T)}$ $\pm 2\sigma$	$\delta^{44}Ca$ (‰) $\pm 2\sigma$
OG-5	1	L. Eo.	46[1]	N	5.4	113	2.60	1.98	0.40	-0.62	18.3	3.4	0.512320 ± 16	0.1124	0.512282 ± 16	-7.0 ± 0.3	0.26 ± 0.11
D4/01	1	L. Eo.	46[1]	Mm	3.9	167	2.59	2.94	0.25	-0.89	6.6	1.1	0.512285 ± 10	0.1008	0.512255 ± 10	-7.5 ± 0.2	0.42 ± 0.08
D10/01	1	L. Eo.	46[1]	S	3.2	179	2.59	n.d.	n.d.	n.d.	1.056[2]	0.187[2]	0.512286 ± 8	0.1071	0.512254 ± 10	-7.5 ± 0.2	n.d.
D17/01	1	L. Eo.	46[2]	N	5.7	133	2.52	2.57	0.29	-0.91	10.0	1.9	0.512291± 16	0.1149	0.512256 ± 16	-7.4 ± 0.3	0.39 ± 0.04
32a/01	1	L. Eo.	46.0[2)]	Mm	6.1	199	3.06	1.99	0.49	-0.87	9.9	1.8	0.512268 ± 22	0.1100	0.512235 ± 22	-7.9 ± 0.4	0.52 ± 0.12
S1/02a	1	L. Eo.	50.5[1]	N	5.3	142	2.64	2.47	0.36	-0.77	29.0	5.1	0.512272 ± 10	0.1064	0.512238 ± 10	-7.8 ± 0.2	0.38 ± 0.04
S17/02	2	L. Eo.	53[1]	P	n.d.	120	2.71	1.21	0.84	-0.53	19.7	4.0	0.512199 ± 12	0.1228	0.512156 ± 12	-9.4 ± 0.2	0.27 ± 0.03
S18/02	3	L. Eo.	53[1]	P	4.4	165	2.66	1.09	1.20	-0.25	85.4	16.4	0.512164 ± 10	0.1162	0.512124 ± 10	-10.0 ± 0.2	0.35 ± 0.09
S19/02	2	L. Eo.	60[1]	P	2.9	121	2.39	1.92	0.35	-0.53	8.6	1.6	0.512228 ± 16	0.1125	0.512182 ± 16	-8.9 ± 0.3	n.d.
S16/02	2	U. Ma.	66[1]	P	4.0	118	2.59	0.98	1.00	-0.25	17.1	3.5	n.d.	n.d.	n.d.	n.d.	0.36 ± 0.12
S20/02	2	U. Ma.	66[1]	P	2.4	105	2.47	1.12	0.80	-0.36	26.4	5.3	0.512198 ± 10	0.1214	0.512146 ± 10	-9.6 ± 0.2	0.34 ± 0.04
S29/03	2	U. Ma.	66[1]	P	2.3	121	2.52	0.88	1.42	-0.15	24	4.7	0.512173 ± 10	0.1185	0.512122 ± 10	-10.1 ± 0.2	n.d.
S30/03	2	U. Ma.	66[1]	P	2.6	132	2.57	0.83	1.51	-0.13	19	3.8	0.512145 ± 10	0.1210	0.512093 ± 10	-10.6 ± 0.2	0.23 ± 0.01
S7/02	4	U. Ma.	66.7[2)]	P	5.3	319	2.50	1.18	1.04	-0.69	280	57	0.512290 ± 10	0.1231	0.512236 ± 10	-7.8 ± 0.2	0.27 ± 0.06
OG-4	1	U. Ma.	67.2[2)]	N	5.3	139	2.55	1.48	0.57	-0.45	8.4	1.7	0.512345 ± 10	0.1124	0.512291± 18	-6.8 ± 0.3	n.d.
S13/02	1	U. Ma.	68.2[2)]	P ± S	5.1	145	2.62	1.62	0.48	-0.72	37.4	7.5	0.512371± 16	0.1213	0.512317 ± 16	-6.3 ± 0.3	0.24 ± 0.06
S6/02	1	L. Ma.	69.0[2)]	N	5.8	102	2.70	2.08	0.41	-0.81	59	10.5	0.512316 ± 10	0.1077	0.512259 ± 10	-7.4 ± 0.2	0.23 ± 0.06
OG-12	1	L. Ma.	70.3[2)]	N	6.0	151	2.57	1.45	0.49	-0.50	10.0	2.1	0.512333 ± 14	0.1270	0.512275 ± 14	-7.1 ± 0.3	n.d.
D8/01	1	L. Ma.	70.6[2)]	N	6.0	145	2.58	n.d.	n.d.	n.d.	0.520[2]	0.101[2]	0.512290 ± 10	0.1175	0.512236 ± 10	-7.8 ± 0.2	0.28 ± 0.01
D26/01	1	L. Ma.	70.8[2)]	N	5.6	221	2.77	1.25	0.53	-0.37	11	2.4	0.512342 ± 16	0.1391	0.512282 ± 16	-6.9 ± 0.2	0.28 ± 0.01
S5 64-65a	1	L. Ma.	71[1]	P	6.1	152	2.68	1.28	0.51	-0.48	21.0	4.2	0.512322 ± 10	0.1210	0.512264 ± 10	-7.3 ± 0.2	0.36 ± 0.17

Table 4. (continued)

Sample no	A.	Str.	T (Ma)	CFA phase	CO_2 (wt%)	Sr/P ($\times 10^{-4}$)	Ca/P	$(La/Sm)_N$	$(Sm/Yb)_N$	Ce/Ce*	Nd ($\mu g\ g^{-1}$)	Sm ($\mu g\ g^{-1}$)	$^{143}Nd/^{144}Nd$ ($\pm 2\sigma \times 10^{-6}$) (measured)	$^{147}Sm/^{144}Nd_{(T)}$	$^{143}Nd/^{144}Nd_{(T)}$ ($\pm 2\sigma \times 10^{-6}$)	$\varepsilon Nd_{(T)} \pm 2\sigma$	$\delta^{44}Ca$ (‰) $\pm 2\sigma$
AT-85	5	U. Ca.	71.1[2)]	P	3.8	153	2.69	0.97	1.00	-0.07	205	42	0.512152 ± 10	0.1239	0.512093 ± 10	-10.6 ± 0.2	n.d.
S10/02	1	U. Ca.	71.4[2)]	N	5.2	220	2.59	1.95	0.32	-0.41	7.4	1.3	n.d.	n.d.	n.d.	n.d.	0.35 ± 0.02
D9/01	1	U. Ca.	71.9[2)]	Mm	6.1	204	2.58	1.72	0.22	-0.34	0.084[3)]	0.016[3)]	0.512205 ± 20	0.1152	0.512151 ± 20	-9.5 ± 0.4	0.49 ± 0.00
D29/01	1	L. Ma.	72.0[2)]	N	5.9	186	2.62	1.90	0.35	-0.71	8.4	1.6	0.512362 ± 10	0.1152	0.512308 ± 10	-6.4 ± 0.2	0.39 ± 0.07
Dis 13	1	U. Ca.	72.0[2)]	N	5.9	219	2.68	2.18	0.43	-0.63	7.3	1.4	0.512363 ± 10	0.1160	0.512308 ± 10	-6.4 ± 0.2	0.32 ± 0.10
S15/02	7	U. Ca.	72[1)]	P	4.4	121	2.50	1.41	0.64	-0.70	29.0	6.0	0.512390 ± 16	0.1252	0.512333 ± 16	-6.0 ± 0.3	n.d.
S12/02	1	U. Ca.	72[1)]	P	4.5	124	2.54	1.04	1.20	-0.37	22.7	4.6	0.512399 ± 10	0.1226	0.512343 ± 10	-5.8 ± 0.2	0.33 ± 0.01
D9/98	6	U. Ca.	72[1)]	P	4.2	132	2.48	1.20	1.03	-0.38	36.3	7.2	0.512409 ± 12	0.1200	0.512354 ± 12	-5.5 ± 0.2	0.27 ± 0.07
SG/45	5	U. Ca.	72[1)]	P ± S	2.8	95	2.47	1.76	0.77	-0.23	5.8	1.0	0.512270 ± 12	0.1043	0.512222 ± 12	-8.1 ± 0.2	n.d.
OG-9	1	U. Ca.	72.0[2)]	P	3.8	104	2.46	1.52	0.44	-0.54	6.5	1.3	0.512329 ± 18	0.1210	0.512272 ± 18	-7.1 ± 0.3	n.d.
B2/L8	1	U. Ca.	72.0[2)]	P	4.1	142	2.53	1.23	0.51	-0.53	39	8.3	0.512336 ± 8	0.1287	0.512274 ± 8	-7.1 ± 0.2	n.d.
D12/01	1	U. Ca.	72.1[2)]	P	5.4	113	2.40	1.92	0.28	-0.74	0.068[3)]	0.012[3)]	0.512373 ± 42	0.1067	0.512323 ± 42	-6.2 ± 0.8	0.45 ± 0.02
B2/29	1	U. Ca.	72.1[2)]	P	n.d.	n.d.	n.d.	n.d.	n.d.	n.d.	0.296[3)]	0.062[3)]	0.512349 ± 13	0.1264	0.512289 ± 13	-6.8 ± 0.2	n.d.
D18/01	1	U. Ca.	72.5[2)]	In	4.5	157	2.65	1.80	0.38	-0.96	10.0	2.0	0.512357 ± 1	0.1210	0.512300 ± 1	-6.6 ± 0.2	0.35 ± 0.04
B2/L7	1	U. Ca.	72.5[2)]	P	3.8	135	2.46	1.30	0.50	-0.75	41.0	8.5	0.512356 ± 10	0.1254	0.512297 ± 10	-6.7 ± 0.2	0.19 ± 0.06
OG-11	1	U. Ca.	73[1)]	P	5.6	124	2.58	1.52	0.41	-0.61	6.3	1.3	0.512345 ± 16	0.1248	0.512284 ± 16	-6.9 ± 0.3	n.d.
SG/40	5	U. Ca.	72.6[2]	P ± S	3.8	153	2.56	1.27	0.49	-0.42	20	4.1	0.512306 ± 12	0.1240	0.512247 ± 12	-7.6 ± 0.2	0.25 ± 0.07
AS-1	7	U. Ca.	73[1)]	P	4.0	137	2.48	1.48	0.60	-0.49	11.9	2.3	0.512384 ± 16	0.1169	0.512328 ± 16	-6.0 ± 0.2	0.44 ± 0.13
15/31	1	U. Ca.	73[1)]	P	n.d.	n.d.	n.d.	n.d.	n.d.	n.d.	n.d.	n.d.	n.d.	n.d.	n.d.	n.d.	0.34 ± 0.08
D11/01	1	U. Ca.	73[1)]	S	2.2	150	2.40	1.96	0.33	-0.64	5.6	1.1	0.512303 ± 24	0.1188	0.512246 ± 24	-7.6 ± 0.4	n.d.
OG-1	1	U. Ca.	73[1)]	P	5.0	150	2.62	1.11	0.73	-0.53	38	8	0.512351 ± 10	0.1273	0.512290 ± 10	-6.8 ± 0.2	n.d.

Table 4. (continued)

Table 4. (continued)

Sample no	A.	Strat.	T (Ma)	CFA phase	CO_2 (wt%)	Sr/P ($\times 10^{-4}$)	Ca/P	$(La/Sm)_N$	$(Sm/Yb)_N$	Ce/Ce*	Nd ($\mu g\ g^{-1}$)	Sm ($\mu g\ g^{-1}$)	$^{143}Nd/^{144}Nd$ (measured)	$^{147}Sm/^{144}Nd_{(T)}$	$^{143}Nd/^{144}Nd_{(T)}$	$\varepsilon Nd_{(T)}$	$\delta^{44}Ca$ (‰) $\pm 2\sigma$
B2/L5	1	U. Ca.	73[1]	P	2.9	134	2.40	1.67	0.35	-0.58	6.8	1.3	0.512368 ± 18	0.1156	0.512312 ± 18	-6.4 ± 0.3	n.d.
B2/L4	1	U. Ca.	73.0[2]	P	3.1	131	2.32	1.40	0.45	-0.47	6.7	1.4	0.512374 ± 20	0.1264	0.512314 ± 20	-6.3 ± 0.4	n.d.
B2/L2	1	U. Ca.	73.3[2]	P	n.d.	116	2.40	1.57	0.42	-0.58	8.1	1.6	0.512383 ± 14	0.1195	0.512326 ± 14	-6.1 ± 0.3	n.d.
B2/L6	1	U. Ca.	73[1]	P	3.1	158	2.45	1.57	0.39	-0.65	8.1	1.6	0.512363 ± 10	0.1195	0.512306 ± 10	-6.5 ± 0.2	n.d.
B2/L3	1	U. Ca.	73.5[2]	P	3.1	114	2.36	1.63	0.39	-0.60	5.8	1.2	0.512375 ± 22	0.1252	0.512315 ± 22	-6.3 ± 0.4	0.29 ± 0.02
B2/L1	1	U. Ca.	73.5[2]	P	3.2	114	2.43	1.41	0.41	-0.51	9.4	1.9	0.512400 ± 20	0.1223	0.512341 ± 20	-5.8 ± 0.4	0.28 ± 0.01
SG/32	5	U. Ca.	74.5[2]	P ± S	3.3	94	2.44	1.28	0.52	-0.23	6.2	1.2	0.512349 ± 28	0.1171	0.512292 ± 28	-6.7 ± 0.4	0.30 ± 0.04
SG/34	5	U. Ca.	74.7[2]	P ± S	3.2	91	2.49	0.97	0.79	-0.13	11	2.2	0.512250 ± 10	0.1210	0.512191 ± 10	-8.7 ± 0.2	0.35 ± 0.03
S1/71	1	U. Ca	75[1]	P	n.d.	n.d.	n.d.	n.d.	n.d.	n.d.	n.d.	n.d.	n.d.	n.d.	n.d.	n.d.	0.35 ± 0.15
D2/01	1	U. Ca.	75[1]	N	5.3	n.d.	n.d.	n.d.	n.d.	n.d.	0.024[3]	0.0045[3]	0.512395 ± 10	0.1134	0.512339 ± 10	-5.8 ± 0.2	0.22 ± 0.07
D3/01	1	U. Ca.	75[1]	S	3.8	140	2.44	3.8	140	2.44	0.083[3]	0.016[3]	0.512303 ± 18	0.1166	0.512246 ± 8	-7.7 ± 0.4	0.30 ± 0.00
SG/38	5	U. Ca.	75.0[2]	P ± S	3.4	89	2.43	1.31	0.55	-0.24	4.5	0.9	0.512275 ± 12	0.1210	0.512216 ± 12	-8.2 ± 0.2	n.d.
SG/15	5	U. Ca.	75.1[2]	P ± S	4.1	121	2.52	0.87	0.99	-0.07	40	8	0.512182 ± 10	0.1210	0.512123 ± 10	-10.1 ± 0.2	n.d.
SG/27	5	U. Ca.	75.3[2]	P ± S	3.9	96	2.46	1.22	0.46	-0.47	1.2	0.25	0.512355 ± 22	0.1260	0.512293 ± 22	-6.7 ± 0.4	n.d.
SG/12	5	U. Ca.	76.0[2]	P ± S	4.5	129	2.58	0.72	1.08	-0.05	27	5.8	0.512257 ± 12	0.1299	0.512192 ± 12	-8.7 ± 0.2	n.d.
34/01p	1	U. Ca.	78[1]	P	n.d.	n.d.	n.d.	n.d.	n.d.	n.d.	n.d.	n.d.	n.d.	n.d.	n.d.	n.d.	0.20 ± 0.12
34/01s	1	U. Ca.	78[1]	S	n.d.	n.d.	n.d.	n.d.	n.d.	n.d.	n.d.	n.d.	n.d.	n.d.	n.d.	n.d.	0.24 ± 0.00
D14/01	1	U. Ca.	78[1]	N	6.0	160	2.70	2.85	0.17	-0.79	2.5	0.47	0.512378 ± 16	0.1240	0.512315 ± 16	-6.3 ± 0.3	0.43 ± 0.12
D15/01	1	U. Ca.	78[1]	S	6.2	124	2.70	2.61	0.19	-0.64	2.4	0.48	0.512255 ± 16	1210	0.512193 ± 16	-8.7 ± 0.3	0.29 ± 0.12
D30/01	1	L. Ca.	81[1]	S	3.6	122	2.42	1.83	0.50	-0.72	0.913[3]	0.177[3]	0.512360 ± 10	0.1173	0.512298 ± 16	-6.6 ± 0.2	0.01 ± 0.11
D6/01	1	Sa.-Ca.*	83[1]	S	3.0	n.d.	n.d.	n.d.	n.d.	n.d.	0.665[2]	0.125[2]	0.512349 ± 11	0.1137	0.512287 ± 12	-6.8 ± 0.2	0.06 ± 0.10

Table 4. (continued)

Table 4. (continued)

Sample no	A.	Strat.	T (Ma)	CFA phase	CO_2 (wt%)	Sr/P ($\times 10^{-4}$)	Ca/P	$(La/Sm)_N$	$(Sm/Yb)_N$	Ce/Ce*	Nd ($\mu g\ g^{-1}$)	Sm ($\mu g\ g^{-1}$)	$^{143}Nd/^{144}Nd$ (measured)	$^{147}Sm/^{144}Nd_{(T)}$	$^{143}Nd/^{144}Nd_{(T)}$	$\varepsilon Nd_{(T)}$	$\delta^{44}Ca$ (‰) $\pm 2\sigma$
D27/01	1	Sa.-Ca.*	83[1]	S	5.7	135	2.47	1.32	1.07	-0.42	4.486[3]	1.57[3]	0.512336 ± 10	0.1425	0.512259 ± 10	-7.4 ± 0.2	0.12 ± 0.06
S2/02	1	Sa.-Ca.*	83[1]	N	6.0	169	2.61	1.80	0.50	-0.61	4.5	0.9	0.512354 ± 10	0.1210	0.512288 ± 10	-6.8 ± 0.2	0.28 ± 0.01
32/01p	1	Sa.-Ca.*	83[1]	P	n.d.	n.d.	n.d.	n.d.	n.d.	n.d.	5.1	1.02	0.512305 ± 10	0.1210	0.512239 ± 10	-7.8 ± 0.2	-0.02 ± 0.11
32/01s	1	Sa.-Ca.*	83[1]	S	n.d.	n.d.	n.d.	n.d.	n.d.	n.d.	5.1	1.02	0.512316 ± 8	0.1210	0.512250 ± 8	-7.6 ± 0.2	0.13 ± 0.03
ZS/18	1	U. Co.	86[1]	P ± S	6.1	179	2.65	1.43	0.60	-0.36	46	9.4	0.512347 ± 8	0.1236	0.512277 ± 8	-7.0 ± 0.2	0.24 ± 0.10
ZS/21	1	U. Co.	86[1]	P ± S	5.4	175	2.61	1.47	0.67	-0.64	73	15	0.512363 ± 8	0.1243	0.512293 ± 8	-6.7 ± 0.3	n.d.
ZS/23	1	U. Co.	86[1]	P ± S	5.2	176	2.66	1.49	0.68	-0.64	73	14.8	0.512358 ± 12	0.1226	0.512289 ± 12	-6.8 ± 0.2	n.d.
Ar-2	8	L. Co.	88[1]	P ± S	n.d.	109	2.54	2.19	0.39	-0.86	6.3	1.15	0.512355 ± 10	0.1104	0.512294 ± 10	-6.7 ± 0.2	0.25 ± 0.03
Ar-10a	8	L. Co.	88[1]	P ± S	4.8	112	2.56	2.11	0.38	-0.86	7.0	1.28	0.512360 ± 10	0.1106	0.512298 ± 10	-6.6 ± 0.2	0.24 ± 0.05
Ar-10b	8	L. Co.	88[1]	P ± S	4.7	113	2.68	2.28	0.38	-0.84	7.2	1.3	0.512325 ± 10	0.1092	0.512264 ± 10	-7.3 ± 0.2	0.26 ± 0.05
Ar-21	8	L. Co.	88[1]	P ± S	4.7	120	2.68	2.11	0.38	-0.78	6.1	1.11	0.512349 ± 20	0.1101	0.512288 ± 20	-6.8 ± 0.3	0.19 ± 0.05
Ar-20c	8	L. Co.	88[1]	P ± S	4.7	113	2.68	2.28	0.38	-0.86	6.4	1.17	0.512345 ± 16	0.1106	0.512284 ± 16	-6.9 ± 0.3	0.26 ± 0.09
S31/03	8	L. Co.	88[1]	P ± S	4.7	102	2.77	2.20	0.35	-0.70	2.1	0.4	0.512370 ± 8	0.1152	0.512306 ± 38	-6.5 ± 0.3	0.32 ± 0.03
S32/03	8	L. Co.	88[1]	P ± S	2.20	0.35	-0.70	3.9	94	2.44	1.7	0.3	0.512391± 8	0. 1067	*	-6.0 ± 0.2	0.30 ± 0.04
6007	8	L. Co.	88.8[2]	P ± S	2.05	0.90	-0.53	6.0	187	2.91	2.8	0.5	n.d.	n.d.	n.d.	n.d.	0.27 ± 0.09
6014	4	L. Co.	88.8[1]	P ± S	5.8	187	2.79	1.50	1.09	-0.51	6.3	1.2	0.512314 ± 10	0.1152	0.512247 ± 10	-7.6 ± 0.2	0.40 ± 0.04
S33/03	8	M. Tur.	91[1]	P ± S	4.4	99	2.82	1.42	1.43	-0.53	56	11	0.512411 ± 8	0.1188	0.512341 ± 8	-5.8 ± 0.2	0.02 ± 0.03
S34/03	8	M. Tur.	91[1]	P ± S	5.6	91	2.49	0.97	4.04	-0.36	117	26	0.512418 ± 8	0.1344	0.512339 ± 8	-5.8 ± 0.2	0.01 ± 0.04
S3/02	1	M. Tur.	91[1]	N	6.1	152	2.48	0.45	7.2	0.00	880	200	0.512411 ± 8	0.1375	0.512329 ± 8	-6.0 ± 0.2	-0.09 ± 0.13
D1/01	6	U. Cen.	94[1]	N	5.7	104	2.52	0.93	2.16	-0.19	12.79[3]	2.75[3]	0.512413 ± 8	0.1300	0.512333 ± 8	-5.9 ± 0.2	n.d.
S4/02	9	L. Cen.	96[1]	Mm	5.7	106	2.59	1.38	1.22	-0.34	13.3	2.5	0.512146 ± 12	0.1137	0.512075 ± 12	-11.0 ± 0.2	n.d.

Table 4. (continued)

Table 4. (continued)

Sample no	A.	Strat.	T (Ma)	CFA phase	CO_2 (wt%)	Sr/P ($\times 10^{-4}$)	Ca/P	$(La/Sm)_N$	$(Sm/Yb)_N$	Ce/Ce*	Nd ($\mu g\ g^{-1}$)	Sm ($\mu g\ g^{-1}$)	$^{143}Nd/^{144}Nd$ (measured)	$^{147}Sm/^{144}Nd_{(T)}$	$^{143}Nd/^{144}Nd_{(T)}$	$\varepsilon Nd_{(T)}$	$\delta^{44}Ca$ (‰) $\pm 2\sigma$
S5/02	9	L. Cen.	96[1]	Mm	6.0	139	2.59	0.91	2.83	-0.16	56	10.8	0.512121 ± 8	0.1167	0.512047 ± 8	-11.5 ± 0.2	n.d.
D42/01	10	L. Alb.	106[1]	N	3.0	210	2.65	0.98	2.67	-0.20	470	88	0.512123 ± 10	0.1133	0.512054 ± 10	-11.4 ± 0.2	-0.07 ± 0.01
D7/01	1	L. Alb.	106[1]	Mm	6.1	n.d.	n.d.	n.d.	n.d.	n.d.	18.52[3]	3.747[3]	0.512210 ± 12	0.1224	0.512126 ± 12	-10.0 ± 0.2	0.09 ± 0.12
D43/01	10	L. Alb.	106[1]	N	4.2	200	2.63	1.05	4.55	-0.19	390	75	0.512142 ± 10	0.1163	0.512061 ± 10	-11.2 ± 0.2	-0.04 ± 0.02
D49/01	10	L. Alb.	106[1]	N	3.3	214	2.59	0.95	3.25	-0.31	800	142	0.512148 ± 10	0.1074	0.512074 ± 10	-11.0 ± 0.2	-0.23 ± 0.06
S27/03	11	L. Alb.	110[1]	N	2.0	87	2.43	1.45	148	-0.01	25	4.3	0.512065 ± 12	0.1040	0.511992 ± 12	-12.6 ± 0.2	0.03 ± 0.02
D45/01	10	U. Apt.	114[1]	N	3.4	212	2.59	n.d.	n.d.	-0.46	615	110	0.512160 ± 8	0.1082	0.512084 ± 8	-10.8 ± 0.2	-0.11 ± 0.03
S26/03	11	U. Apt.	114[1]	N	5.6	177	2.58	1.21	2.51	0.00	60	11	0.512065 ± 8	0.1108	0.511982 ± 8	11.0 ± 0.2	n.d.
S25/03	11	L. Bar.	125[1]	N	2.3	123	2.52	0.51	2.77	-0.08	32	7.0	0.512083 ± 10	0.1323	0.511975 ± 10	-12.8 ± 0.2	-0.26 ± 0.05
S24/03	11	L. Haut.	130[1]	N	2.3	127	2.52	0.92	1.75	-0.17	35	7.4	0.512134 ± 14	0.1279	0.512029 ± 14	-11.9 ± 0.3	- 0.19 ± 0.05

1 – Israel (Negev); 2 – Morocco (Ganntour); 3 – Tunisia (Gafsa); 4 – Greece (Ionian zone); 5 – Egypt (Red sea coast); 6 – Jordan (Al Abiad, Rusaifa); 7 – Syria (Er Rakheime); 8 – Turkey (Mardin-Mazidagi); 9 – S. England (Isle of Wight, Lyme Regis); 10 – SE France (Fossé Voncontien); 11 – Helvetic Alps.

L. – Lower; M. – Middle; U. – Upper; Eo. – Eocene; Ma. – Maastrichtian; Ca. – Campanian; Sa-Ca* - Santonian-Campanian transition; Co. – Coniacian; Tu. – Turonian; Ce. – Cenomanian; Alb. – Albian; Apt. – Aptian; Bar. – Barremian; Haut. – Hauterivian.

N – nodular; Mm – megafossil molds; S – skeletal; P – pelletal; In – intraclastic

(T) Initial composition at time T of the sample.

T[1] – estimated chronostratigraphic ages according to the stratigraphic position of the samples in time scales of Gradstein et al. (1995) and Berggren et al. (1995).

T[2] – measured Sr ages

[3] 20% glacial acid acetic dissolution; for other samples 1/3 HNO_3 dissolution was used.

Table 5. Comparison of $\varepsilon_{Nd\,(T)}$ values in CFA for various Campanian-Eocene stratigraphic intervals in different sites along the Tethyan phosphate province.

Stage	T (Ma)	1	2	3
L. Eo.	46.0	-7.5 ± 0.2		
	50.5	-7.8 ± 0.2		
	53			-9.7 ± 0.2
	60			-8.9 ± 0.3
U. Ma.	66			-10.1 ± 0.2
	66.7	-7.8 ± 0.2		
	67.2	-6.8 ± 0.3		
	68.2	-6.3 ± 0.3		
L. Ma.	70.8	-6.9 ± 0.2		
	71	-7.3 ± 0.2	-10.6 ± 0.2	
U. Ca	72.0	-6.4 ± 0.2	-8.1 ± 0.2	
	72.5	-6.7 ± 0.2	-7.6 ± 0.2	
	75.0	-6.7 ± 0.3	-9.1 ± 0.2	
	76.0		-8.7 ± 0.2	

Eo. – Eocene; Ma. – Maastrichtian; Ca – Campanian; U – upper; L – lower;
§ – Sr ages; other T are estimated biostratigraphic ages.
1 – Israel (Negev); 2 – Egypt (Red sea coast); 3 – Morocco (Ganntour)

Table 6. P and Ca accumulation rates and bulk sedimentation rates over the Cretaceous – Eocene succession in the Negev area.

Stage	Stratigraphy		T (Ma)	$n^{(1)}$	P acc. rate (μmole.cm^{-2}.kyr^{-1})	Bulk sed. rate (cm.kyr^{-1})	Sources $^{(1)}$	$n^{(2)}$	Ca acc. rate (μmole. cm^{-2}.kyr^{-1})	Sources $^{(2)}$
U. Eo.	Qez'iot Fm.		38-35	2	25 ± 10	3.3	1	4	24 ± 10	1, 3
M. Eo.	Matred Fm.		43.7-38	5	40 ± 20	1.4	3, 53,	17	12 ± 1.2	2, 3, 6, 20, 53,
L. Eo.	Paran Fm.		49-43.7	8	300 ± 220	2.5 ± 1.0	2, 3, 6, 53			
	Mor Fm.		52.3-49	4	90 ± 40	1.3 ± 0.6	6, 53, this work			
Pal.	Taqiya		65-53	12	70 ± 40	0.6 ± 0.2	1, 2, 6, 19, 21, 53, this work	11	3.3 ± 1.3	1, 2, 6, 19-21, 53, this work
Ma.	Ghareb Fm.	M.	70-65	7	110 ± 40	0.7 ± 0.3	1, 35,	10	7.7 ± 1.4	1, 2, 6, 35, 53, 21, this work
		O. Sh..	72-70	6	630 ± 170	1.4 ± 0.5	1, 27, 35, 43,			
U. Ca	Mishash Fm.	Ph. U.	74-72	31	1470 ± 650	0.4 ± 0.2	4, 5, 7, 9-14, 16, 24-26, 28, 31, 33, 36-42, 46-52, 54-61	10	3.2 ± 1.9	3, 8, 15, 43, 45, 54
		Po. U.	75.5-74	3	930 ± 90	0.8 ± 0.2	8, 34, this work			
		Ph.-Ca U.	79-75.5	2	630 ± 50	0.8 ± 0.5	8, this work			
U. Co – L. Ca	Menuha Fm.	Up.	83-80.5	2	170 ± 15	0.9 ± 0.3	2, 3, 6, 20, 21,32, 53	10	11 ± 1.6	6, 20, 53
		L.	87-83	9	115 ± 30	1.3 ± 0.3	2, 8, 20.			
U. Tu – Co	Zihor Fm.		89-87	4	45 ± 10	2.1 ± 0.3	1, 2, 3, 6, 19-22, 53	6	23 ± 3.6	3, 20, 53
U. Tu	Gerofit Fm.		90.5-89	15	210 ± 130	9.2 ± 2.9	19, 20, 32,	29	100 ± 8.6	1-3, 6, 20, 22, 53
L. – M. Tu	Ora shale Fm.		94-90.5	9	35 ± 15	1.8 ± 0.1	1, 2, 3, 6, 20, 21	10	13.9 ± 1.3	1-3, 6
L. Alb. – U. Ce.	Hazera Fm.	Av. + Ta.	95.8-94	4	50 ± 40	5.3 ± 1.5	3, 6, 20, 21, 32	19	74 ± 2.6	2, 3, 6, 20, 30, 32
		Za.	97-95.8	1	20	5.0	3	10	33 ± 6.2	1-3, 32, 20, 44
		Yo..	99-96.8	4	25 ± 15	1.6 ± 0.7	3, 6, 20, 32	6	16.3 ± 6.7	3, 6, 20, 32
		He.	103 (?) - 99	2	35 ± 15	3.5	3, 6	4	38 ± 5.2	1-3, 20

Eo. – Eocene; Pal. – Paleocene; Ma – Maastrichtian; Ca – Campanian; Co – Coniacian; Tu – Turonian; Ce. – Cenomanian; Alb. – Albian; U. – upper; M – middle; L. – lower.
M. – marly Mbr; O. sh. – Oil Shale Mbr.; Ph. U. – Phosphorite unit; Po. U. – Porcelanite unit; Ph.–Ca U. – Phosphatic carbonate unit; Av. – Avnon Mbr. Ta – Tamar Mbr.; Za. – Zafit Mbr.; Yo. – Yorqe'am Mbr; He. – Hevyon Mbr.
$n^{(1)}$ – number of sections quantified for P acc. and sed. rates; $n^{(2)}$ – number of sections quantified for Ca rate.
T from Lewy (1990) and Zohar (2004) ; time scales used – Gradstein et al. (1995) – Mesozoic; and Berggren et al. (1995) – Cenozoic.

Table 7. C_{org}:N_{org} ratios, and $\delta^{13}C_{org}$ and $\delta^{15}N_{org}$ values in Negev succession (Upper Coniacian-Middle Eocene) and in phosphate samples (Campanian) of Egypt (Red sea)

Sample no	Stratigr. interval	TOC[(1)] (wt%)	C_{org}[(2)] (wt%)	N_{org} (wt%)	C:N_{org} (atomic)	$\delta^{13}C_{org}$ (‰)	$\delta^{15}N_{org}$ (‰)
M-13/39.1-40.3	9	0.3	1.7	0.07	28.0	- 25.37	4.27
M-13/47.0-49.5	9	0.5	2.5	0.13	23.3	- 25.92	3.46
M-13/52.1-54.1	9	0.3	2.4	0.13	21.1	- 26.07	4.79
M-13/58.0-59.6	9	0.2	0.9	0.05	23.3	- 25.88	2.95
M-13/65.1-66.7	9	0.3	1.9	0.10	22.8	- 26.21	4.08
M-13/71.5-74.5	9	0.3	1.7	0.09	23.3	- 26.23	4.81
M-13/79.0-82.0	9	0.4	2.2	0.12	22.5	- 27.11	4.35
M-13/88.4-91.4	9	0.3	3.9	0.12	40.0	- 26.90	7.11
M-13/98.5-101.0	9	0.4	1.8	0.07	28.0	- 26.96	3.35
M-7/297	8	0.3	0.8	0.08	12.0	- 26.94	6.62
M-7/300	8	0.2	0.5	0.13	4.4	- 26.00	- 2.96
M-7/309	8	0.4	1.1	0.15	9.0	- 26.21	- 0.80
M-7/327	8	0.2	0.9	0.09	11.6	- 26.08	7.01
M-7/336	8	0.4	1.2	0.09	16.6	- 25.51	6.58
M-7/338	8	0.4	1.1	0.09	15.0	- 25.93	6.46
M-7/341	8	0.4	1.1	0.10	12.8	- 26.15	6.16
M-7/344	8	0.5	1.1	0.09	15.0	- 26.29	6.23
M-7/345	8	0.5	1.3	0.11	15.7	- 26.20	6.68
M-7/347	8	1.0	2.1	0.16	15.4	- 26.62	5.09
B-124/8.0-9.5	7	0.3	1.0	0.11	10.0	- 26.40 (-26.69)	9.18
B-124/12.0-13.0	7	0.2	1.1	0.09	15.0	- 26.39	7.17
B-124/13.5-14.0	7	0.2	1.1	0.14	9.0	- 26.52	7.70
B-124/14.0-14.5	7	0.2	1.0	0.11	10.0	- 26.90	8.29
B-124/15.5-16.5	7	0.2	0.8	0.10	8.5	- 27.10	7.26
B-124/16.5-17.0	7	0.2	0.7	0.08	12.0	- 26.62 (-26.45)	7.63
B-124/17.0-17.3	7	0.3	0.9	0.10	14.0	- 26.77	8.93
B-124/24.0-25.0	7	0.3	1.2	0.18	7.7	- 26.82	6.50
B-124/28.8-29.1	6	4.1	13.4	n.d.	n.d.	- 28.86	n.d.
B-124/29.1-29.3	6	11.3	27.8	n.d.	n.d.	- 29.14	n.d.
B-124/30.3-31.0	6	9.4	22.0	0.96	26.9	- 29.41 (-29.11)	5.23
B-124/32.0-32.7	6	8.0	24.7	0.93	30.9	- 29.27	3.08
B-124/36.3-37.0	6	8.8	21.9	0.97	29.3	- 28.61 (-28.31)	5.48
B-124/37.0-37.7	6	12.4	38.4	1.03	41.6	- 29.04	5.26
B-124/37.7-38.4	6	8.3	23.7	1.00	27.7	- 29.07	5.55
B-124/38.4-39.2	6	6.9	22.4	1.16	22.7	- 29.46	5.66
B-124/45-45.6	6	7.9	28.4	1.04	31.7	- 28.81	5.15
B-124/48.0-48.6	6	9.6	26.2	1.00	30.7	- 28.99	5.53
B-124/50.4-51.0	6	7.8	23.5	1.09	24.4	- 29.25 (-28.93)	4.55
B-124/58.8-59.4	6	9.3	32.6	1.26	30.1	- 29.13 (-28.54)	4.88
B-124/60.0-60.7	6	9.5	35.4	1.27	32.6	- 29.52	4.83
B-124/60.7-61.5	6	11.3	40.5	1.26	37.4	- 29.57 (-28.95)	4.85
B-124/62.2-63.0	6	12.4	32.3	1.08	34.9	- 29.50	3.54
B-124/63.0-63.5	6	11.6	39.6	1.30	35.8	- 29.65	4.98
B-124/63.5-64.0	6	11.4	40.6	1.19	39.7	- 30.30	5.63
B-124/65.0-65.5	6	15.4	45.6	1.50	35.5	- 29.67	5.82
B-124/65.5-66.0	6	15.4	44.7	1.66	31.5	- 30.26 (-29.75)	5.35
B-17/13	5	5.2	35.1	0.83	49.5	- 28.61	4.52
B-17/12	5	7.4	40.4	0.91	51.7	- 29.32	5.66

Table 7 (continued)

Sample no	Strat.	TOC[1] (wt%)	C_{org}[2] (wt%)	N_{org} (wt%)	C:N_{org} (atomic)	$\delta^{13}C_{org}$ (‰)	$\delta^{15}N_{org}$ (‰)
B-17/11	5	5.3	26.8	0.62	50.7	- 28.55	4.66
B-17/10	5	4.1	12.0	n.d.	n.d.	- 28.76	n.d.
B-17/9	5	2.8	20.7	0.55	44.1	- 28.58	4.28
B-17/8	5	2.9	21.1	0.51	48.6	- 29.03	4.27
B-17/7	5	8.0	28.9	0.68	50.2	- 28.87	3.92
B17/6	5	2.3	4.0	0.09	55.0	- 28.86	4.15
B17/5	5	5.5	21.7	0.48	52.9	- 29.06	4.53
B17/3	5	5.0	18.0	0.89	55.1	- 29.36	4.37
B17/2	5	6.8	26.0	0.62	49.0	- 29.43	3.77
B17/1	5	3.3	10.9	0.42	30.3	- 29.03	4.08
ATT7 beta[3]	5+4	0.7	1.99	0.09	25.8	-12.57	5.57
Q25C[3]	4+5	2.53	3.62	0.17	24.9	-29.85	5.94
Q22A[3]	4+5	19.3	32.2	0.84	44.6	-27.47	7.41
ATT5 gamma[3]	4+5	4.0	4.2	0.17	28.9	-27.82	5.88
NMT1[3]	4+5	n.d.	34.8	0.86	47.2	-27.46	7.57
Q11[3]	4+5	2.7	3.6	0.11	38.2	-27.82	5.78
Q25B[3]	4+5	2.7	6.7	0.13	60.1	-16.59	6.12
ATT 5H 2[3]	4+5	4.0	3.4	0.13	30.5	-27.67	5.93
Q2[3]	4+5	2.1	2.1	0.08	30.6	-27.23	5.96
S1 53.0-54.0	4	7.2	9.1	0.29	38.0	-29.10 (-29.34)	4.01
S1 55.0-56.0	4	7.4	9.8	0.31	36.8	-29.33	4.48
S1 57.0-58.0	4	15.8	26.2	0.65	47.4	-28.51 (-28.57)	4.34
S1 60.0-61.0	4	15.8	19.4	0.47	48.5	-28.46	3.59
S1 63.0-64.0	4	11.5	15.9	0.40	47.1	-27.82 (-28.21)	4.58
S1 65.0-66.0	4	7.2	9.9	0.28	40.0	-28.71	5.88
S1 67.0-68.0	4	4.5	5.8	0.21	32.0	-29.37	8.47
S1 69.0-70.0	4	8.3	10.7	0.31	40.0	-28.51	6.62
S1 71.0-72.0	3	10.0	15.4	0.44	40.9	-28.21	4.34
S1 72.0-73.0	3	7.4	12.0	0.35	39.6	-28.56	3.96
S1 74.0-75.0	3	4.5	5.6	0.21	30.6	-29.48	4.70
S1 77.0-78.0	3	8.5	20.4	0.52	45.7	-28.45	3.66
S1 78.0-79.0	3	12.1	19.2	0.49	45.7	-28.40 (-28.41)	4.09
S1 82.0-83.0	3	7.9	19.4	0.56	40.2	-29.22 (-29.32)	3.07
S1 84.0-85.0	3	3.8	7.8	0.26	35.5	-29.42	3.87
S1 86.0-87.0	3	6.6	17.9	0.52	42.2	-29.70	3.02
S1 88.0-89.0	3	8.3	15.7	0.45	41.1	-29.47 (-29.65)	2.93
S1 90.0-91.0	3	12.2	29.6	0.84	41.0	-29.65	4.23
S1 94.0-95.0	3	9.5	24.0	0.64	44.2	-28.70	-0.08
S1 98.0-99.0	3	10.8	17.3	0.44	46.4	-27.90	2.37
S1 100.0-101.0	3	5.4	8.8	0.25	42.9	-28.50	4.55
S1 101.0-102.0	3	6.3	13.3	0.33	48.2	-28.69 (-29.82)	4.24
S1 102.0-103.0	3	8.8	23.3	0.54	51.0	-28.92	3.53
S1 104.0-105.0	3	5.7	11.0	0.29	46.0	-28.52	4.75
S1 106.0-107.0	3	7.0	10.1	0.14	84.0	-29.66 (-29.01)	3.76
ZS-28/73.3	2	16.7	70.6	1.34	61.9	- 30.17	2.79
ZS-28/78.0	2	4.4	5.8	0.19	35.5	- 28.80	5.19
ZS-28/78.9	2	7.6	33.8	0.87	45.3	- 27.58	3.46
ZS-28/79.3	2	3.8	10.0	0.34	34.6	- 29.13	4.58
ZS-28/79.5	2	2.1	2.45	0.06	50.0	- 29.50	2.01
ZS-28/81.8	2	10.4	31.6	0.77	47.6	- 28.81	2.70

Table 7 (continued)

Sample No	Stratigr. interval	TOC[(1)] (wt%)	C_{org}[(2)] (wt%)	N_{org} (wt%)	C_{org}:N_{org} (atomic)	$\delta^{13}C_{org}$ (‰)	$\delta^{15}N_{org}$ (‰)
ZS-28/85.5	2	8.7	39.8	1.00	46.7	- 29.40	3.03
ZS-28/85.8	2	2.7	2.9	0.07	48.0	- 29.12	3.15
ZS-28/87.0	2	2.0	2.1	0.05	56.6	- 29.03	2.59
ZS-28/90.0	2	10.0	18.1	0.36	35.7	- 28.91	3.08
ZS-28/91.5	2	7.1	16.6	0.48	40.5	- 28.91	4.59
ZS-28/93.0	1	1.7	24.7	0.84	34.1	- 26.45	0.40
ZS-28/95.7	1	1.6	1.7	0.05	46.6	- 28.92	n.d.
ZS-28/96.0	1	2.8	15.6	0.67	27.6	- 28.20	5.53
ZS-28/96.3	1	3.4	n.d.	0.85	n.d.	n.d.	- 0.54
ZS-28/96.5	1	4.3	3.96	0.09	55.0	- 28.79	n.d.
ZS-28/97.0	1	0.3	31.5	0.95	38.9	- 28.63	5.86
ZS-28/97.5	1	n.d.	3.1	0.72	4.9	- 28.35	1.10
ZS-28/97.7	1	n.d.	n.d.	0.94	n.d.	n.d.	- 0.74
ZS-28/99.8	1	n.d.	n.d.	0.96	n.d.	n.d.	- 0.18
ZS-28/102.0	1	n.d.	n.d.	0.19	n.d.	n.d.	4.57

(1) Zihor (?)-Menuha Fms (Upper Coniacian-Lower Santonian); (2) Menuha Fm. (Lower Campanian);
(3) Phosphatic Carbonate unit, Mishash Fm. (Up. Campanian);(4) Porcelanite unit, Mishash Fm. (Up. Campanian);
(5) Phosphorite unit, Mishash Fm. (Uppermost Campanian); (6) Oil Shale Mbr., Ghareb Fm. (L. Maastrichtian);
(7) Chalky-Marly Mbr., Ghareb Fm. (Up. Maastrichtian); (8) Taqiye Fm. (Paleocene); Paran Fm. (Lower-Middle Eocene).
[(1)] – in bulk samples; [(2)] – in the organic fraction. [(3)] – Egyptian (Red Sea) phosphate samples.
$\delta^{13}C$ values in parentheses are values measured in the Geochemistry Division of the Geological Survey of Israel.
All the other C and N results are from the Department of Geology and Geophysics of the University of Hawaii.

Table 8. TOC, $C_{:org}$: $N_{:org}$ and $C_{org.}$:P_{org} ratios in various intervals over the Upper Coniacian-Middle Eocene Negev succession

Sample No	Strat. Interv.	TOC[1] (wt %)	C_{org}[2] (wt %)	C_{org}[3] (wt %)	N_{org}[3] (wt %)	P_{org}[4] (wt%)	C_{org}[3]:N_{org}[3] (atomic)	C_{org}[2]: P_{org}[4] (atomic)
M13/39.1-40.3	8	0.3	1.4	1.7	0.07	0.0107	28.0	337
M13/58.0-59.6	8	0.2	0.8	0.9	0.05	0.0150	23.3	137
M13/65.1-66.7	8	0.3	1.9	1.9	0.10	0.0102	22.8	480
M13/88.4-91.4	8	0.3	3.2	3.9	0.12	0.0108	40.0	765
B-124/8.0-9.5	7	0.3	0.6	1.0	0.11	0.0744	10.6	20
B124/13.5-14.0	7	0.2	0.8	1.1	0.14	0.0476	10.0	43
B-124/16.5-17.0	7	0.2	0.5	0.7	0.08	0.0496	10.2	26
B124/24.0-25.0	7	0.3	1.3	1.2	0.18	0.0924	7.7	36
B-124/25.0-25.5	7	0.3	1.6	n.d.	n.d.	0.0450	n.d.	94
B-124/30.3-31.0	6	9.4	23.1	22.0	0.96	0.0450	26.7	1371
B-124/36.3-37.0	6	8.8	17.8	21.9	0.97	0.0223	26.3	2117
B-124/45.0-45.6	6	7.9	26.3	28.4	n.d.	0.0354	n.d.	1990
B-124/50.4-51.0	6	7.8	28.6	23.5	1.09	0.0174	25.1	4252
B-124/58.8-59.4	6	9.3	36.2	32.6	1.26	0.0393	30.1	2511
B-124/60.75-61.5	6	11.3	42.5	40.5	1.26	0.0095	37.4	11956
B-124/65.5-66.0	6	15.4	46.7	44.7	1.66	0.0189	31.4	6480
B17/1	5	3.3	22.8	10.9	0.42	0.0298	30.3	1973
B17/4	5	5.5	32.6	21.7	0.89	0.0270	52.9	3116
B17/8	5	2.9	34.4	21.1	0.51	0.263	48.6	3373
B17/11	5	5.3	51.5	26.8	0.62	0.0288	50.7	4615
S-1/53.0-54.0	4	7.2	4.7	9.1	0.29	0.0029	36.6	4348
S-1/57.0-58.0	4	15.8	19.7	26.2	0.65	0.0270	46.9	1885
S-1/63.0-64.0	4	11.5	11.7	15.9	0.40	0.0063	46.4	4870
S-1/78.0-79.0	3	12.1	12.7	19.2	0.49	0.0045	45.7	7552
S-1/82.0-83.0	3	7.9	17.2	19.4	0.56	0.0127	40.3	3580
S-1/88.0-89.0	3	8.3	13.7	15.7	0.45	0.0066	40.7	5703
S-1/101-102	3	6.3	17.9	13.3	0.33	0.0059	47.1	7844
S-1/106.0-107.0	3	7.0	9.5	10.1	0.14	0.0370	84.0	719
ZS28/1 (73.3)	2	16.7	63.4	70.6	1.34	0.0388	61.9	4216
ZS28/7 (79.3)	2	3.8	8.3	10.0	0.34	0.0139	34.6	1542
ZS28/9 (81.8)	2	10.4	40.9	31.6	0.77	0.0115	47.6	9178
ZS28/13 (87.0)	2	2.0	2.4	2.1	0.05	0.0083	56.6	745
ZS28/16 (93.0)	1	1.7	23.1	24.7	0.84	0.0173	34.1	3446
ZS28/18 (96.0)	1	2.8	26.6	15.6	0.67	0.0662	27.6	1036
ZS28/21 (97.0)	1	0.3	1.3	31.5	0.95	0.0325	38.9	103
ZS28/23 (97.5)	1	n.d.	0.8	3.1	0.72	0.0398	4.9	52

(1) Zihor (?)-Menuha Fms (Upper Coniacian-Lower Santonian); (2) Menuha Fm. (Lower Campanian); (3) Phosphatic Carbonate unit, Mishash Fm. (Up. Campanian);(4) Porcelanite unit, Mishash Fm. (Up. Campanian); (5) Phosphorite unit, Mishash Fm. (Uppermost Campanian); (6) Oil Shale Mbr., Ghareb Fm. (L. Maastrichtian); (7) Chalky-Marly Mbr., Ghareb Fm. (Up. Maastrichtian); Paran Fm. (Lower-Middle Eocene).

[1] in bulk samples

[2] GSI measurements

[3] University of Hawaii measurements

[4] Hebrew University (Rehovot) measurements

Table 9. $C_{(org)}$ accumulation rates along the Upper Coniacian -Lower-Middle Eocene succession of the Negev

Stratigr. interval	T[1] (Ma)	Thickness (m)	TOC (wt%) (mean)	$C_{(org)}$ accum. rate ($\mu moleC_{(org)}.cm^{-2}.kyr^{-1}$)
9	3.0[2]	49.0[2)]	0.33 ± 0.08	540 ± 130
8	5.7[2]	50.0[2]	0.43 ± 0.22	380 ± 190
7	3.2[2]	16.0[2]	0.23 ± 0.05	120 ± 30
6	1.8	41.0	10.0 ± 2.8	22760 ± 6400
5	1.8	11.0	4.88 ± 1.86	2980 ± 1100
4	1.3	16.0	9.71 ± 4.20	11940 ± 5100
3	3.7	35.0	7.92 ± 2.40	7490 ± 2200
2	4.3	18.5	6.86 ± 4.49	2950 ± 1900
1	0.9[2]	4.0[2]	2.35 ± 1.43	1040 ± 600

(1) Zihor (?)-Menuha Fms (Upper Coniacian-Lower Santonian); (2) Menuha Fm. (Lower Campanian); (3) Phosphatic Carbonate unit, Mishash Fm. (Up. Campanian);(4) Porcelanite unit, Mishash Fm. (Up. Campanian); (5) Phosphorite unit, Mishash Fm. (Uppermost Campanian); (6) Oil Shale Mbr., Ghareb Fm. (L. Maastrichtian); (7) Chalky-Marly Mbr., Ghareb Fm. (Up. Maastrichtian); (8) Taqiye Fm. (Paleocene); Paran Fms. (Lower-Middle Eocene).

[1] Estimated from Sr isotopic measurements and where these are lacking, T was estimated from the stratigraphic position of the samples in time scales of Gradstein et al. (1995) and Berggren et al. (1995).

[2] Uncomplete section

תקציר

כדי להבין את השנויים בקצבי הפוספוגנזה לאורך הזמן, וכן האם הם משקפים שינויים בצירקולציה הימית או בעצמת הבלייה היבשתית, נבחנה התפתחות הפוספוגנזה של התטיס במהלך הקרטיקון-איאוקן. 26 אופקי פוספוריט רצופים, המייצגים טווח זמן של קרוב ל- 90 מליון שנה בין ההוטריבין לאיאוקן התיכון, נבדקו להרכב האיזוטופי של Sr, Ca, ו- Nd בפאזה הפרנקוליטית. כמו כן, חושבו קצבי ההצטברות של הזרחן ושל הקלציום וקצבי הסדימנטציה לאורך הקרטיקון התיכון–איאוקן בנגב, זאת כדי לברר את היחסים הדדיים בין השינויים האיזוטופיים לבין עצמת הפוספוגנזה. TOC (%), ויחסי C:N:P, $\delta^{13}C$, $\delta^{15}N$ בפרקציה האורגנית של חתך המשקעים של הקוניאק-איאוקן בנגב , ושל חתך הפוספוריט במצריים (קמפן עליון), נמדדו במטרה להעריך את מידת הרגנרציה ומחזור הנוטריאנטים ע"י הצירקולציה הימית .

מהממצאים מתקבלות המסקנות הבאות : 1) $\delta^{44}Ca$ ו- $\varepsilon_{Nd(T)}$ מראים מגמות השתנות דומות בזמן, עם עליה תלולה לאחר הקנומן-טורון ושיאים אחדים בקמפן העליון ; 2) יש שוני מובהק בערכי ה- $\varepsilon_{Nd(T)}$ בין הפוספוריט של ישראל וזה של מצרים בתקופת הקמפן, וכן שוני בערכי ה- $\varepsilon_{Nd(T)}$ בין הפוספוריט של ישראל וזה של צפון אפריקה בתקופת המאסטריכט-איאוקן ; 3) שיאי ה- $\delta^{44}Ca$ ו- $\varepsilon_{Nd(T)}$ בקמפן העליון בנגב חופפים שיא בקצב ההצטברות של הזרחן, ומינימום בקצבי ההצטברות של הקלציום וקצבי הסדימנטציה ; 4) אין בד"כ התאמה בין ההתפתחות בהרכב האיזוטופי של ה- Sr ושל ה- Ca ו- Nd בטווח הזמן שנבדק ; 5) TOC (wt%), C:N:P , $\delta^{13}C$, ו- $\delta^{15}N$ בפרקציה האורגנית של המשקעים, משתנים בו-זמנית.

ההשתנות הבו-זמנית של $\varepsilon_{Nd(T)}$, $\delta^{44}Ca$, TOC, $\delta^{13}C$, $\delta^{15}N$, יחד עם קצבי הצטברות הזרחן בקרטיקון התיכון-איאוקן בנגב מצביעה על חשיבותם של גורמים פלאוגיאוגרפיים ואוקיאנוגרפיים בהצטברות הפוספט. העליה התלולה ב- $\varepsilon_{Nd(T)}$ לאחר הקנומן העליון מצביעה על כניסה מוגברת של מי הפסיפיק אל תוך התטיס, הנובעת מעליה הגלובלית של פני הים בקרטיקון העליון והגברת הצירקולציה הימית. העליה ב- $\varepsilon_{Nd(T)}$ משקפת גם החלשה בתרומת ה- Nd היבשתי כתוצאה מהתפשטות הים על פני היבשות. העליה המקבילה בערכי ה- $\delta^{44}Ca$ משקפת ירידה בשטף של Ca^{+2} יבשתי יחד עם התפשטות ניכרת של שטחי הסדימנטציה הקרבונטית במדפי היבשת. הגידול בקצבי ההצטברות של הזרחן בתקופת הקמפן משקף אף הוא את האפקט המשולב של עלית פני הים עם אפקטים הנובעים מטקטוניקת הלוחות. שני אלה יחדיו גורמים לצירקולציה ימית ואטמוספרית מתאימה בים התטיס.

ערכי $\delta^{13}C$ ו-$\delta^{15}N$ הנמוכים בפרקציה האורגנית של משקעי הקמפן-מאסטריכט בנגב מעידים על פעילות מוגברת של upwelling חופי המזרים זרחן מומס לעמודת המים בים התטיס המזרחי. פעילות זו נובעת מהגברת הצירקולציה הימית באזור זה במיוחד, כפי שמשתקף בערכי ה- $\varepsilon_{Nd(T)}$. חוסר ההתאמה בין ההתפתחות הגיאוכימית בהרכב האיזוטופי של Sr ושל ה- Ca-Nd בטווח הזמן שנבדק מצביעה כנראה על חוסר קשר ישיר בין קצבי הבלייה היבשתית לבין עצמת הפוספוגנזה. בנוסף לכך, השוני בערכי $\varepsilon_{Nd(T)}$ בין הפוספוריטים של מזרח התיכון ושל צפון אפריקה מרמז על מקורות ימיים שונים של הזרחן בשני האזורים הללו.